Electronic Supplementary Material (ESI) for Physical Chemistry Chemical Physics.

Supporting Information

For

Aromaticity *versus* Regioisomeric Effect of β-Substituents in Porphyrinoids

Yuhang Yao,[†,§] Yu Rao,[†,§] Yiwei Liu,[†] Liang Jiang,[‡] Jin Xiong,[†] Yingjie Fan,[†] Zhen Shen,*[‡] Jonathan L. Sessler*[,#,Δ] and Jun-Long Zhang*[,†]

[†]Beijing National Laboratory for Molecular Sciences, State Key Laboratory of Rare Earth Materials Chemistry and Applications, College of Chemistry and Molecular Engineering, Peking University, Beijing 100871, P. R. China

[‡]State Key Laboratory of Coordination Chemistry, School of Chemistry and Chemical Engineering, Nanjing University, Nanjing 210093, P. R. China

[#]Institute for Supramolecular Chemistry and Catalysis, Shanghai University, Shanghai, 200444, P. R. China

[Δ]Department of Chemistry, The University of Texas at Austin, Austin, Texas 78712-1224, USA

Outline

1. Synthesis and characterization. 4

General information. 4

Synthesis. 5

Analysis of the *cis* isomer product in 1,3-dipolar cycloaddition. 10

2. Photophysical properties, electrochemistry measurement and computation details. 11

Electrochemistry measurement. 11

X-ray diffraction measurement. 11

Computational details. 12

3. Supporting Tables and Figures. 13

Table S1-S3. Crystal data and structure refinements. 13

Table S4-S6. Average length and standard deviations of selected chemical bonds for **3-5**. 16

Table S7. Photophysical and electrochemical data for the **1-5**. 20

Table S8. Reversibility of redox waves in *cis*-**3** with different scan rate of CV measurements. 21

Table S9. Change in the NICS(1) values in the middle ring and the sub-rings. 22

Table S10. Chemical shift values for the *β*-H signals and ΔQ_L absorption values for compounds discussed in this paper. 23

Figure S1-S8. ^{1}H NMR spectra. 24

Figure S9-S16. ^{13}C NMR spectra. 28

Figure S17-S24. ^{19}F NMR spectra. 32

Figure S25-S32. HR-MS (ESI). 36

Figure S33-S40. FT-IR spectra. 40

Figure S41-S50. COSY and NOSEY spectra. 44

Figure S51-S56. X-ray structures. 54

Figure S57-S60. Normalized excitation spectra. 57

Figure S61-S68. Lifetime measurements. 59

Figure S69-S70. Absolute quantum yields. 67

Figure S77-S80. Cyclic Voltammograms. 71

Figure S81. Cyclic Voltammograms of *cis*-**3** in DCM with different scan rates. 73

Figure S82. Average NICS(1) value *vs* average $\delta_{\beta\text{-Hs}}$ for **1-5** in this work. 73

Figure S83. Correlation between regioisomeric effect and aromaticity estimated by average chemical shifts of N-Hs in cis/trans-isomers. 74

Figure S84. Correlation between regioisomeric effect and aromaticity estimated by average chemical shifts of *β*-Hs in cis/trans-isomers. 74

Figure S86. Observed Q band energy *versus* the calculated HOMO–LUMO gap in **1-5**. 75

Figure S87. The experimental Q band wavelength *versus* the theoretical Q band wavelength in **1-5**. 76

Figure S88. The oscillator strength, *f*, of the Q_L band *versus* the calculated ΔHOMO in **1-5**. 76

Figure S89. HOMO-LUMO gap at the optimized S_0 geometries *vs* $Q_L(0,0)$ band for **1-5** in this work. 77

4. Reference: 78

1. Synthesis and characterization.

General information.

All reagents and materials were purchased from commercial suppliers and used as received unless otherwise indicated. All photographs were taken using a Nikon D5300 camera. UV-vis spectra were recorded on an Agilent 8453 UV-vis spectrometer equipped with an Agilent 89090A thermostat (± 0.1 ^{o}C). ESI-MS spectra were recorded on Bruker APEX IV Fourier Transform Ion Cyclotron Resonance Mass Spectrometer using electrospray ionization. Mass spectrometric simulations were carried out using the IsoPro v3.0 package. MALDI-TOF-MS were recorded on an AB Sciex 5800 MALDI-TOF/TOF mass spectrometer. ^{1}H and ^{13}C NMR spectra were recorded on a Bruker-400 MHz instrument, ^{19}F NMR spectra were recorded on a Bruker-500 MHz instrument. ^{1}H and ^{13}C NMR spectra were referenced to tetramethylsilane as an internal standard. For the ^{19}F NMR spectra, trifluoroacetic acid (-77.5 ppm) was used as an external reference. 2D-NMR (COSY and NOSEY) experiments were carried out using a Bruker-500 MHz instrument using $CDCl_3$ as the solvent. Fluorescence spectra were recorded on a NanoLog FL3-2iHR infrared fluorescence spectrometer or an UltraFast Lifetime Spectrofluorometer (Delta Flex), while lifetime and steady state spectra were recorded using FLS-920 and FLS-980 spectrometers. The absolute quantum yields were determined using an integrating sphere on the FLS-980 spectrometer. IR spectra were recorded on a Tensor 27 FTIR or a Spectrum Spotlight 200 FT-IR microscopic.

Synthesis.

Meso-tetrakispentafluorophenylporphyrin, *cis*- and *trans*-porphodilactone

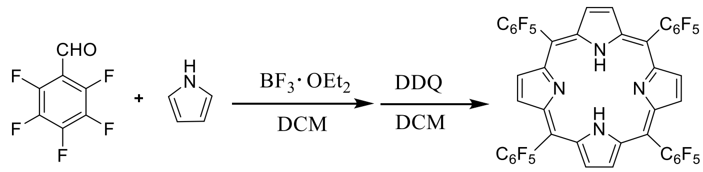

Scheme S1. Synthetic procedure used to prepare the control system F20 Porphyrin

Meso-tetrakispentafluorophenylporphyrin (F_{20} Porphyrin) was synthesized according to the literature as shown in Scheme S1.[1]

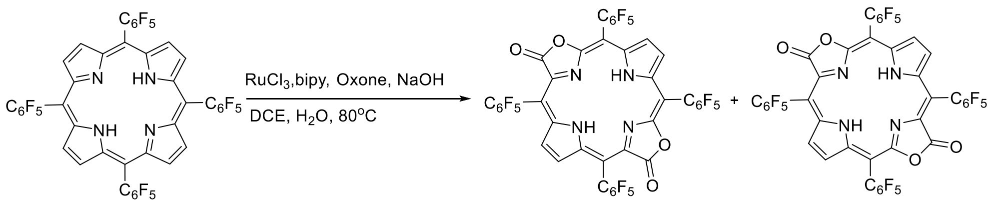

Scheme S2. Synthetic procedure of *cis*/*trans*-**1**

cis-Porphodilactone (*cis*-**1**) and *trans*-porphodilactone (*trans*-**1**) were synthesized and separated according to the literature as shown in Scheme S2.[2]

Synthesis of 2.

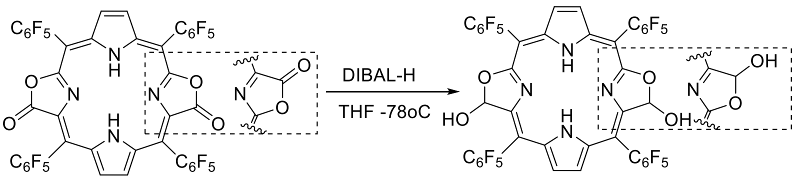

Scheme S3. Synthetic procedure of *cis*/*trans*-**2**

Cis-**1** or *trans*-**1** was dissolved in dry THF. Excess DIBAL-H (0.1 M in hexanes) was added under nitrogen at -78 ℃.[3] Then, the solution was allowed to warm to room temperature and to react for 2 hours. After this point in time, water was added into the reaction mixture. Purification on a silica gel column using ethyl acetate (EA) /petroleum ether (PE) (1:5) as an eluent yielded *cis*- and *trans*-**2**.

Cis-**2**: yield 90%; ^{1}H NMR (400 MHz, Chloroform-d) δ 8.18 (s, 2H), 7.66 (d, *J* = 2.1 Hz, 2H), 7.44 (d, *J* = 10.1 Hz, 2H), 3.72 (t, *J* = 10.8 Hz, 2H), 1.25 (s, 1H), 0.79 (s, 1H).

^{19}F NMR (377 MHz, Chloroform-d) δ -135.39 (ddd, *J* = 24.5, 16.0, 8.2 Hz), -137.28 – -137.96 (m), -140.02 (dd, *J* = 24.0, 8.6 Hz), -151.92 (td, *J* = 21.1, 9.0 Hz), -152.20 (t, *J* = 20.8 Hz), -161.26 (ddtt, *J* = 67.5, 29.6, 22.5, 7.8 Hz). MALDI-TOF-MS m/z: Calcd. For $C_{42}H_{10}F_{20}N_4O_4$ $[M+H]^+$ 1014.037721, found 1014.036329. IR (cm^{-1}): 1261, 1089, 1018, 914, 798, 755, 730, 719. UV-Vis absorption (CH_2Cl_2): λ_{max} (lg ε) = 346 (4.93), 378 (5.03), 443 (3.83), 470 (3.97), 502 (4.44), 606 (3.67), 659 (4.02), 722 (4.56).

Trans-**2**: yield 90%; ^{1}H NMR (400 MHz, Chloroform-d) δ 8.36 (d, *J* = 4.2 Hz, 2H), 8.28 (d, *J* = 4.5 Hz, 2H), 7.78 (d, *J* = 9.6 Hz, 2H), 4.03 (d, *J* = 9.9 Hz, 2H), -1.35 (s, 2H). ^{19}F NMR (377 MHz, Chloroform-d) δ -135.01 (dd, *J* = 25.0, 9.5 Hz), -137.57, -137.82, -139.40 (dd, *J* = 23.9, 8.1 Hz), -139.60 (dd, *J* = 24.6, 8.1 Hz), -151.56 (t, *J* = 21.0 Hz), -152.44 (td, *J* = 21.0, 9.7 Hz), -160.87, -161.12, -161.34 – -161.95 (m). MALDI-TOF-MS m/z: Calcd. For $C_{42}H_{10}F_{20}N_4O_4$ $[M+H]^+$ 1014.037721, found 1014.038852. IR (cm^{-1}): 1519, 1498. UV-Vis absorption (CH_2Cl_2): λ_{max} (lg ε) = 345 (4.91), 382 (4.98), 450 (3.46), 478 (3.58), 510 (4.37), 689 (3.65), 750 (4.81).

Synthesis of 3.

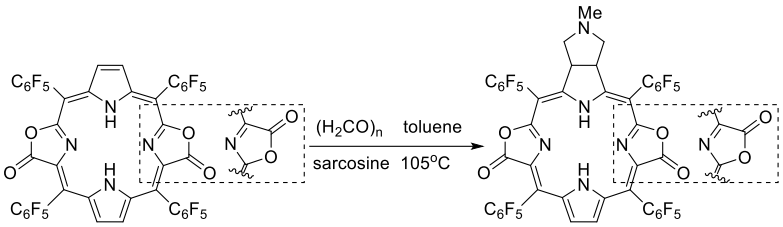

Scheme S4. Synthetic procedure leading to *cis- and trans*-**3**

Cis-**1** or *trans*-**1** (0.015 mmol) was dissolved in dry toluene along with 6 mg (0.067 mmol) sarcosine and 2.6 mg (0.087 mmol) paraformaldehyde.[4] This purple solution was heated at 105 ℃ and stirred for 12 h in a Schleck tube under N_2. During this time the color of the mixture changed to orange. This reaction was monitored by observing the solution under a UV lamp at 365 nm. Purification was carried out on a small silica gel column using CH_2Cl_2/PE (1:1) as the eluent. This gave unreacted *cis*-**1** or *trans*-**1**; then, using dichloromethane as an eluent, *cis*- and *trans*-**3** were obtained.

Cis-**3**: yield 57%; ^{1}H NMR (400 MHz, Chloroform-d) δ 7.23 (d, *J* = 2.1 Hz, 2H), 6.53 (s, 1H), 5.45 (s, 1H), 4.35 (d, *J* = 3.7 Hz, 2H), 2.73 (s, 2H), 2.53 (d, *J* = 3.2 Hz,

2H), 2.22 (s, 3H). ^{13}C NMR (101 MHz, $CDCl_3$) δ 163.7, 159.6 – 159.4, 158.8, 134.9, 127.9, 121.7, 112.8, 85.0, 61.5, 47.6, 40.7. ^{19}F NMR (471 MHz, Chloroform-d) δ -135.54 (dd, *J* = 24.9, 8.5 Hz), -138.25 – -138.71 (m), -139.32 (d, *J* = 18.5 Hz), -150.00, -151.33, -159.48 (d, *J* = 8.5 Hz), -159.69 (d, *J* = 8.0 Hz), -160.80 – -161.30 (m). ESI-MS m/z: Calcd. For $C_{45}H_{14}F_{20}N_5O_4$ $[M+H]^+$ 1068.072095, found 1068.071241. IR (cm^{-1}): 1774, 1716, 1610. UV-Vis absorption (CH_2Cl_2): λ_{max} (lg ε) = 372 (5.12), 383 (5.15), 478 (3.94), 511 (4.32), 549 (4.67).

Trans-**3**: yield 66%; ^{1}H NMR (400 MHz, $CDCl_3$) δ 7.59 (dd, *J* = 11.2, 9.3 Hz, 2H), 4.60 (d, *J* = 5.6 Hz, 2H), 4.13 (s, 1H), 3.48 (s, 1H), 2.86 (d, *J* = 8.5 Hz, 2H), 2.61 – 2.52 (m, 2H), 2.23 (s, 3H). ^{13}C NMR (101 MHz, Acetone) δ 162.7, 150.7, 134.4, 134.1, 129.7, 126.7, 123.0, 121.5, 61.9, 48.5, 40.0. ^{19}F NMR (471 MHz, Chloroform-d) δ -135.99 – -138.34 (m), -138.84, -139.94, -147.81 (d, *J* = 283.4 Hz), -150.37 (d, *J* = 356.5 Hz), -157.64 (d, *J* = 215.8 Hz), -158.74, -159.85 (d, *J* = 148.8 Hz), -160.33 – -161.38 (m). ESI-MS m/z: Calcd. For $C_{45}H_{14}F_{20}N_5O_4$ $[M+H]^+$ 1068.072095, found 1068.072539. IR (cm^{-1}): 1772, 1631, 1600. UV-Vis absorption (CH_2Cl_2): λ_{max} (lg ε) = 381 (4.93), 403 (5.09), 573 (4.32), 620 (4.47).

Synthesis of 4.

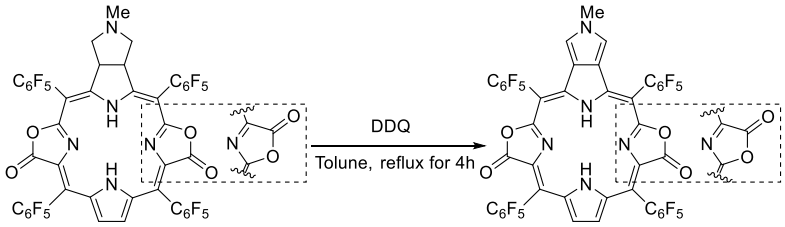

Scheme S5. Synthetic procedure used to access *cis*- and *trans*-**4**

Cis-**3** or *trans*-**3** (0.056 mmol) was dissolved in 20 mL toluene along with 150 mg (0.661 mmol) DDQ. The solution was heated at reflux for 6 hours. Purification was carried on a neutral aluminum oxide column protected from light. PE : CH_2Cl_2 (DCM) =1:1 was used as eluent to give the violet product *cis*- or *trans*-**4**.

Cis-**4**: yield 87%; ^{1}H NMR (400 MHz, Chloroform-*d*) δ 7.79 (d, *J* = 2.2 Hz, 2H), 6.71 (s, 2H), 4.06 (s, 3H), 3.51 (s, 1H), 2.39 (s, 1H). ^{13}C NMR (126 MHz, Chloroform-*d*) δ 164.8, 157.6, 141.5, 134.9, 128.3, 124.1, 122.5, 117.3, 109.7, 84.1, 38.4. ^{19}F NMR

(471 MHz, Chloroform-*d*) δ -137.09 (dd, *J* = 23.2, 8.2 Hz), -139.09 (dd, *J* = 23.6, 7.8 Hz), -150.30 (dd, *J* = 23.9, 17.9 Hz), -151.56 (t, *J* = 20.9 Hz), -159.22 – -160.47 (m), -160.99 – -161.65 (m). MALDI-TOF-MS m/z: Calcd. For $C_{45}H_9F_{20}N_5O_4$ $[M+H]^+$ 1063.032970, found 1063.033600. IR (cm^{-1}): 1774, 1605. UV-Vis absorption (CH_2Cl_2): λ_{max} (lgε) = 376 nm (4.85), 393 nm (5.10), 415 nm (5.40), 546 nm (4.25), 573 nm (4.36), 595 nm (4.38).

Trans-**4**: yield 90%; ^{1}H NMR (400 MHz, Chloroform-*d*) δ 8.21 (d, *J* = 12.6 Hz, 2H), 6.85 (s, 1H), 6.77 (s, 1H), 4.15 (s, 3H), 0.79 (s, 1H), 0.19 (s, 1H). ^{13}C NMR (126 MHz, $CDCl_3$) δ 165.3, 151.2, 139.4, 138.4, 135.0, 134.9, 127.7, 124.6, 124.2, 123.0, 116.7, 116.4, 38.6.^{19}F NMR (471 MHz, Chloroform-*d*) δ -137.17 (dd, *J* = 54.0, 15.4 Hz), -138.28 (d, *J* = 15.8 Hz), -138.96 (d, *J* = 15.7 Hz), -150.12 (t, *J* = 20.9 Hz), -150.82 (q, *J* = 20.1 Hz), -151.52 (t, *J* = 20.7 Hz), -159.25 – -159.93 (m), -160.07 – -160.48 (m), -160.67 – -160.97 (m), -161.25 – -161.81 (m). Calcd. For $C_{45}H_9F_{20}N_5O_4$ $[M+H]^+$ 1063.032970, found 1063.034118. IR (cm^{-1}): 1753, 1591. UV-Vis absorption (CH_2Cl_2): λ_{max} (lgε) = 393 nm (5.50), 409 nm (5.05), 431 nm (5.17), 586 nm (4.17), 614 nm (4.23), 668 nm (4.65).

Synthesis of 5.

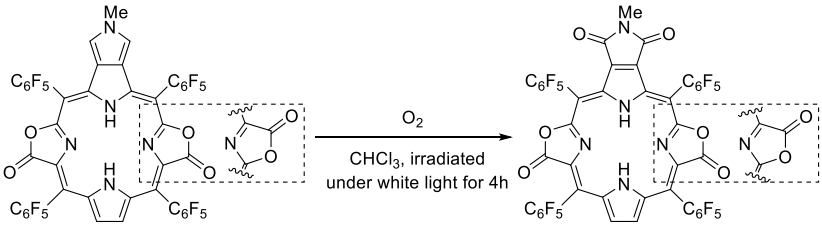

Scheme S6. Synthetic procedure used to obtain *cis*- and *trans*-**5**

Cis-**4** or *trans*-**4** (0.042 mmol) was dissolved in 20 mL chloroform. The solution was saturated with oxygen. Then, it was irradiated in a photoreactor and irradiated. Over the course of 4 h, the solution changed from violet to dark red. The volatiles were removed using a rotary evaporator. Purification was carried on a silica gel column. PE : DCM = 8:1 was used to separate the red product, consisting of *cis*- or *trans*-**5** depending on the choice of starting material.

Cis-**5**: yield 16%. ^{1}H NMR (500 MHz, Chloroform-d) δ 8.76 (s, 2H), 3.30 (s, 3H), -

1.05 (s, 1H), -1.64 (s, 1H). ^{13}C NMR (126 MHz, Chloroform-d) δ 164.2, 161.8, 139.4, 133.9, 130.8, 128.1, 106.7, 25.3. ^{19}F NMR (471 MHz, Chloroform-d) δ -138.28 – -138.54 (m), -138.69 (dd, *J* = 23.6, 8.0 Hz), -149.49 (d, *J* = 21.0 Hz), -149.56, -149.77 (t, *J* = 21.4 Hz), -160.27 – -160.55 (m), -161.24 – -161.44 (m). MALDI-TOF-MS m/z: Calcd. For $C_{45}H_7F_{20}N_5O_6$ $[M+H]^+$ 1093.007149, found 1093.008387. IR (cm^{-1}):1774, 1724. UV-Vis absorption (CH_2Cl_2): λ_{max} (lgε) =432 (5.31), 526 (4.18), 568 (4.00), 658 (3.92), 722 (4.86).

Trans-**5**: yield 18%. ^{1}H NMR (500 MHz, Chloroform-d) δ 8.80 – 8.67 (m, 2H), 3.25 (s, 3H), -0.66 (s, 1H), -0.69 (s, 1H). ^{13}C NMR (126 MHz, Chloroform-d) δ 164.0, 163.6, 162.2, 161.9, 156.6, 154.4, 143.7, 142.7, 138.8, 134.6, 134.0, 132.8, 130.5, 130.4, 128.5, 128.2, 107.2, 101.5, 25.2. ^{19}F NMR (471 MHz, Chloroform-d) δ -136.61 – -137.28 (m), -137.74 – -138.51 (m), -138.71 – -139.06 (m), -139.96 – -140.63 (m), -148.51 (t, *J* = 20.9 Hz), -149.40 (t, *J* = 20.8 Hz), -150.06 (t, *J* = 21.1 Hz), -150.71 (t, *J* = 20.8 Hz), -159.63 (dd, *J* = 21.6, 14.3 Hz), -160.37 (dd, *J* = 21.7, 14.4 Hz), -161.42 (dd, *J* = 21.5, 15.4 Hz), -161.76 (dd, *J* = 21.3, 15.4 Hz). MALDI-TOF-MS m/z: Calcd. For $C_{45}H_7F_{20}N_5O_6$ $[M+H]^+$ 1093.007149, found 1093.005622. IR (cm^{-1}): 1786, 1720. UV-Vis absorption (CH_2Cl_2): λ_{max} (lgε) =423(5.19), 524(4.00), 564(4.25), 640(4.02), 702(4.75).

Analysis of the *cis* isomer product in 1,3-dipolar cycloaddition.

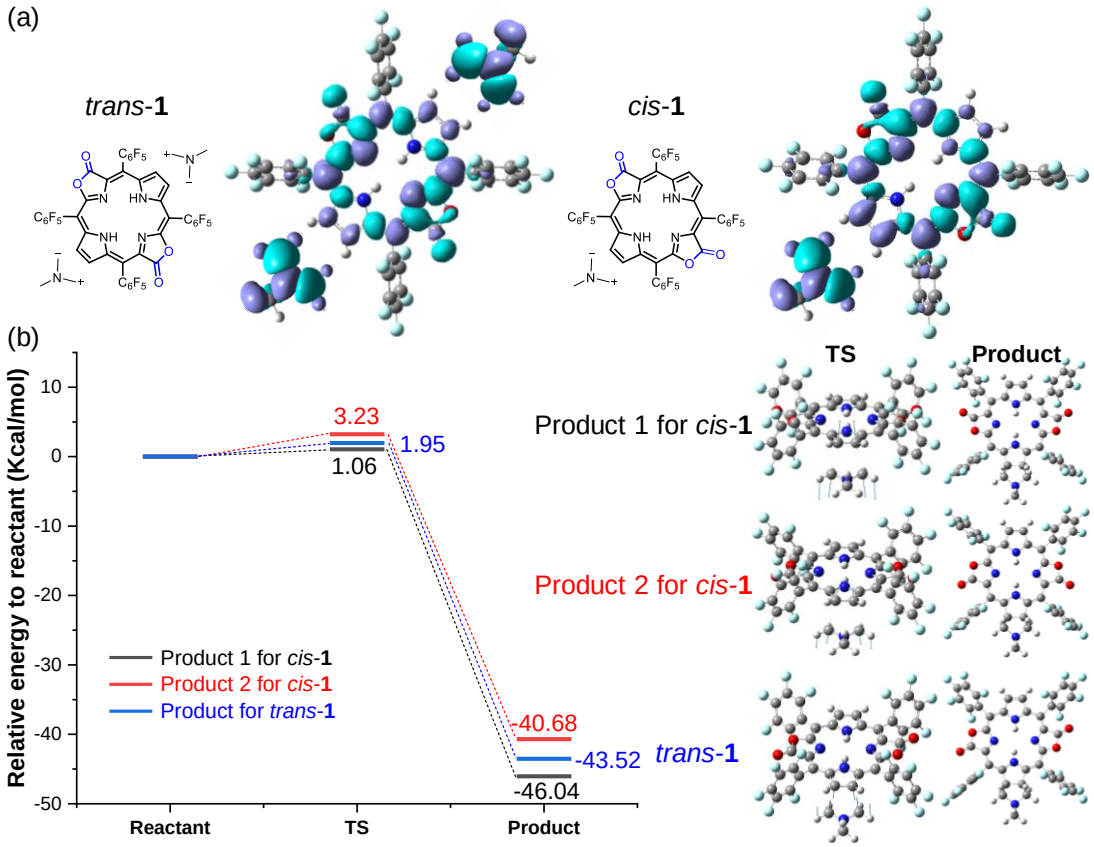

Scheme S7. (a) Dual descriptor for explaining 1,3-dipolar cycloaddition of *cis*/*trans*-**1** and (b) energy diagram for reaction coordinates as well as the structures of transition states and products for 1,3-dipolar cycloaddition of *cis*/*trans*-**1**.

Dual descriptor,[5] which is often used to predict the chemical reactivity of cycloaddition reaction, as shown in scheme S7, is evenly distributed in the two sides of lactone moieties in *trans* isomer, while distributed more in the side of saturated oxygen atom than carbonyl group in *cis* isomer. This indicates the favor formation of *cis* isomer in this work (product 1) rather than another possible *cis* isomer (product 2). Further more, the energy diagram for reaction coordinates exhibit a higher energy of transition state and product of another possible *cis* isomer (product 2) compared with the *cis* isomer in this work (product 1), which also suggest the favor formation of *cis* isomer in this work both thermodynamically and kinetically.

2. Photophysical properties, electrochemistry measurement and computation details.

Electrochemistry measurement.

The electrochemistry analyses were conducted using a standard three-electrode configuration on a Shanghai Chenhua CHI660C electrochemical workstation at 25 ºC under argon. Cyclic voltammetric curves were recorded using glassy-carbon working electrode disks of 3 mm diameter (Cypress Systems EE-040). Between scans, the working electrode was subject to a sequence that involved polishing with diamond paste (Buehler) of decreasing sizes (3 to 0.05 μm) interspersed by washings with purified H_2O. The auxiliary electrode was a platinum wire and Ag/AgCl electrode was used as the reference electrode. All glassware used for electrochemical studies was oven dried overnight and allowed to cool to room temperature before use.

X-ray diffraction measurement.

X-ray diffraction data were collected on *Rigaku XtaLAB Pro: Kappa single system* instrument equipped with Mo K*α* source. Suitable crystal was mounted on the diffractometer and cooled under a nitrogen stream as soon as practical after mounting to preclude desolvation. The *CrysAlisPro* program was employed for data processing. The structure was solved using *SHELXT 2014* program[6] and refined against F^2 anisotropically for all non-hydrogen atoms per the full matrix least-squares protocol using the *SHELXL 2016* program in an Olex2 GUI.[7] The *Platon* program package[8] was employed for squeeze processing.

Computational details.

In this work, the hybrid density functional, B3LYP[9] was employed for all calculations using the program package G09[10] (except for the ACID calculations). The 6-31G(d) basis set[11] was used for all atoms subject top geometry optimization, while current density tensor computations were used for the ACID calculations.[12] The 6-31+G(d) basis set was employed in NICS [13] calculation. Geometry optimizations of the singlet ground state (S_0) were carried out using the density functional theory without symmetry constraints. Frequency calculations were performed on the optimized structures to ensure that they represented true minimum energy structures as judged by the absence of imaginary frequency values (i.e. NImag = 0). And the transition states were also confirmed by only one imaginary frequency along the reaction coordinates. The intrinsic reaction coordinate (IRC) calculations were also performed to connect the reactants, transition states and products. NMR shielding tensors were computed using the Continuous Set of Gauge Transformations (CSGT) method[14] and the Gauge-Independent Atomic Orbital (GIAO) method[14c, 15]. ACID plots were constructed using the AICD 2.0 program package[12a] and drawn using Povray 3.7.

3. Supporting Tables and Figures.

Table S1. Crystal data and structure refinement of *cis*/*trans*-**3**.

Compounds	*cis*-**3** (CCDC 1568750)	*trans*-**3** (CCDC 1568751)
molecular formula	$C_{49}H_{21}Cl_3F_{20}N_5O_4$	$C_{45}H_{11}F_{20}N_5O_4$
formula wt (g mol^{-1})	1230.06	1065.59
temperature (K)	180.00(10)	100.00(11)
Radiation (λ, Å)	0.71073	0.71073
crystal system	monoclinic	monoclinic
space group	$I_{1\frac{2}{m}1}$	$C_{1\frac{2}{m}1}$
$a(\text{Å})$	18.9313(9)	25.7880(5)
$b(\text{Å})$	16.3839(12)	16.3752(3)
$c(\text{Å})$	17.3825(10)	12.6133(2)
α (°)	90	90
β (°)	91.048(4)	90.592(2)
γ (°)	90	90
Volume (Å^3)	5390.6(6)	5326.11(17)
Z	4	4
ρ_{calcd} (g cm^{-3})	1.516	1.329
μ (mm^{-1})	0.287	0.134
F (000)	2452	2112
crystal size (mm^3)	0.23×0.21×0.15	0.319×0.236×0.148
Theta range	2.847 to 27.484°	3.5730 to 30.2550°
reflections collected	19233	78894
independent reflections	6392[R(int)=0.0457]	7075[R(int)=0.0116]
Completeness	99.83%	99.72%
goodness-of-fit on ^{2}F	1.064	1.060
final R indices[R>2σ(I)]	$R1^a$=0.0954 wR_2^b=0.2963	$R1^a$=0.0690 wR_2^b= 0.1888
R indices (all data)	$R1^a$=0.1321 wR_2^b=0.2623	$R1^a$=0.0755 wR_2^b= 0.1948
Largest diff. peak and hole (e Å^{-3})	1.647 and -1.297	0.572 and -0.298

Table S2. Crystal data and structure refinement of *cis*/*trans*-**4**.

Compounds	*cis*-**4** (CCDC 1841552)	*trans*-**4** (CCDC 1841553)
molecular formula	$C_{46}H_{10}Cl_3F_{20}N_5O_4$	$C_{46}H_{10}Cl_3F_{20}N_5O_4$
formula wt (g mol^{-1})	1182.94	1182.94
temperature (K)	179.99(10)	179.99(10)
Radiation (λ, Å)	0.71073	0.71073
crystal system	monoclinic	monoclinic
space group	P 21	P 21/n
$a(\text{Å})$	14.5721(8)	19.2843(10)
$b(\text{Å})$	9.2987(6)	8.2608(4)
$c(\text{Å})$	15.8007(10)	28.316(2)
α (°)	90	90
β (°)	90.331(6)	103.985(6)
γ (°)	90	90
Volume ($Å^3$)	2141.0(2)	4377.1(5)
Z	2	4
ρ_{calcd} (g cm^{-3})	1.835	1.795
μ (mm^{-1})	0.358	0.35
F (000)	1168	2336
crystal size (mm^3)	0.2×0.05×0.04	0.4×0.08×0.05
Theta range	2.5730 to 20.7440°	2.1800 to 25.4210°
reflections collected	18279	25827
independent reflections	8264[R(int)=0.0649]	7712[R(int)=0.0492]
Completeness	0.988	0.999
goodness-of-fit on ^2F	1.03	1.027
final R indices[R>2σ(I)]	$R1^a$= 0.0689 wR_2^b = 0.1753	$R1^a$=0.0815 wR_2^b= 0.2162
R indices (all data)	$R1^a$ = 0.1115 wR_2^b = 0.1585	$R1^a$= 0.1256 wR_2^b= 0.1906
Largest diff. peak and hole (e $Å^{-3}$)	0.450 and -0.716	0.908 and -0.959

Table S3. Crystal data and structure refinement of *cis*/*trans*-**5**.

Compounds	*cis*-**5** (CCDC 1851807)	*trans*-**5** (CCDC 1851808)
molecular formula	$C_{45}H_7F_{20}N_5O_6$	$C_{45}H_7F_{20}N_5O_6$
formula wt (g mol^{-1})	1093.56	1093.56
temperature (K)	179.99(11)	100.00(13)
Radiation (λ, Å)	0.71073	0.71073
crystal system	triclinic	monoclinic
space group	P -1	P 21
$a(\text{Å})$	18.2714(3)	33.9547(16)
$b(\text{Å})$	18.3261(2)	8.7071(3)
$c(\text{Å})$	35.2109(6)	58.8064(13)
α (°)	95.7970(10)	90
β (°)	97.4290(10)	93.851(3)
γ (°)	90.0230(10)	90
Volume (Å^3)	11630.3(3)	17346.7(11)
Z	10	16
ρ_{calcd} (g cm^{-3})	1.561	1.675
μ (mm^{-1})	0.159	0.17
F (000)	5400	8640
crystal size (mm^3)	0.6×0.4×0.15	0.3×0.1×0.05
Theta range	1.7070 to 26.5980°	2.1600 to 27.7710°
reflections collected	138185	93886
independent reflections	40971[R(int)=0.0726]	54490[R(int)=0.0925]
Completeness	0.997	99.60%
goodness-of-fit on ^{2}F	1.018	1.09
final R indices[R>2σ(I)]	R1^a = 0.0959 wR_2^b = 0.2193	R1^a = 0.1453 wR_2^b = 0.3615
R indices (all data)	R1^a = 0.1463 wR_2^b = 0.2449	R1^a = 0.2369 wR_2^b =0.3039
Largest diff. peak and hole (e Å^{-3})	1.006 and -0.626	1.619 and -0.952

Table S4. Average length and standard deviations of selected chemical bonds for the core ring present in *cis*/*trans*-**3**.

	cis-**3**		*trans*-**3**	
	Bond	**Length /Å**	**Bond**	**Length /Å**
C-N	C00J-N00D	1.359	C8-N3	1.375
	C00N-N00G	1.308	C6-N2	1.325
	C00R-N00G	1.383	C4-N2	1.380
	C00J-N00F	1.372	C2-N1	1.368
	Average	1.356		1.362
	Standard deviation	0.033		0.025
C-C	C00N-C00K	1.424	C6-C7	1.422
	C00K-C00J	1.365	C7-C8	1.371
	C00R-C00Q	1.381	C4-C3	1.377
	C00Q-C00U	1.405	C3-C2	1.422
	C00U-C011	1.417	C8-C9	1.309
	C011-C011	1.357	C9-C9	1.548
	C013-C00R	1.456	C6-C5A	1.404
	C00J-C00L	1.516	C5B-C4	1.409
	C00L-C00L	1.556	C2-C1	1.415
			C1-C1	1.386
	Average	1.431		1.406
	Standard deviation	0.068		0.060

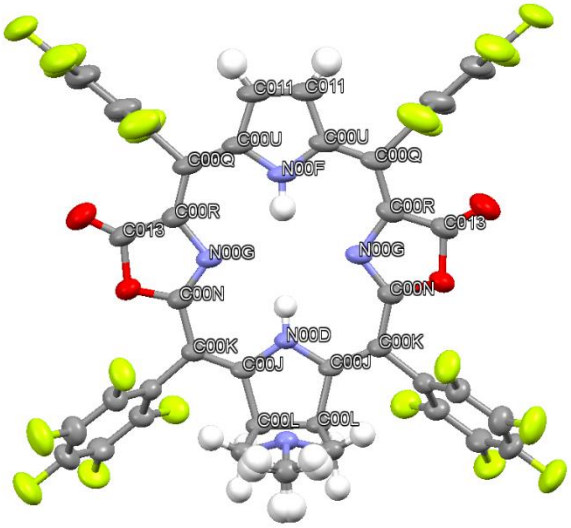

cis-**3**

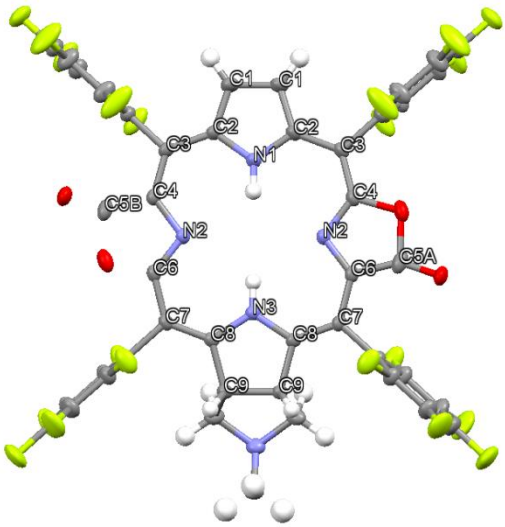

trans-**3**

Table S5. Average length and standard deviations of selected chemical bonds for the core ring present in *cis*/*trans*-**4**.

	cis-**4**		*trans*-**4**	
	Bond	**Length /Å**	**Bond**	**Length /Å**
C-N	C5-N2	1.368	C4-N2	1.359
	C8-N2	1.366	C7-N2	1.380
	C3-N1	1.390	C2-N1	1.363
	C1-N1	1.322	C21-N1	1.315
	C20-N4	1.366	C19-N4	1.395
	C14-N4	1.393	C13-N4	1.372
	C10-N3	1.300	C9-N3	1.348
	C12-N3	1.377	C11-N3	1.366
	C18-N5	1.378	C17-N5	1.355
	C16-N5	1.355	C15-N5	1.376
	Average	1.362		1.363
	Standard deviation	0.029		0.022
C-C	C6-C7	1.378	C5-C6	1.372
	C5-C6	1.405	C5-C4	1.405
	C5-C4	1.413	C3-C4	1.419
	C4-C3	1.364	C3-C2	1.380
	C3-C2	1.474	C1-C2	1.478
	C1-C21	1.419	C21-C20	1.399
	C21-C20	1.396	C20-C19	1.378
	C20-C19	1.437	C19-C18	1.432
	C19-C15	1.407	C18-C14	1.416
	C15-C14	1.447	C14-C13	1.450
	C14-C13	1.378	C13-C12	1.385
	C13-C12	1.399	C11-C12	1.406
	C11-C10	1.485	C10-C11	1.488
	C10-C9	1.373	C9-C8	1.373
	C9-C8	1.406	C8-C7	1.408
	C8-C7	1.412	C7-C6	1.395
	C19-C18	1.399	C14-C15	1.363
	C15-C16	1.374	C18-C17	1.377
	Average	1.409		1.407
	Standard deviation	0.034		0.036

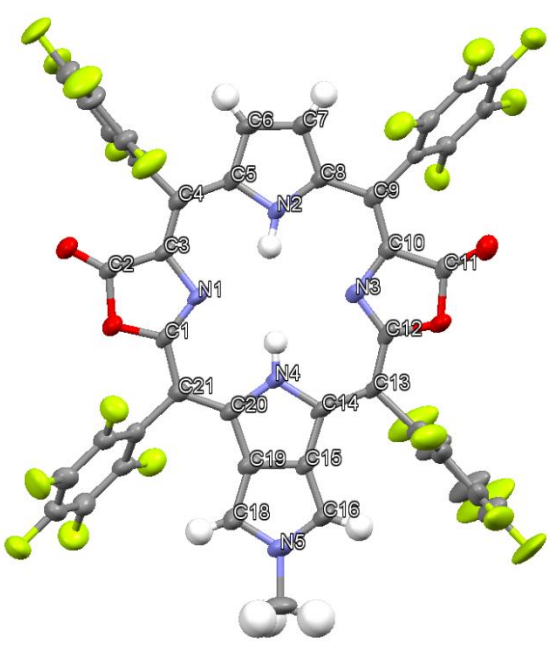

cis-**4**

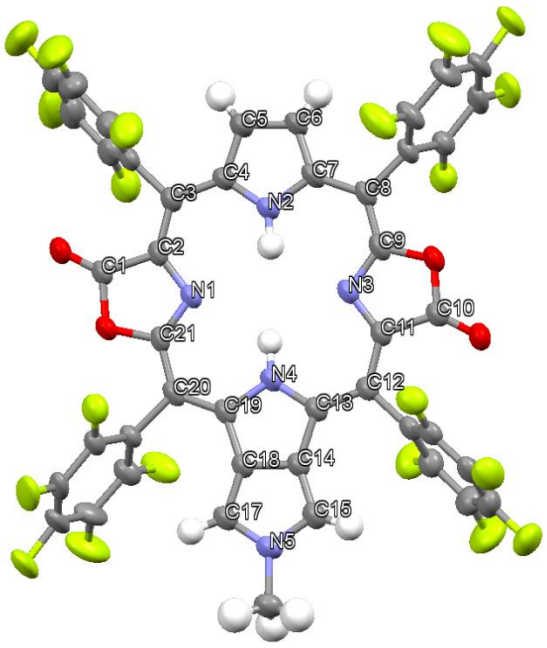

trans-**4**

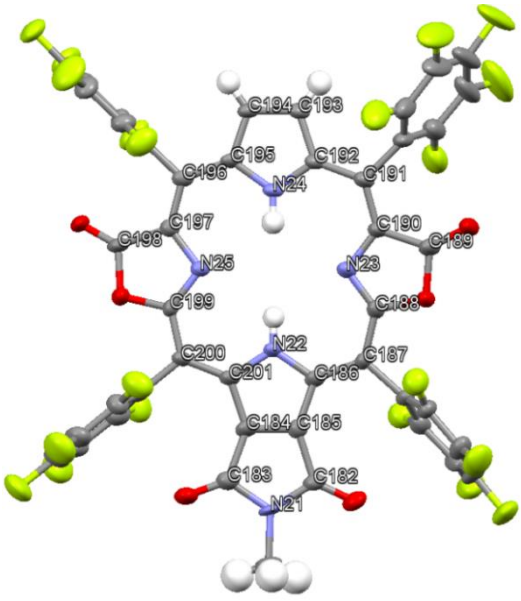

cis-**5**

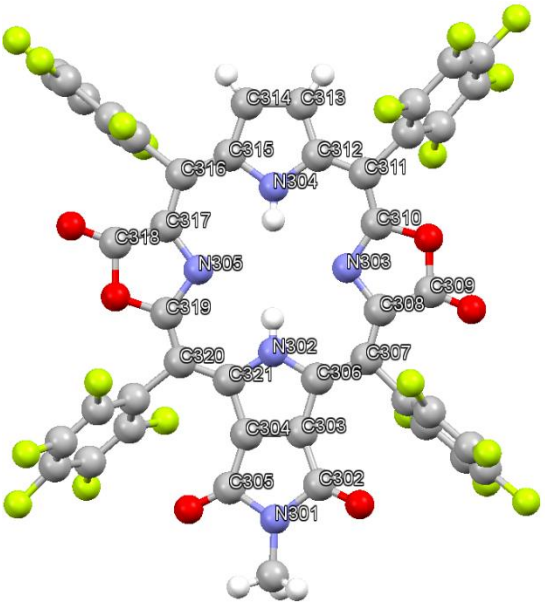

trans-**4**

Table S6. Average length and standard deviations of selected chemical bonds for the core ring present in *cis*/*trans*-**5**.

	cis-**5**		*trans*-**5**	
	Bond	**Length /Å**	**Bond**	**Length /Å**
C-N	C195-N24	1.375	C315-N304	1.415
	C192-N24	1.362	C317-N305	1.400
	C197-N25	1.367	C319-N305	1.399
	C199-N25	1.318	C321-N302	1.351
	C201-N22	1.387	C305-N301	1.471
	C186-N22	1.366	C302-N301	1.464
	C188-N23	1.315	C306-N302	1.357
	C190-N23	1.371	C308-N303	1.388
	C183-N21	1.389	C310-N303	1.388
	C182-N21	1.398	C312-N304	1.407
	Average	1.365		1.404
	Standard deviation	0.028		0.039
C-C	C193-C194	1.350	C313-C314	1.417
	C194-C195	1.414	C314-C315	1.410
	C195-C196	1.392	C315-C316	1.351
	C196-C197	1.377	C316-C317	1.400
	C197-C198	1.473	C317-C318	1.398
	C199-C200	1.394	C319-C320	1.307
	C200-C201	1.384	C320-C321	1.353
	C201-C184	1.437	C321-C304	1.477
	C184-C185	1.367	C304-C303	1.460
	C185-C186	1.424	C304-C305	1.469
	C186-C187	1.401	C302-C303	1.471
	C187-C188	1.416	C303-C306	1.439
	C189-C190	1.478	C306-C307	1.385
	C190-C191	1.382	C307-C308	1.311
	C191-C192	1.407	C308-C309	1.394
	C192-C193	1.423	C310-C311	1.340
	C183-C184	1.492	C311-C312	1.314
	C182-C185	1.505	C312-C313	1.407
	Average	1.418		1.395
	Standard deviation	0.044		0.056

Table S7. Photophysical and electrochemical data for the *cis*/*trans* porphyrinoids **1-5**[a]

Compound	UV-vis λ_{max} [nm] (log ε [M^{-1} cm^{-1}])		fluorescence λ_{max} [nm] (τ [ns])	Φ_F [b]	E_{ox} [c] [V]	E_{red} [c] [V]
	Soret bands	Q bands				
cis-**1** [e]	391(5.11), 408(5.62),	505(4.26), 600 (3.88), 657(4.47)	662, 711 (3.49)	0.090	1.66	−0.44, −0.85
trans-**1** [e]	410(5.56)	512(4.15), 552(4.38), 676(4.89)	678, 755 (3.49)	0.100	1.61	−0.37, −0.87
cis-**2**	346 (4.93), 378 (5.03)	443 (3.83), 470 (3.97), 502 (4.44), 606 (3.67), 659 (4.02), 722 (4.56)	737, 784 (2.11)	0.061	0.94	-0.73, -1.11
trans-**2**	345 (4.91), 382 (4.98)	450 (3.46), 478 (3.58), 510 (4.37), 689 (3.65), 750 (4.81)	754, 828 (2.61)	0.053	0.87	-0.67, -1.08
cis-**3**	372 (5.12), 383 (5.15)	478 (3.94), 511 (4.32), 549 (4.67)	559, 604 (5.10)	0.351	1.52	-0.74, -1.05
trans-**3**	381 (4.93), 403 (5.09)	573 (4.32), 620 (4.47)	635, 683 (5.46)	0.245	1.38	-0.62, -1.03
cis-**4**	376(4.85), 393(5.10), 415(5.40)	546(4.25), 573(4.36), 595(4.38)	617, 666 (8.34)	0.363	1.35	-0.85, -1.14
trans-**4**	393(5.50), 409(5.05), 431(5.17)	586(4.17), 614(4.23), 668(4.65)	692, 746 (3.29)	0.152	1.22	-0.64, -1.10
cis-**5**	432(5.31)	526(4.18), 568(4.00), 658(3.92), 722(4.86)	728, (3.45)	0.209	--[f]	0.0, -0.48, -1.59
trans-***5***	423(5.19)	524(4.00), 564(4.25), 640(4.02), 702(4.75)	707, 764 (3.95)	0.277	--[f]	-0.06, -0.54, -1.64

[a]All photophysical analyses were carried out in anhydrous CH_2Cl_2 at room temperature. [b]Quantum yields were measured using an Edinburgh Analytical Instrument FLS-980 equipped with an integrating sphere except for *cis*/*trans*-**1**. [c]Relative to Fc^+/Fc with the underlying analyses being carried out in CH_2Cl_2 using n-Bu_4NPF_6 as the electrolyte. [d] The HL energy gap was estimated by the difference of E_{ox}^1- E_{re}^1. [e]From ref. 7. [f]No oxidation waves for **5** were observed in CH_2Cl_2.

Table S8. Reversibility of redox waves in *cis*-**3** with different scan rate of CV measurements.

Scan rate ($V \cdot s^{-1}$)	Redox 1 (V)	Redox 2 (V)
0.05	0.622 – 0.555 = 0.067	1.030 – 0.963 = 0.067
0.07	0.622 – 0.555 = 0.067	1.027 – 0.960 = 0.067
0.1	0.622 – 0.555 = 0.067	1.027 – 0.957 = 0.070
0.3	0.625 – 0.540 = 0.085	1.021 – 0.930 = 0.091
0.5	0.640 – 0.543 = 0.097	1.042 – 0.945 = 0.097

Table S9. Change in the NICS(1) values in the middle ring and the sub-rings.

NICS(1) /ppm		middle ring	sub-ring				
			a		*b*	*c*	*d*
1	*cis*	-10.61	-1.23	-1.39	-10.72	-11.58	--
	trans	-11.37	-1.52	-1.17	-11.07	-11.68	--
2	*cis*	-9.88	0.89	0.48	-10.60	-13.22	--
	trans	-10.71	0.90	1.19	-12.12	-10.84	--
3	*cis*	-4.72	-2.52	-2.48	-0.07	-10.01	--
	trans	-6.39	-2.01	-3.09	0.46	-10.07	--
4	*cis*	-7.16	-1.76	-1.66	-4.24	-11.58	-12.76
	trans	-9.23	-1.93	-1.42	-4.81	-12.46	-12.51
5	*cis*	-10.93	-1.63	-1.59	-9.02	-9.78	0.094
	trans	-10.36	-1.38	-1.78	-9.26	-8.66	0.559
Cavaleiro et al.	*cis*	-11.63	--				
	trans	-11.85					
Lindsey et al.	*cis*	-11.12	--				
	trans	-11.88					
chlorophyll	*d*	-10.80	--				
	f	-11.45					
Inhoffen et al.	*cis*	-11.31	--				
	trans	-11.42					
Brückner et al (compund **14**)	*cis*	-9.54	--				
	trans	-10.38					
Brückner et al (compound **16**)	*cis*	-10.23	--				
	trans	-10.89					

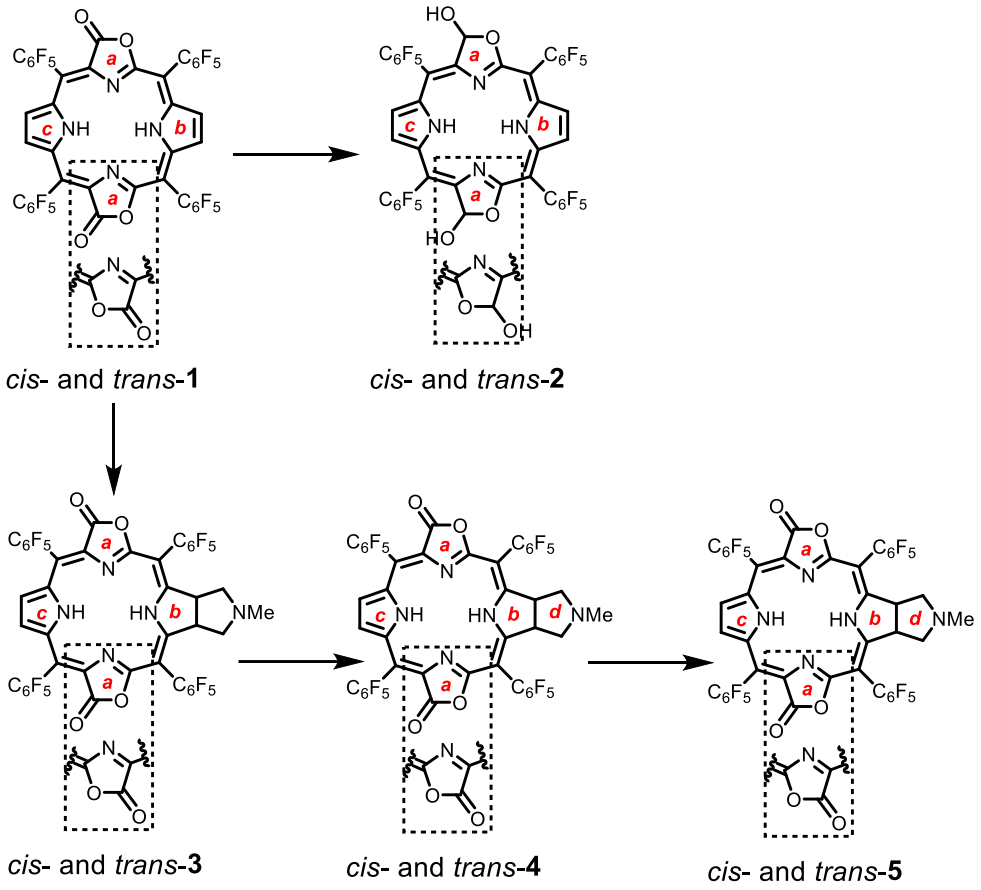

Table S10. Chemical shift values for the *β*-H signals seen in the ^{1}H NMR spectrum (recorded in $CDCl_3$) and ΔQ_L absorption values for compounds discussed in this paper.

		***β*-H NMR/ppm**	**Average /ppm**	**Q_L /nm**	**ΔQ_L /nm**
1	*cis*	8.70 8.52 8.53	8.73	657	19
	trans	8.85		676	
2	*cis*	8.18, 7.66, 7.43	8.12	723	28
	trans	8.35, 8.27, 7.78		751	
3	*cis*	7.23	7.40	549	71
	trans	7.55, 7.60		620	
4	*cis*	7.79	8.00	595	73
	trans	8.20, 8.23		668	
5	*cis*	8.76	8.75	659	20
	trans	8.74		640	

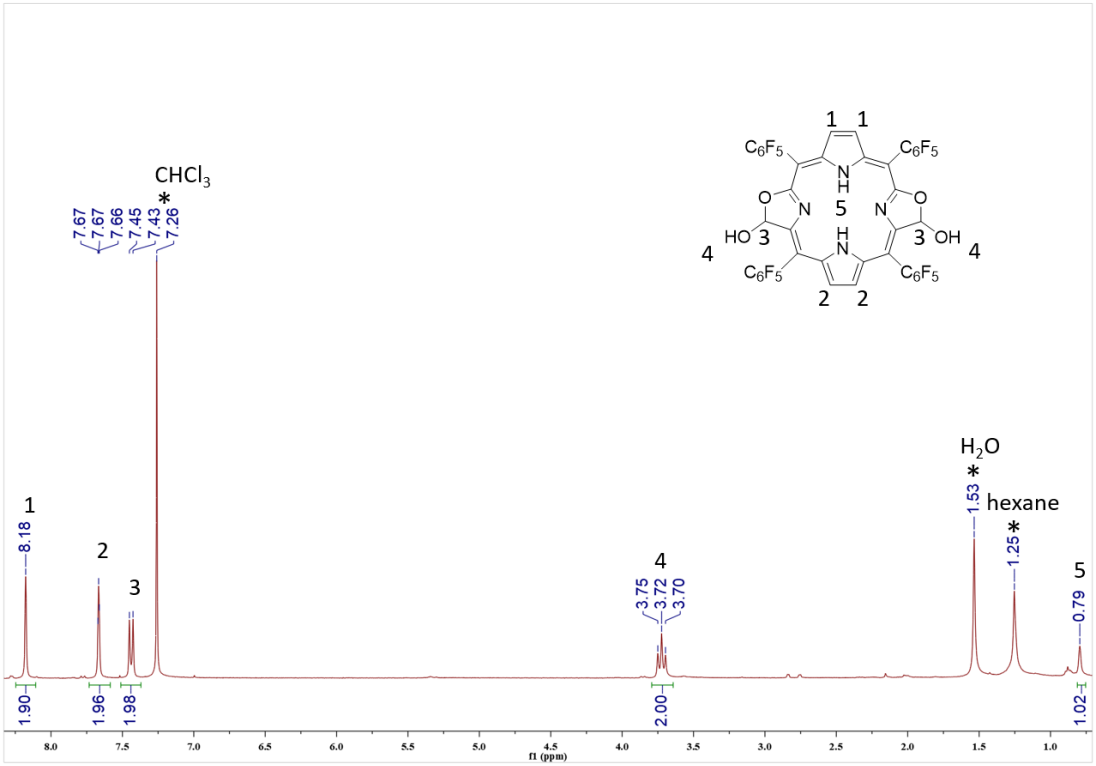

Figure S1. ^{1}H NMR spectrum of *cis*-**2** recorded at room temperature in $CDCl_3$ (* indicates a peak ascribed to residual solvents and impurities).

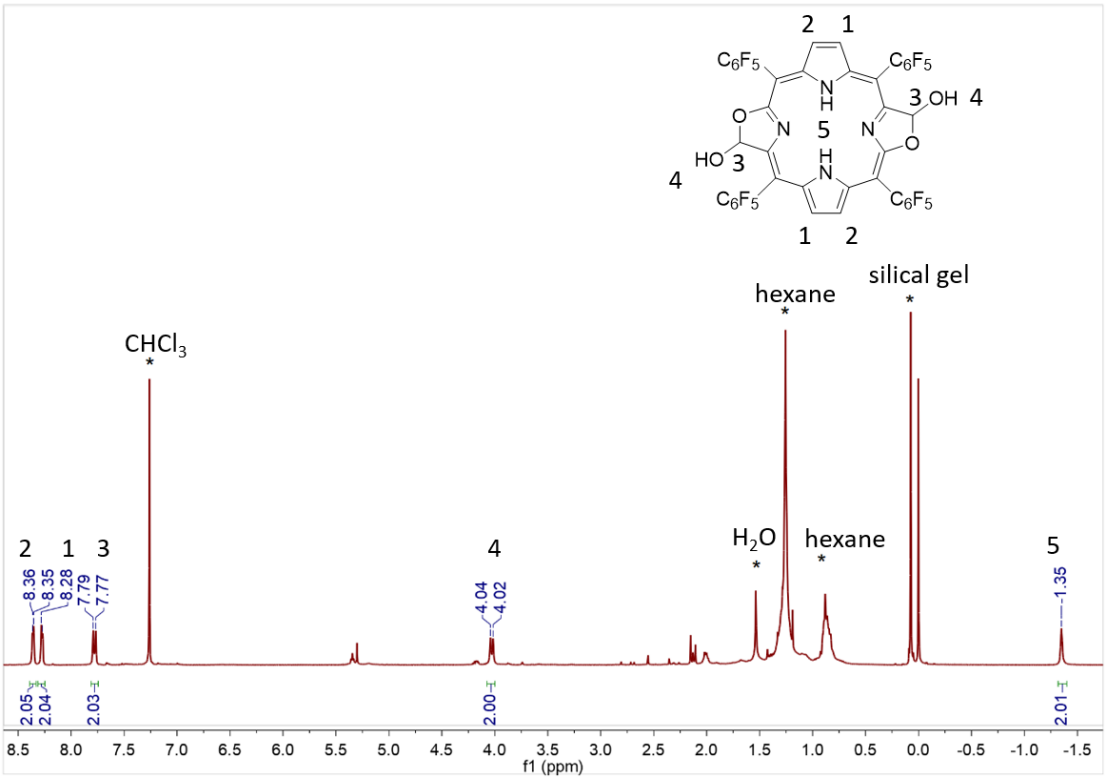

Figure S2. ^{1}H NMR spectrum of *trans*-**2** recorded at room temperature in $CDCl_3$ (* indicates a peak ascribed to residual solvents and impurities).

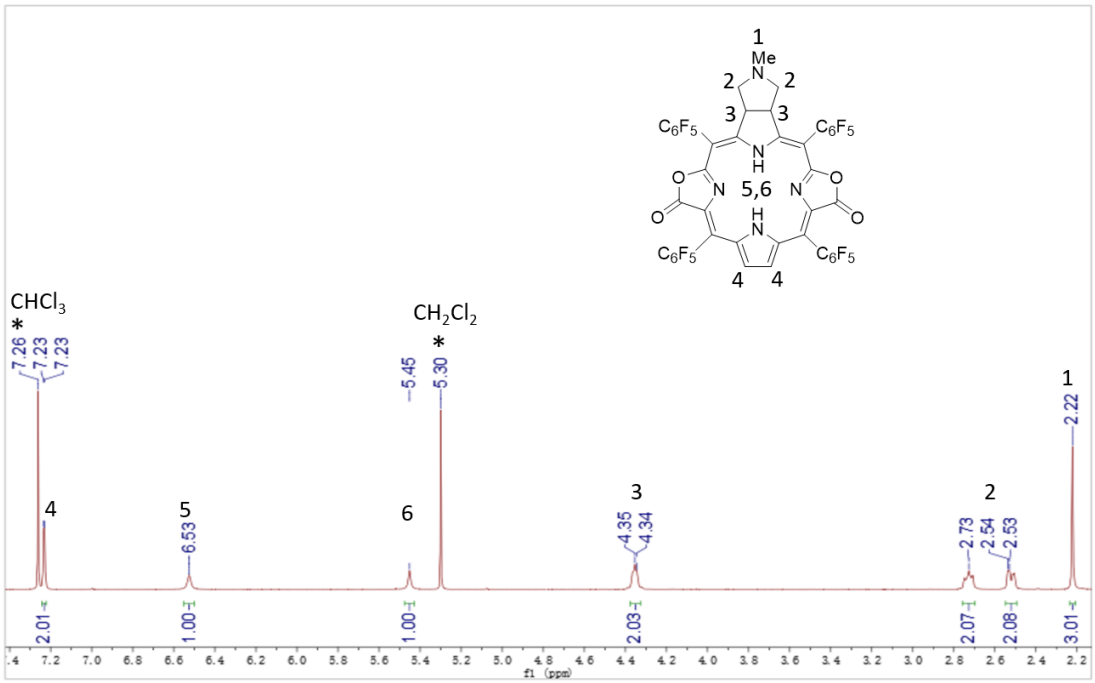

Figure S3. ^{1}H NMR spectrum of *cis*-**3** recorded at room temperature in CD_2Cl_2.

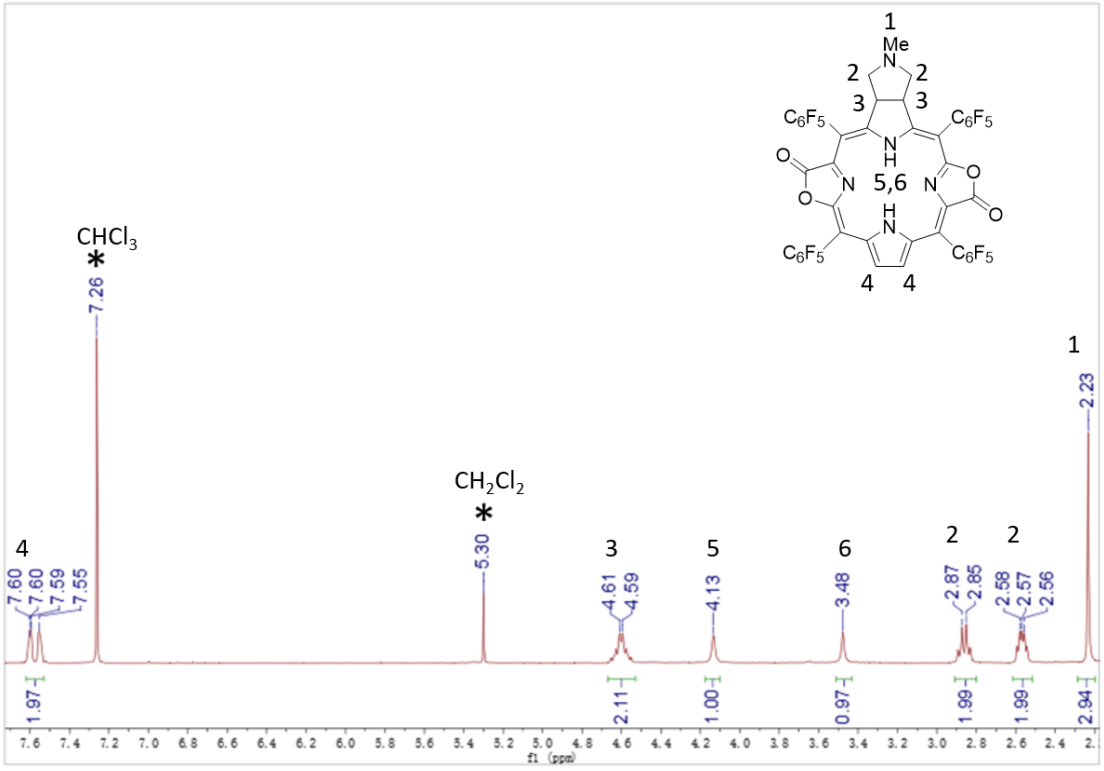

Figure S4. ^{1}H NMR spectrum of *trans*-**3** recorded at room temperature in $CDCl_3$ (* indicates a peak ascribed to residual solvents and impurities).

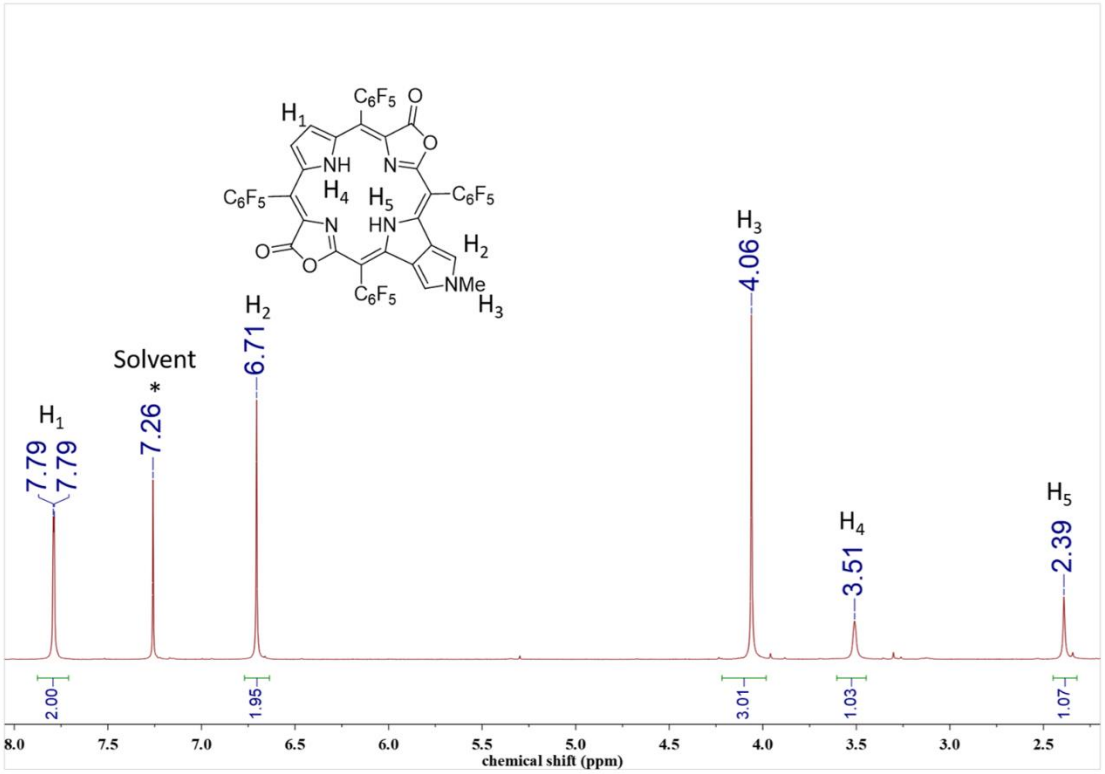

Figure S5. ^{1}H NMR spectrum of *cis*-**4** recorded at room temperature in $CDCl_3$.

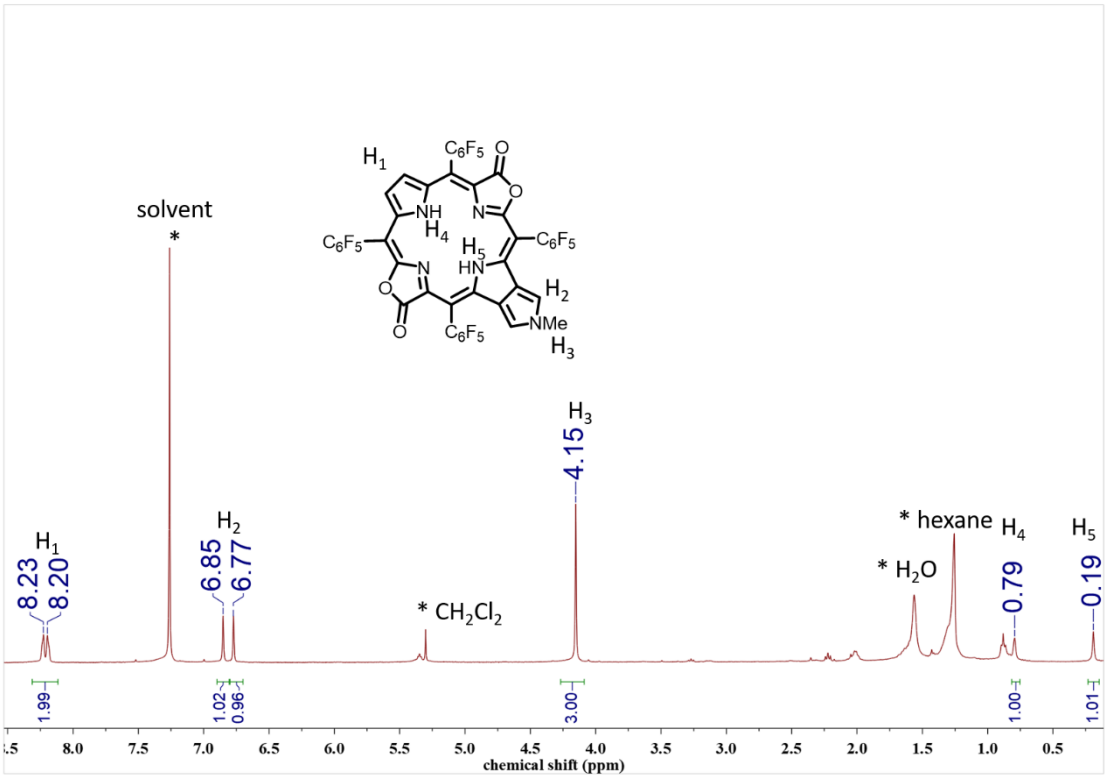

Figure S6. ^{1}H NMR spectrum of *trans*-**4** recorded at room temperature in $CDCl_3$ (* indicates a peak ascribed to residual solvents and impurities).

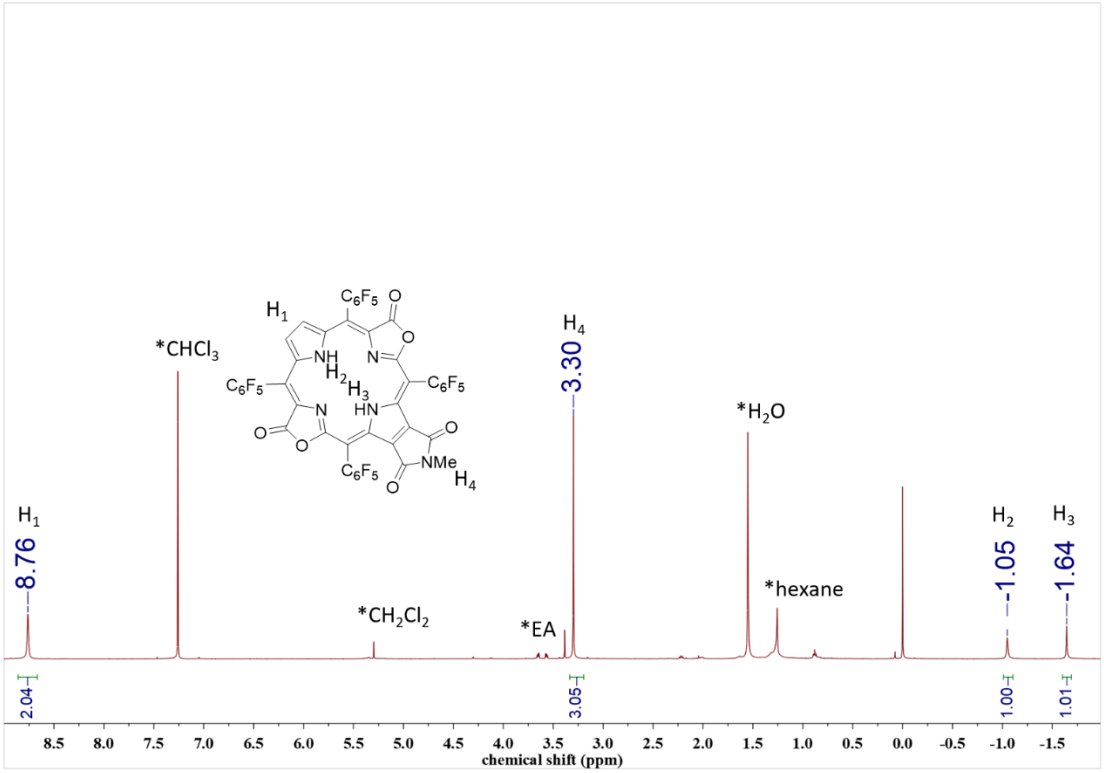

Figure S7. ^{1}H NMR spectrum of *cis*-**5** recorded at room temperature in $CDCl_3$.

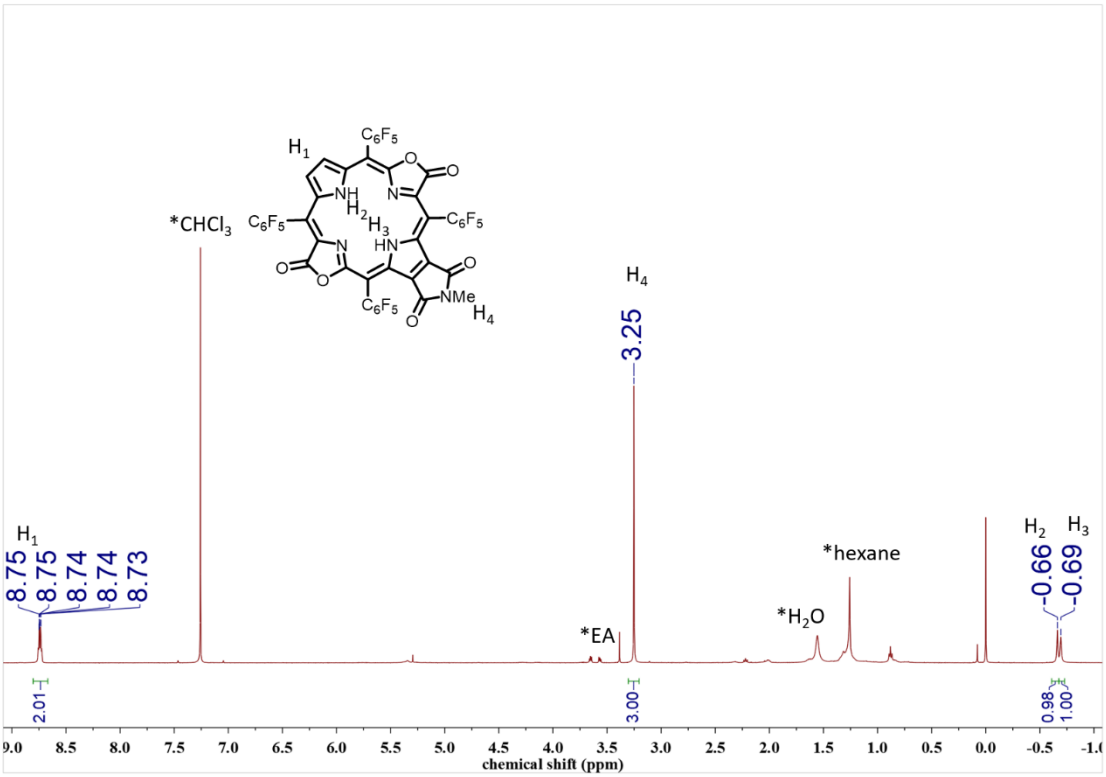

Figure S8. ^{1}H NMR spectrum of *trans*-**5** recorded at room temperature in $CDCl_3$ (* indicates a peak ascribed to residual solvents and impurities).

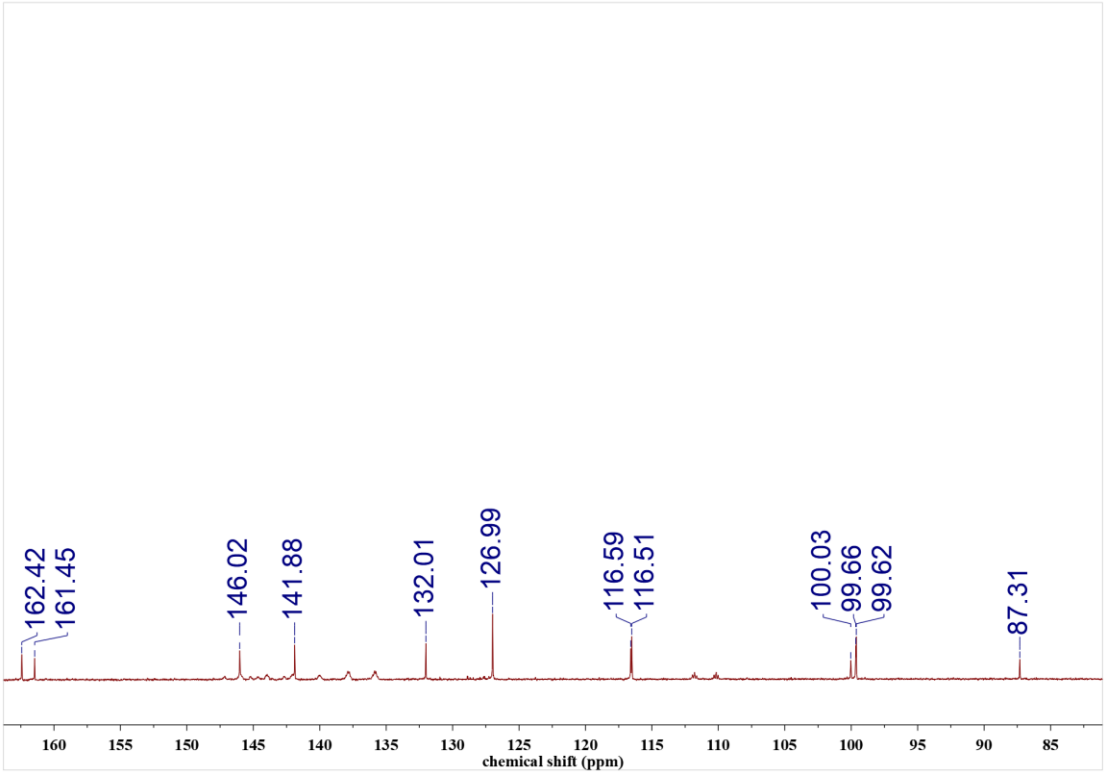

Figure S9. ^{13}C NMR spectrum of *cis*-**2** recorded at room temperature in $CDCl_3$ (* indicates a peak ascribed to residual solvents and impurities).

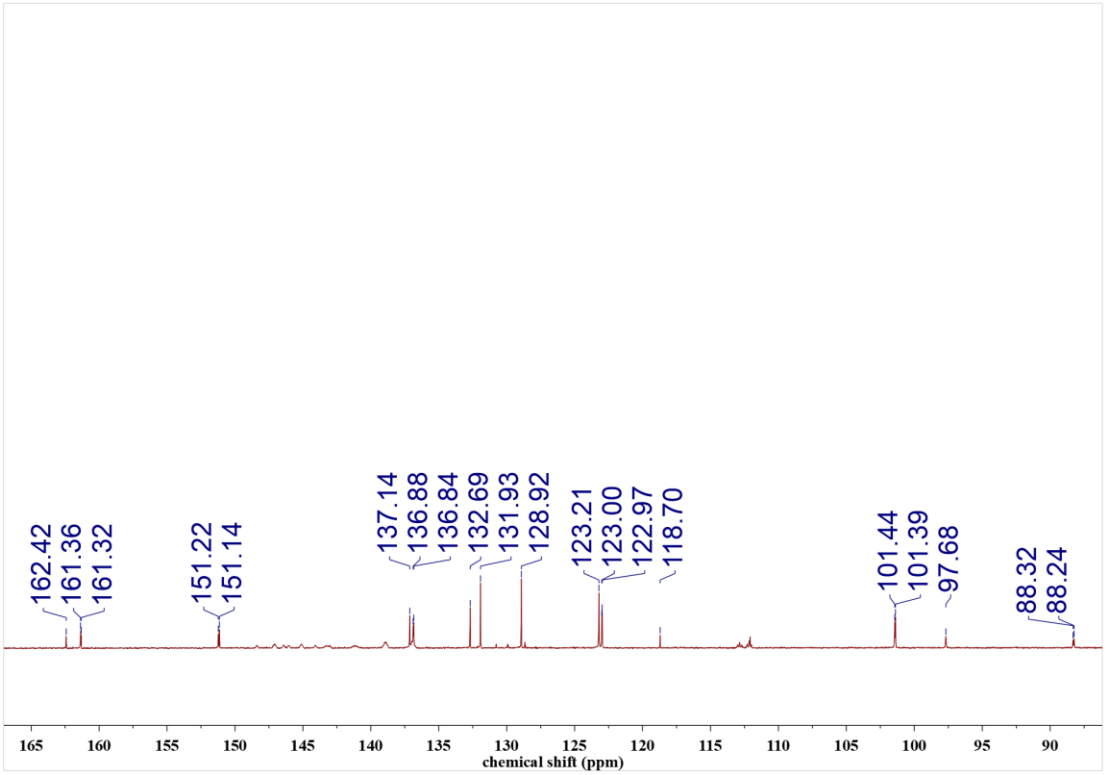

Figure S10. ^{13}C NMR spectrum of *trans*-**2** recorded at room temperature in acetone-d_6 (* indicates peaks ascribed to residual solvents and impurities).

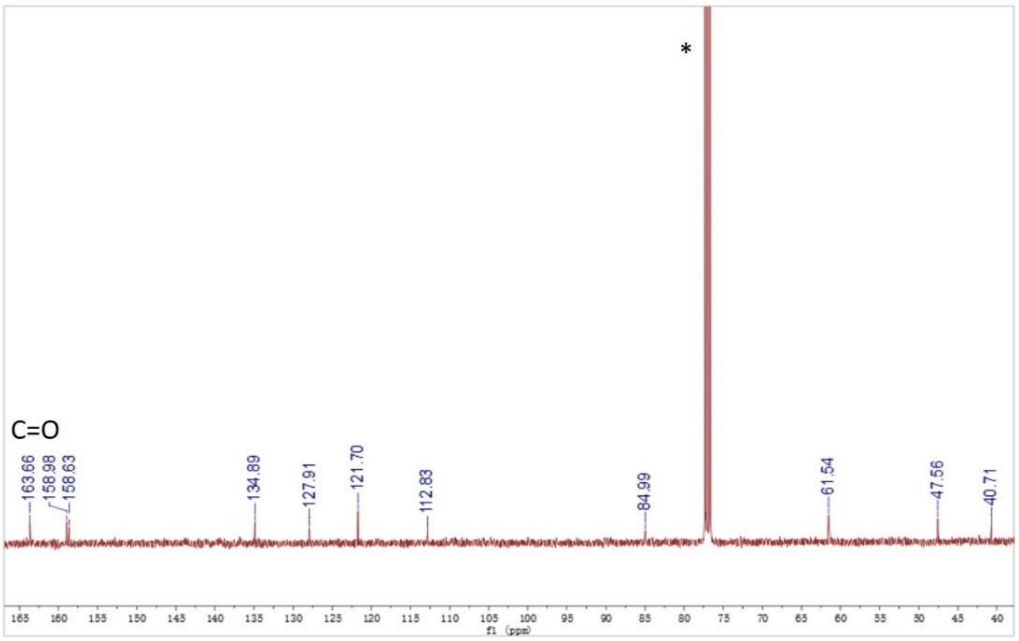

Figure S11. ^{13}C NMR spectrum of *cis*-**3** recorded at room temperature in $CDCl_3$ (* indicates a peak ascribed to residual solvents and impurities).

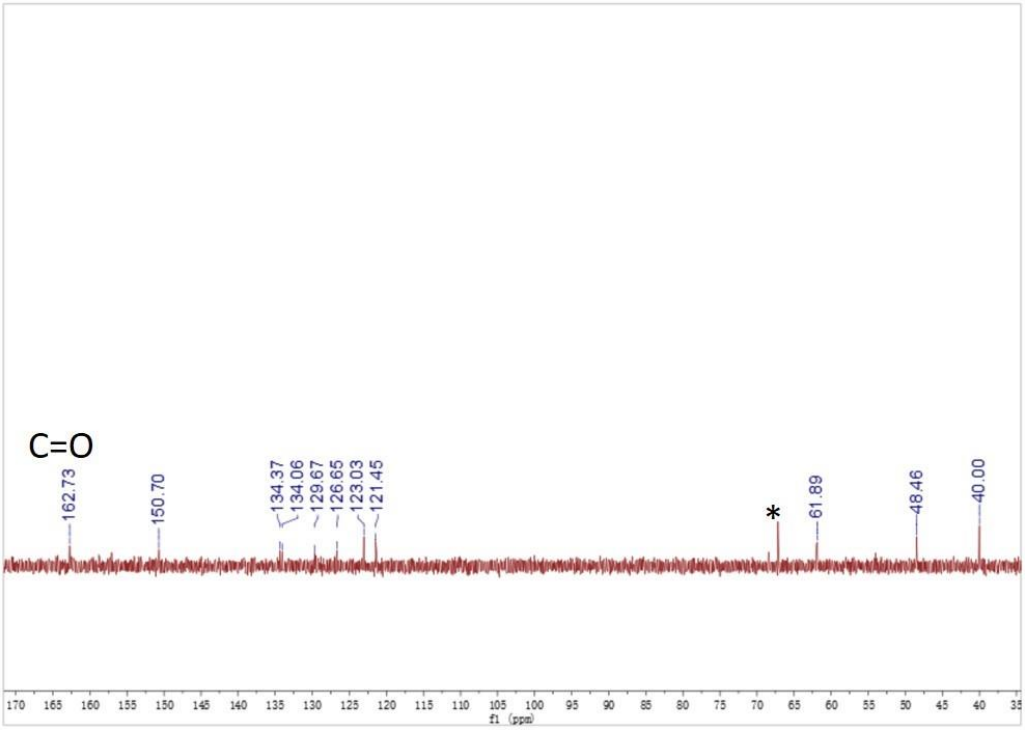

Figure S12. ^{13}C NMR spectrum of *trans*-**3** recorded at room temperature in acetone-d_6 (* indicates peaks ascribed to residual solvents and impurities).

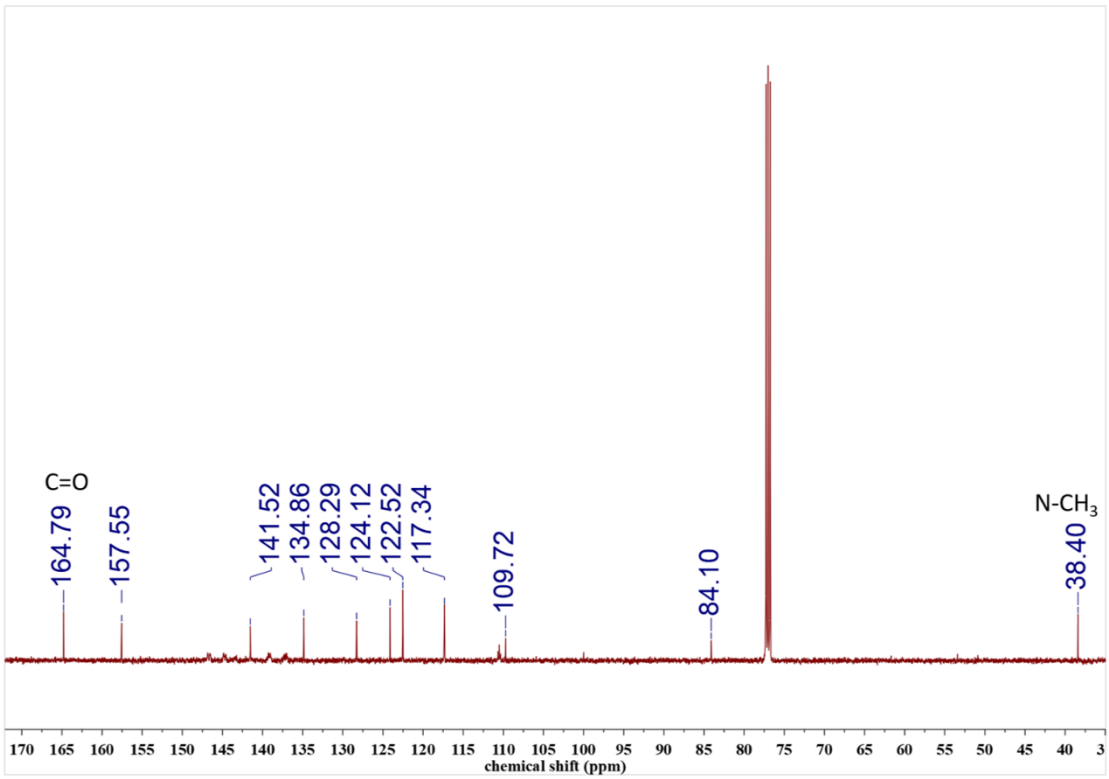

Figure S13. ^{13}C NMR spectrum of *cis*-**4** recorded at room temperature in $CDCl_3$ (* indicates a peak ascribed to residual solvents and impurities).

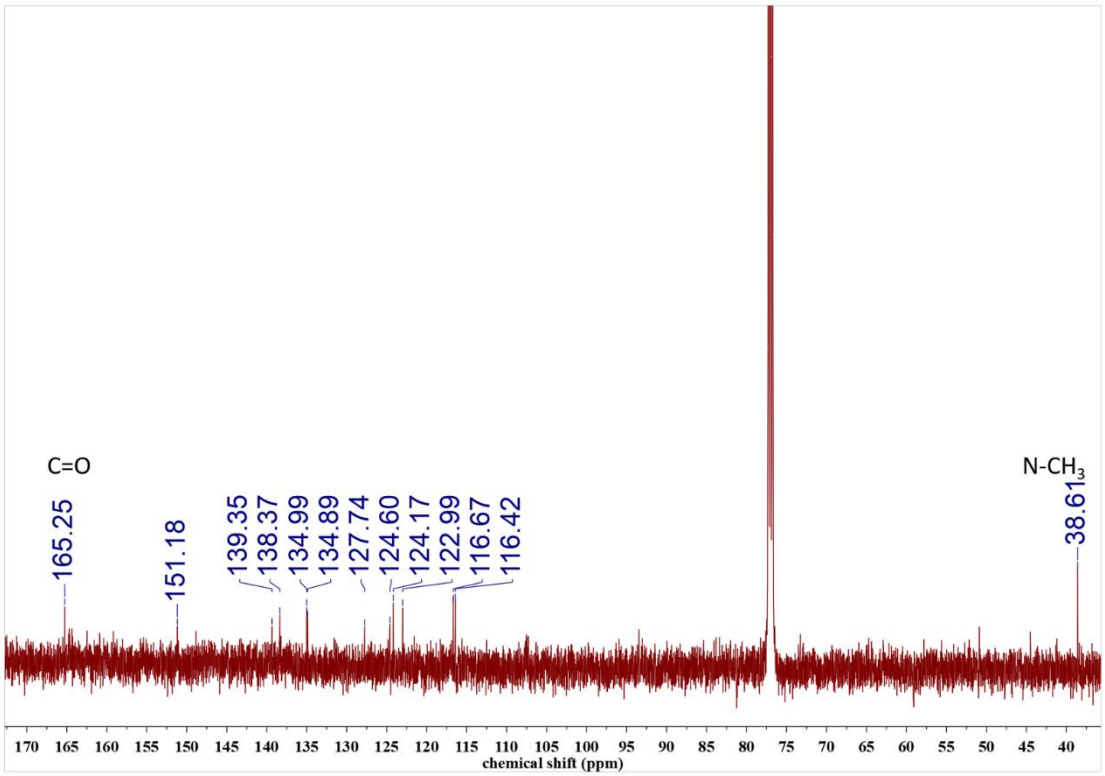

Figure S14. ^{13}C NMR spectrum of *trans*-**4** recorded at room temperature in acetone-d_6 (* indicates peaks ascribed to residual solvents and impurities).

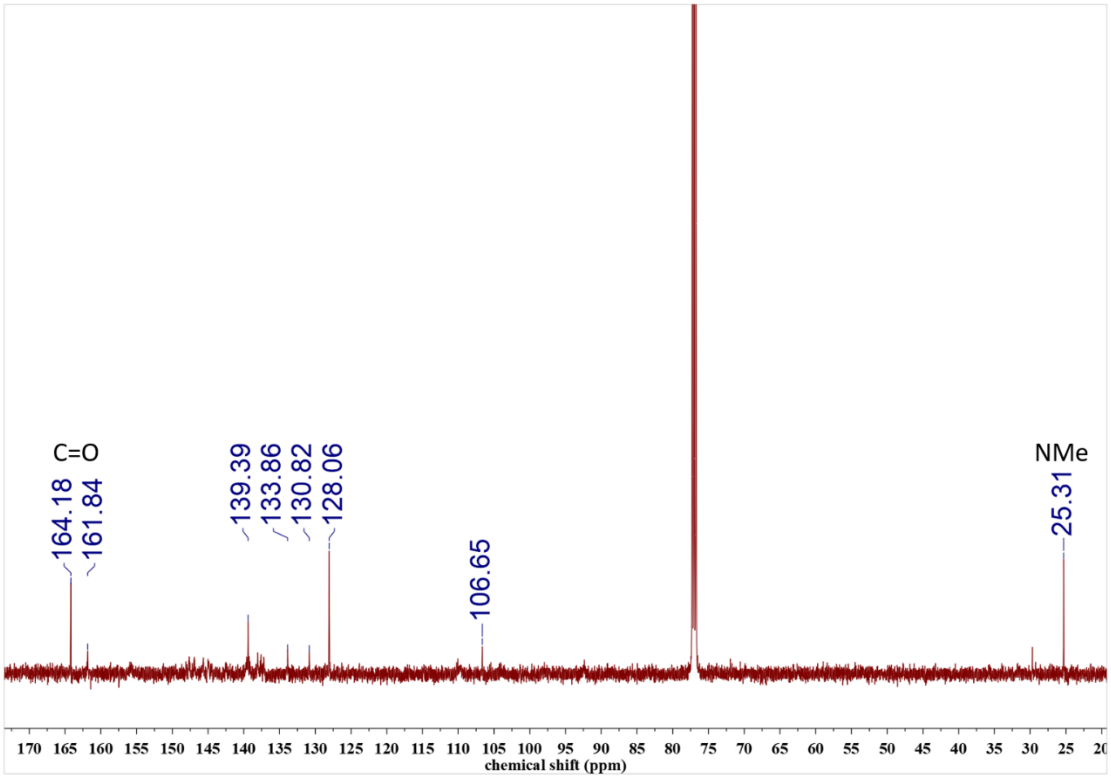

Figure S15. ^{13}C NMR spectrum of *cis*-**5** recorded at room temperature in $CDCl_3$ (* indicates a peak ascribed to residual solvents and impurities).

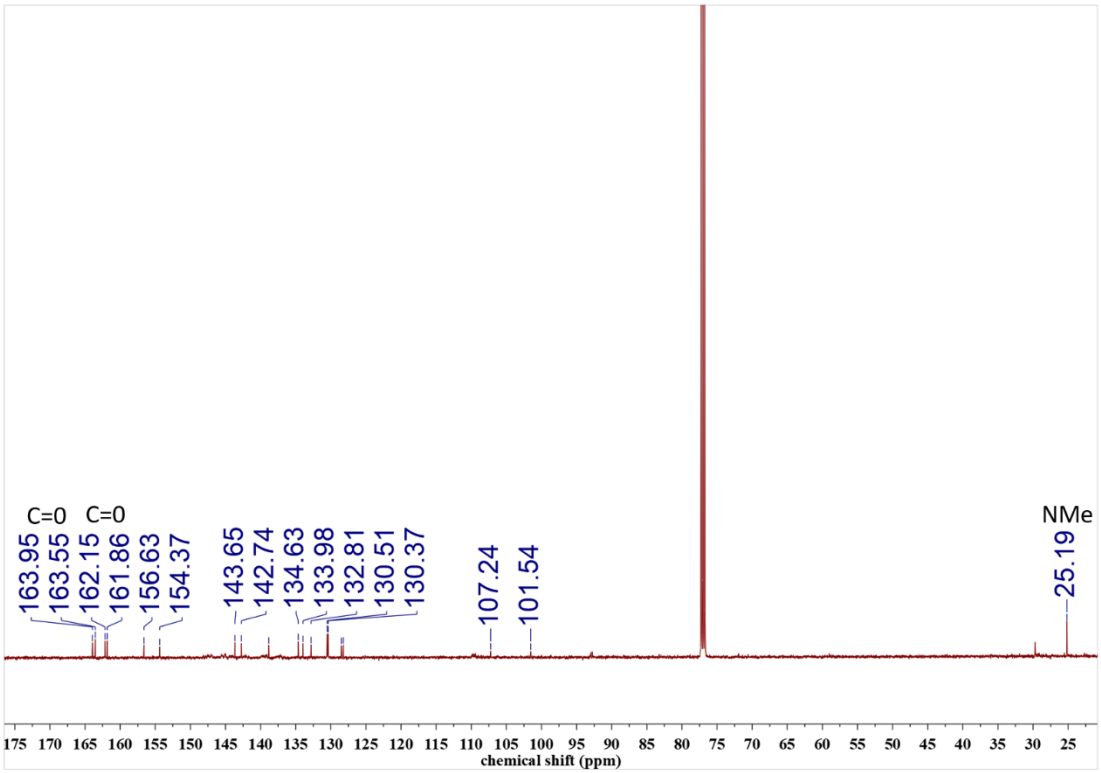

Figure S16. ^{13}C NMR spectrum of *trans*-**5** recorded at room temperature in acetone-d_6 (* indicates peaks ascribed to residual solvents and impurities).

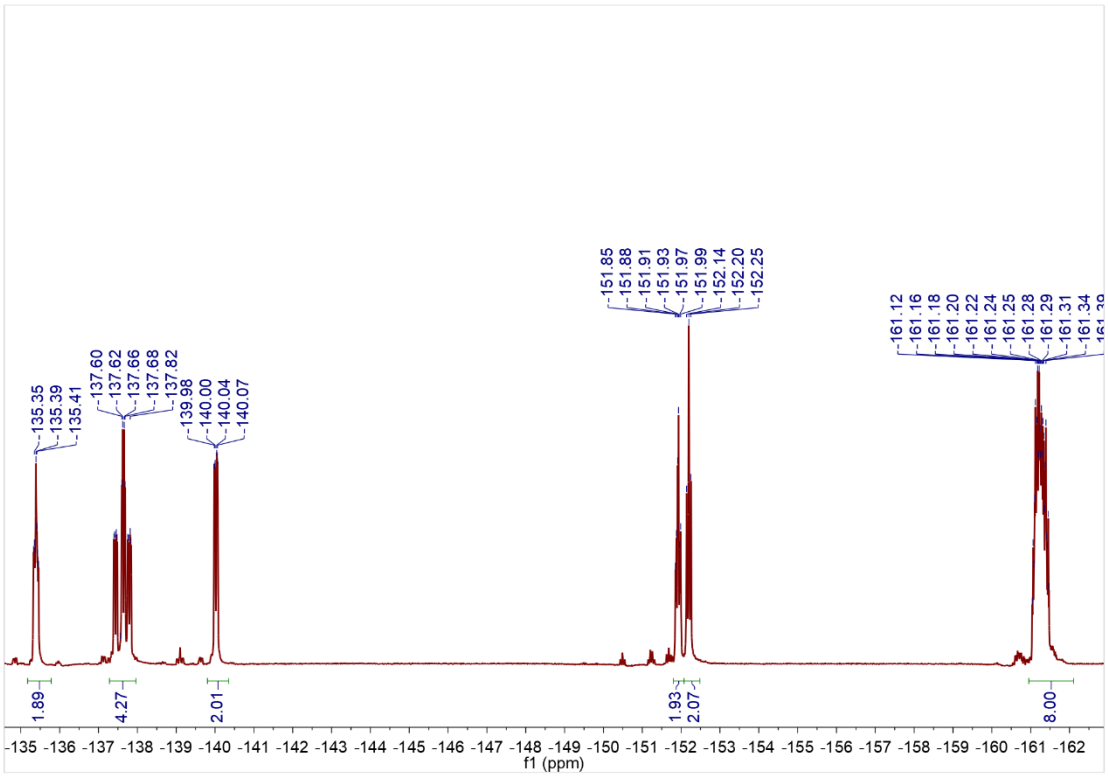

Figure S17. ^{19}F NMR spectrum of *cis*-**2** recorded at room temperature in $CDCl_3$.

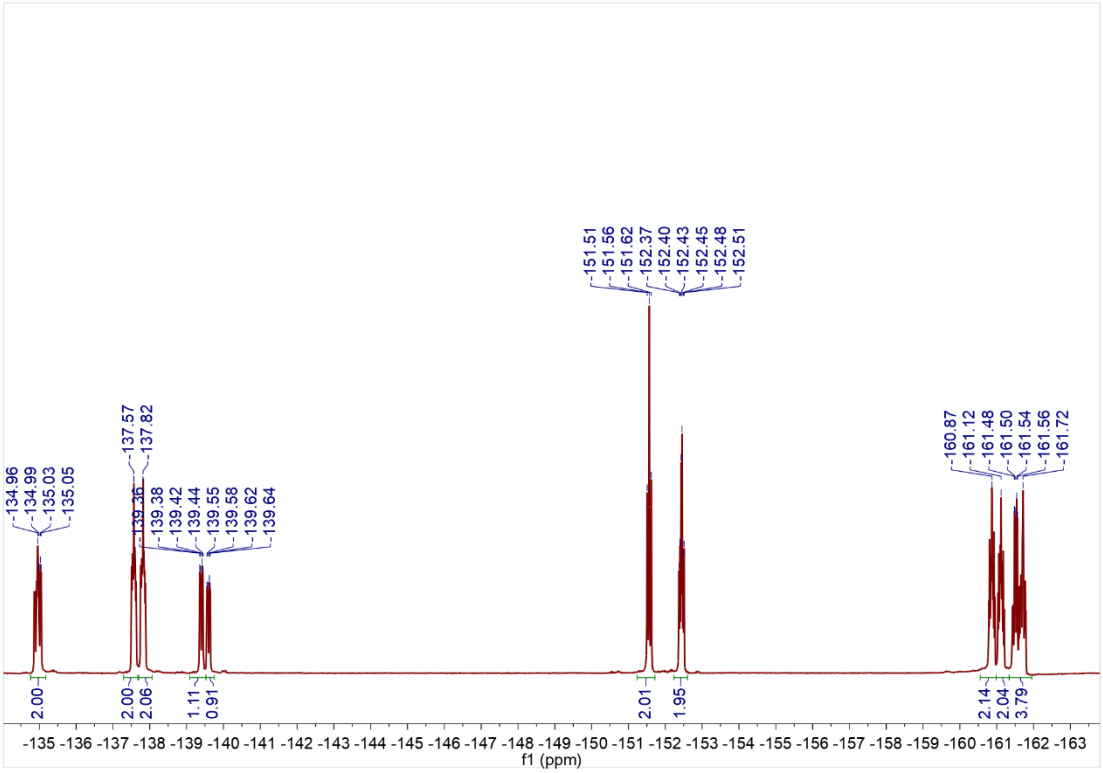

Figure S18. ^{19}F NMR spectrum of *trans*-**2** recorded at room temperature in $CDCl_3$.

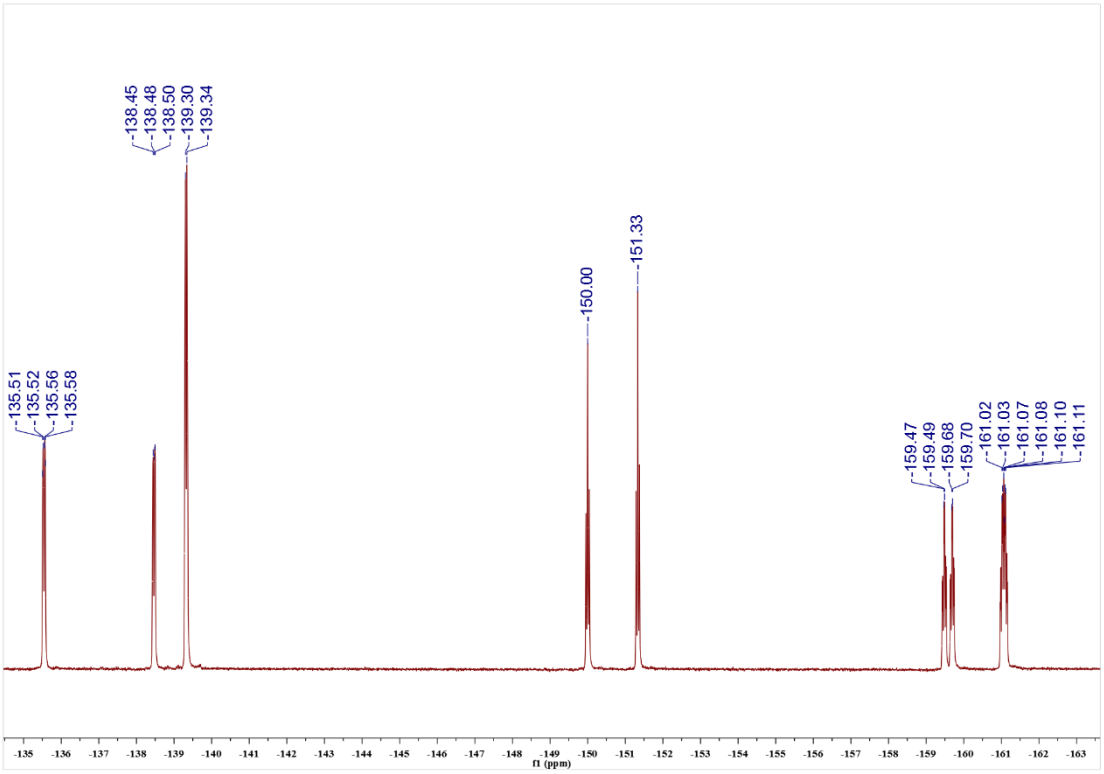

Figure S19. ^{19}F NMR spectrum of *cis*-**3** recorded at room temperature in $CDCl_3$.

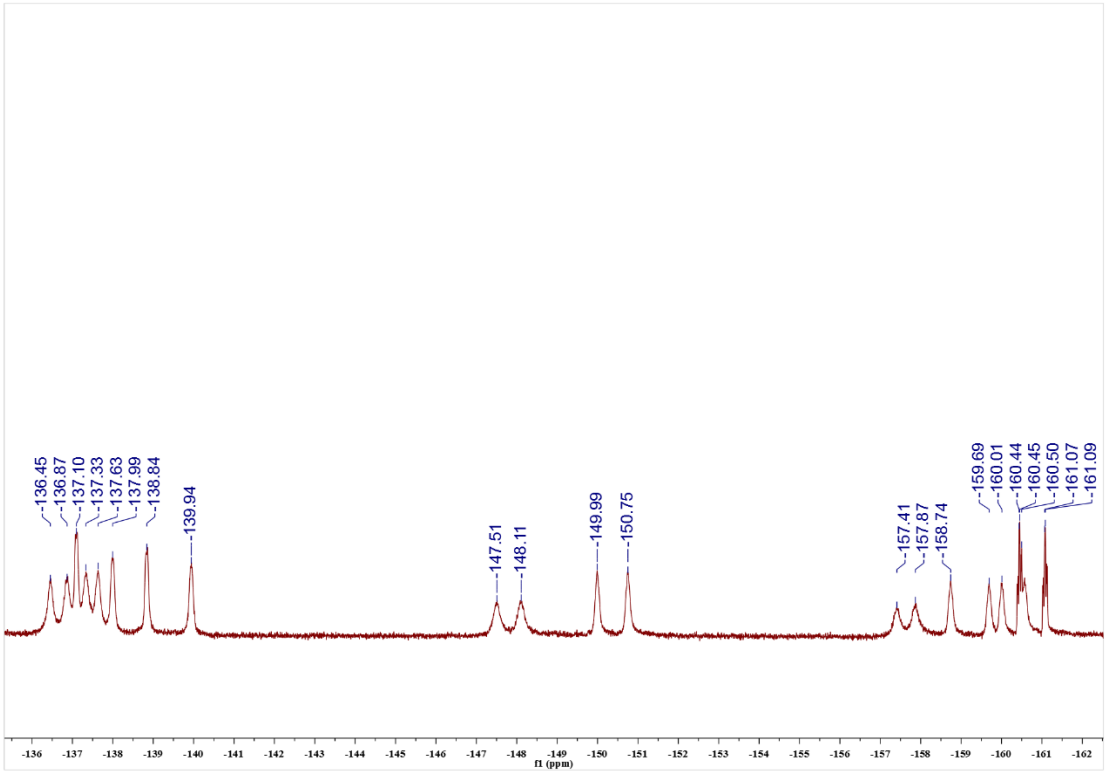

Figure S20. ^{19}F NMR spectrum of *trans*-**3** recorded at room temperature in $CDCl_3$.

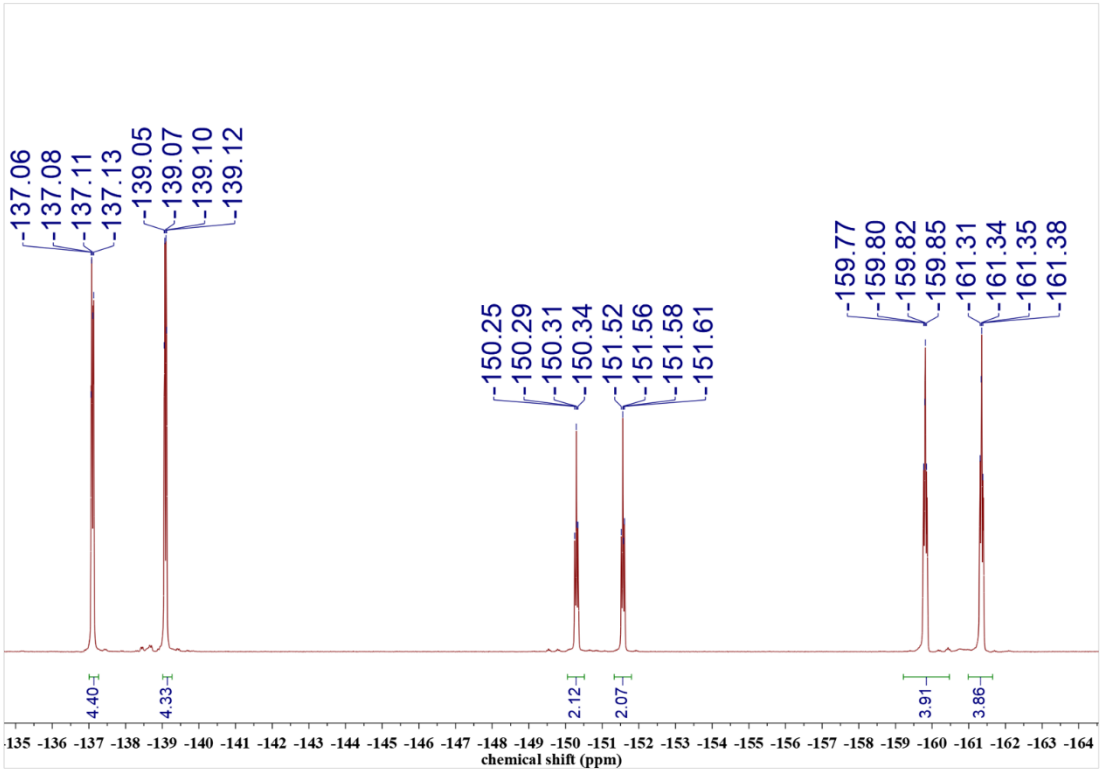

Figure S21. ^{19}F NMR spectrum of *cis*-**4** recorded at room temperature in $CDCl_3$.

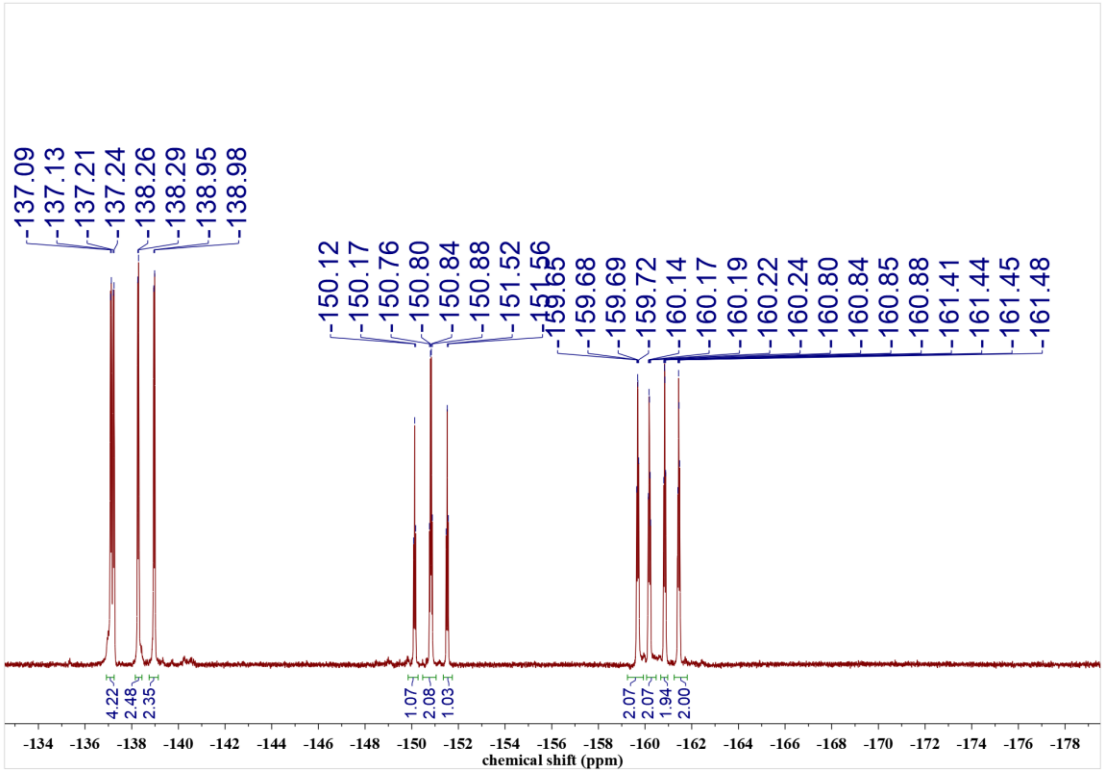

Figure S22. ^{19}F NMR spectrum of *trans*-**4** recorded at room temperature in $CDCl_3$.

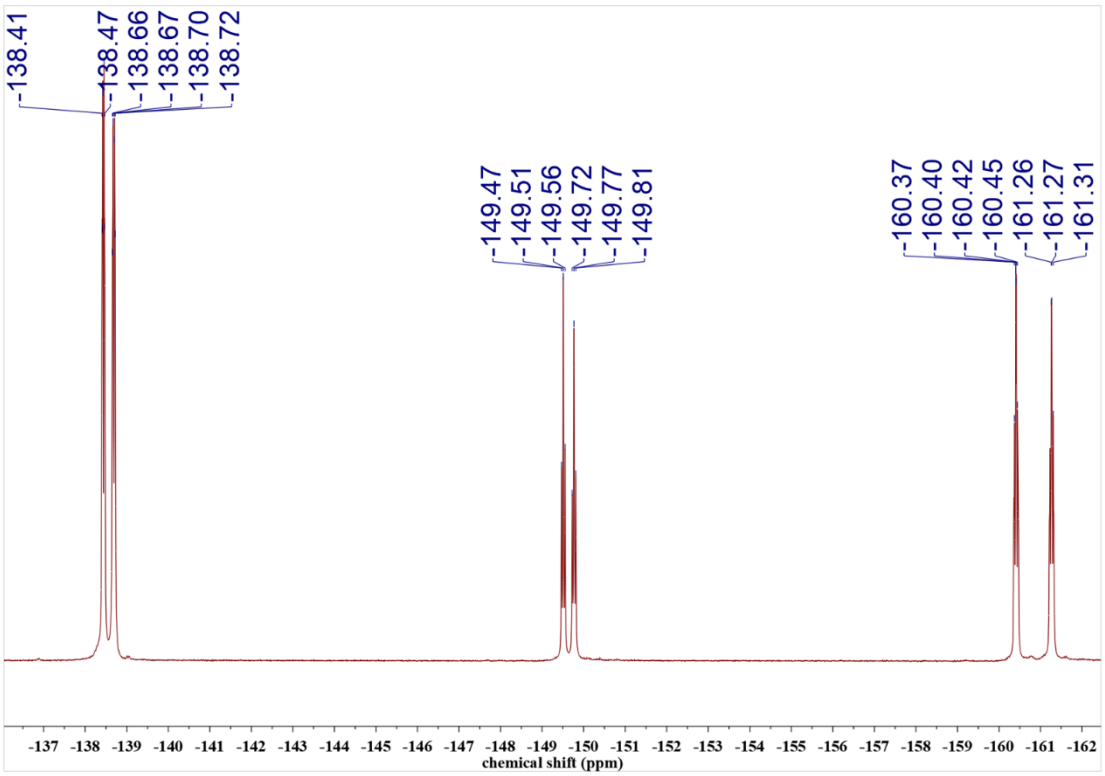

Figure S23. ^{19}F NMR spectrum of *cis*-**5** recorded at room temperature in $CDCl_3$.

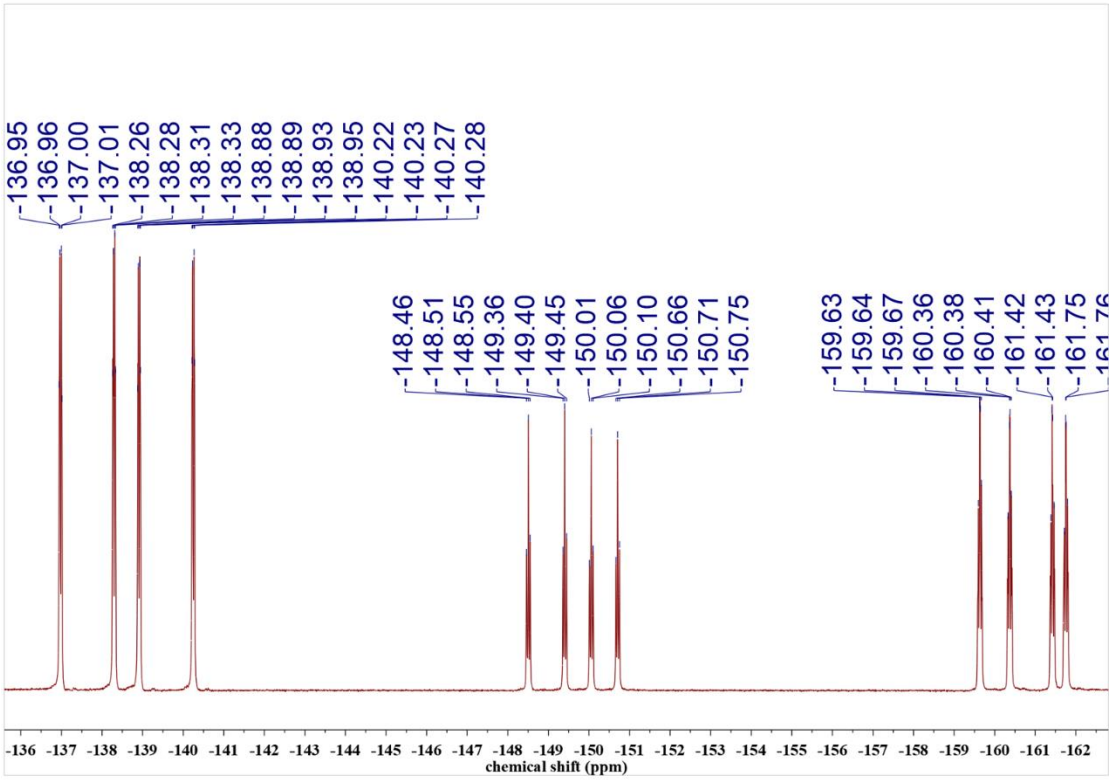

Figure S24. ^{19}F NMR spectrum of *trans*-**5** recorded at room temperature in $CDCl_3$.

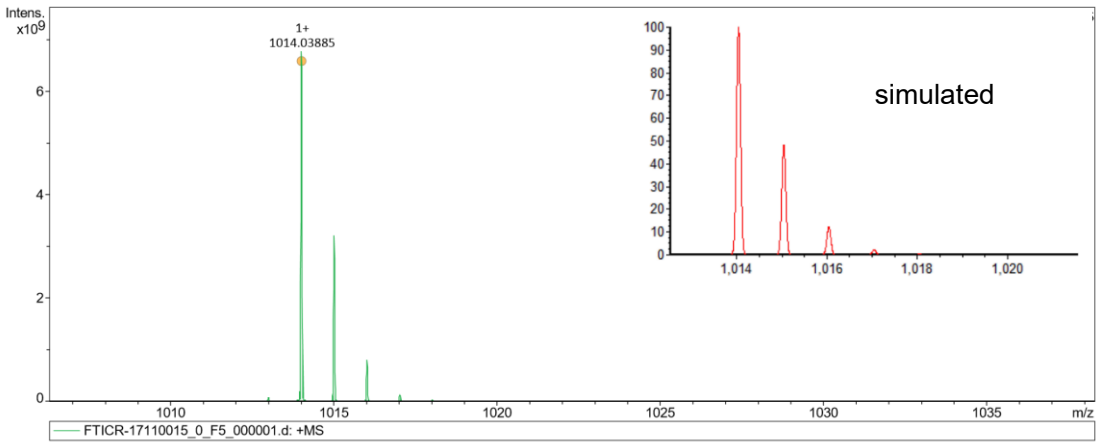

Meas. m/z	#	Ion Formula	Score	m/z	err [ppm]	Mean err [ppm]	mSigma	rdb	e⁻ Conf	N-Rule
1014.038852	1	C42H10F20N4O4	100.00	1014.037721	-1.1	-0.5	n.a.	30.5	odd	ok

Figure S25. HR-MS(ESI) (top) and simulation (bottom) of *cis*-**2**

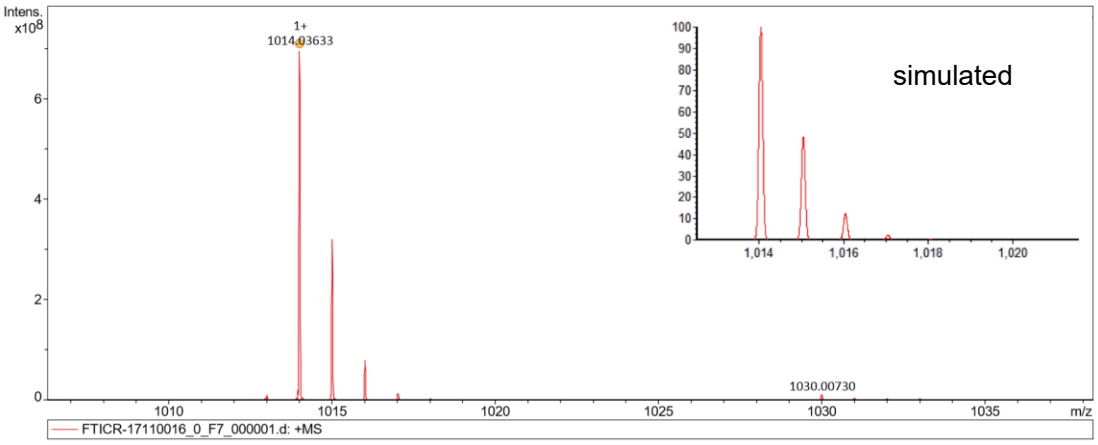

Meas. m/z	#	Ion Formula	Score	m/z	err [ppm]	Mean err [ppm]	mSigma	rdb	e⁻ Conf	N-Rule
1014.036329	1	C42H10F20N4O4	100.00	1014.037721	1.4	1.1	5.6	30.5	odd	ok

Figure S26. HR-MS(ESI) (top) and simulation (bottom) of *trans*-**2**

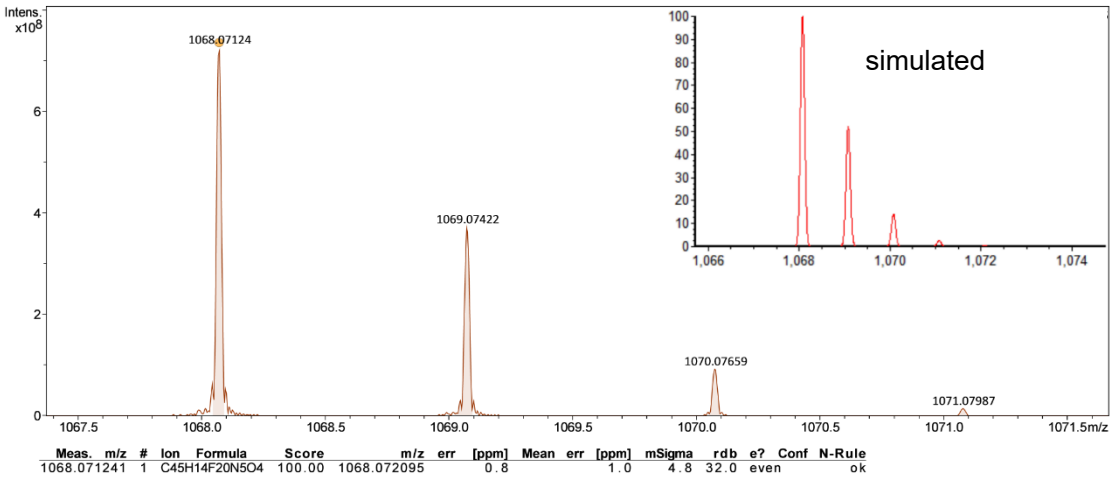

Figure S27. MALDI-TOF-MS (top) and simulation (bottom) of *cis*-**3**

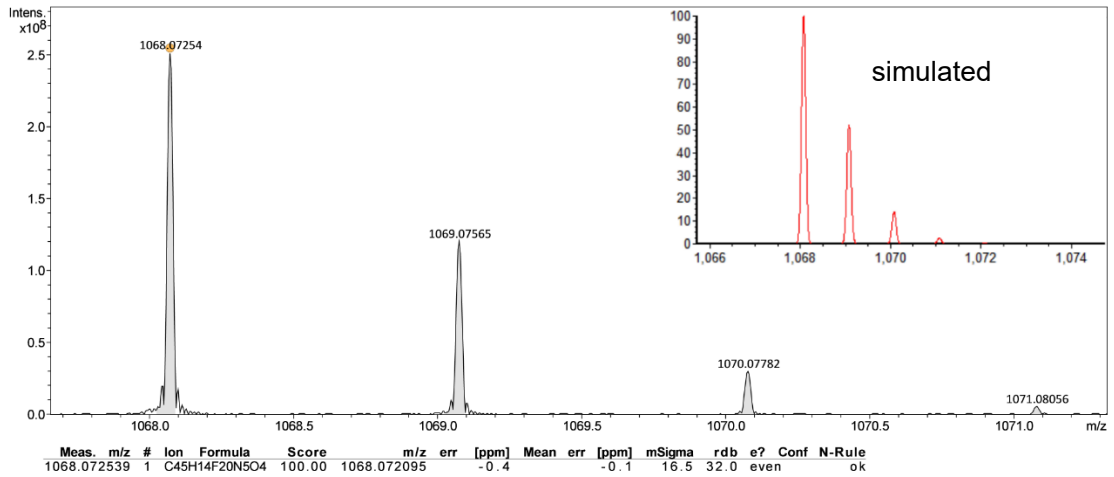

Figure S28. MALDI-TOF-MS (top) and simulation (bottom) of *trans*-**3**

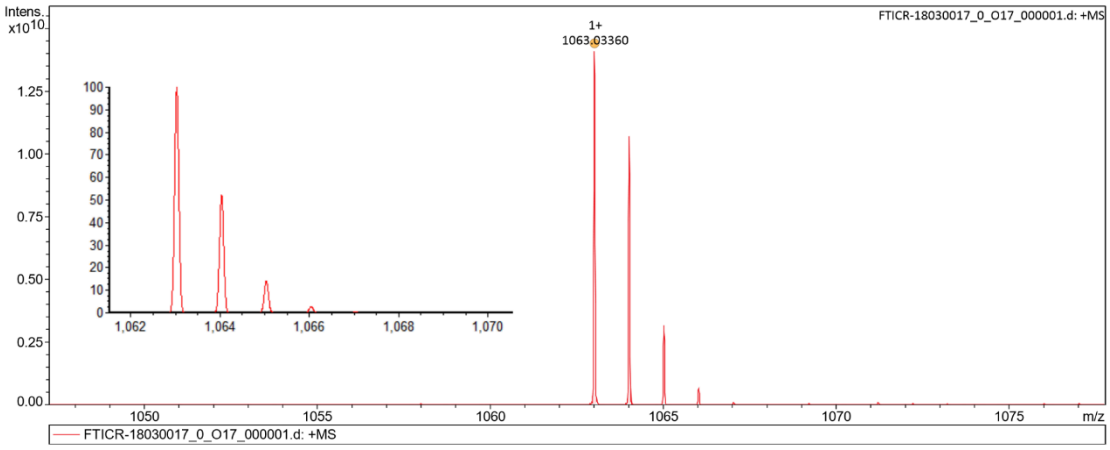

Meas. m/z	#	Ion Formula	Score	m/z	err [ppm]	Mean err [ppm]	mSigma	rdb	e⁻ Conf	N-Rule
1063.033600	1	C45H9F20N5O4	100.00	1063.032970	-0.6	-1.1	131.4	34.5	odd	ok

Figure S29. MALDI-TOF-MS (top) and simulation (bottom) of *cis*-**4**

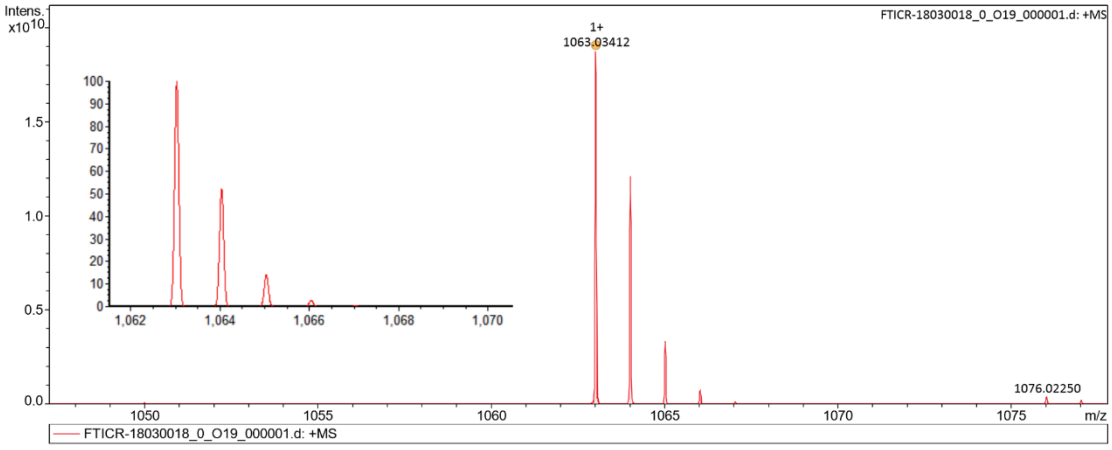

Meas. m/z	#	Ion Formula	Score	m/z	err [ppm]	Mean err [ppm]	mSigma	rdb	e⁻ Conf	N-Rule
1063.034118	1	C45H9F20N5O4	100.00	1063.032970	-1.1	-0.1	73.4	34.5	odd	ok

Figure S30. MALDI-TOF-MS (top) and simulation (bottom) of *trans*-**4**

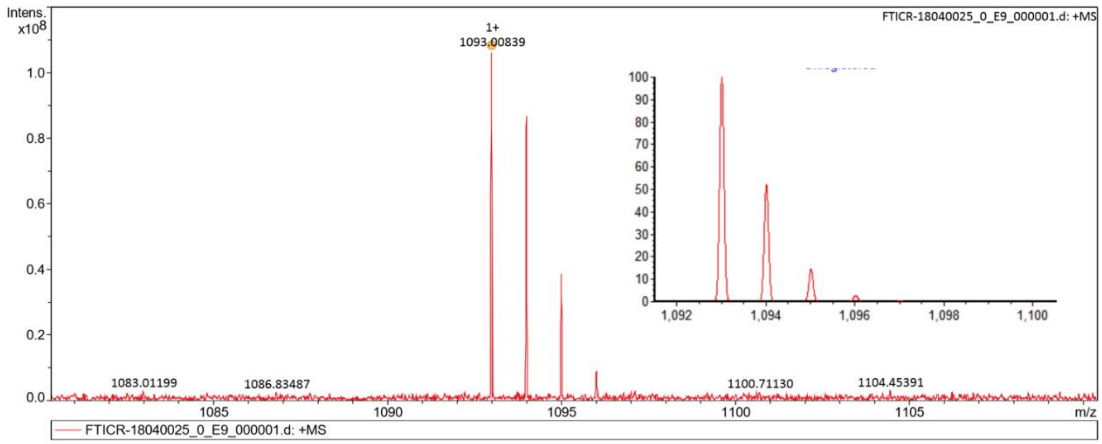

Meas. m/z	#	Ion Formula	Score	m/z	err [ppm]	Mean err [ppm]	mSigma	rdb	e⁻ Conf	N-Rule
1093.008387	1	C45H7F20N5O6	100.00	1093.007149	-1.1	-3.1	191.2	35.5	odd	ok

Figure S31. MALDI-TOF-MS (top) and simulation (bottom) of *cis*-**5**

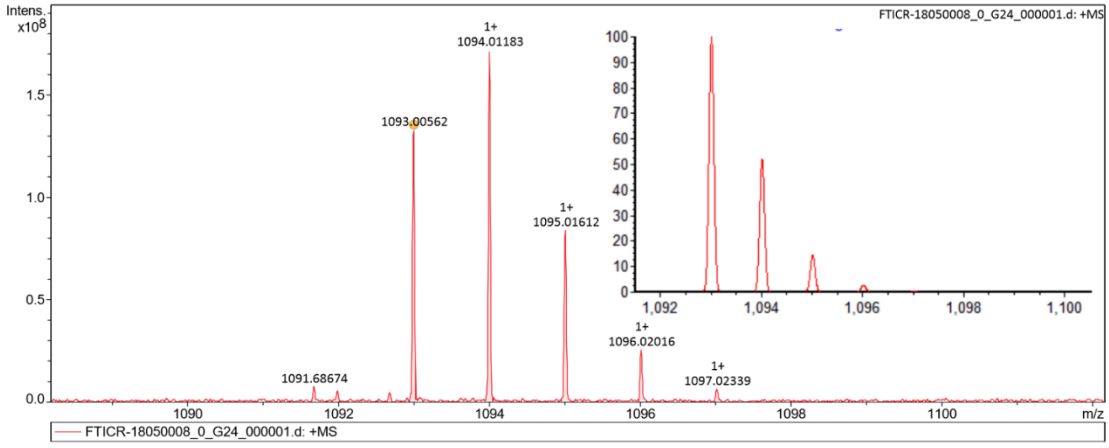

Meas. m/z	#	Ion Formula	Score	m/z	err [ppm]	Mean err [ppm]	mSigma	rdb	e⁻ Conf	N-Rule
1093.005622	1	C45H7F20N5O6	100.00	1093.007149	1.4	-0.8	328.1	35.5	odd	ok

Figure S32. MALDI-TOF-MS (top) and simulation (bottom) of *trans*-**5**

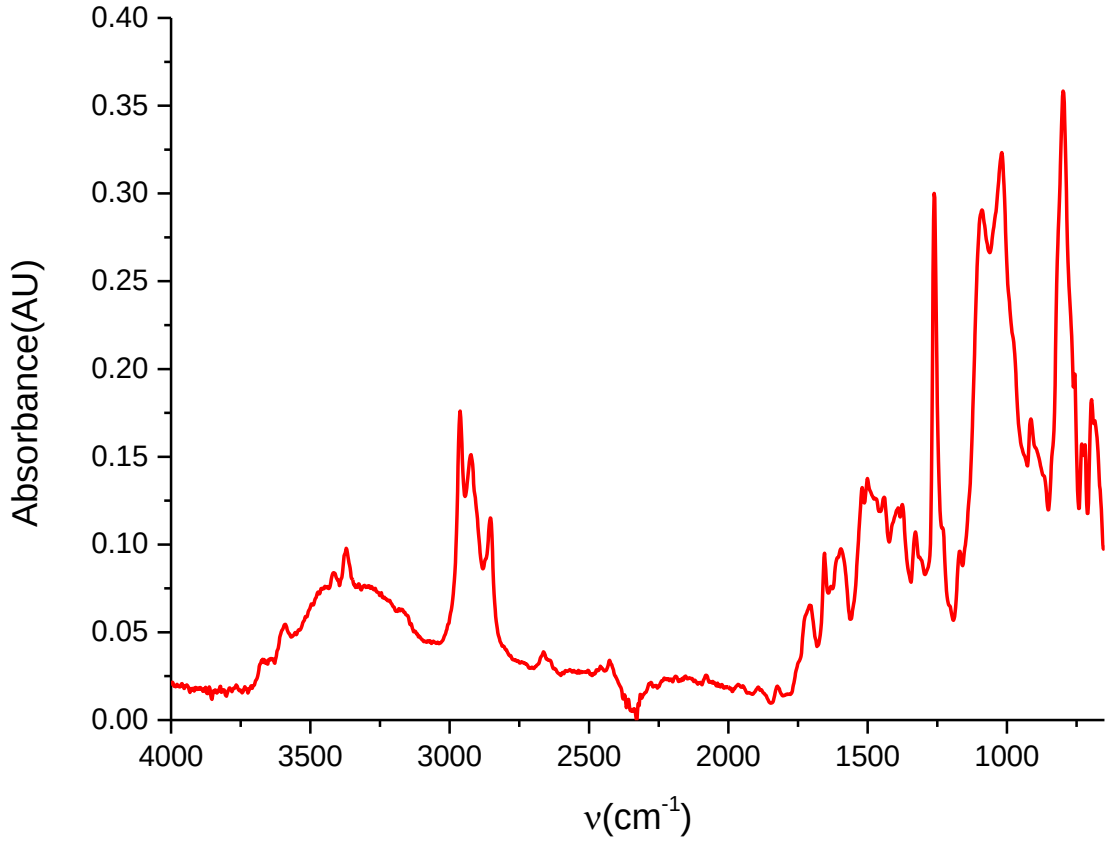

Figure S33. FT-IR spectrum of *cis*-**2.**

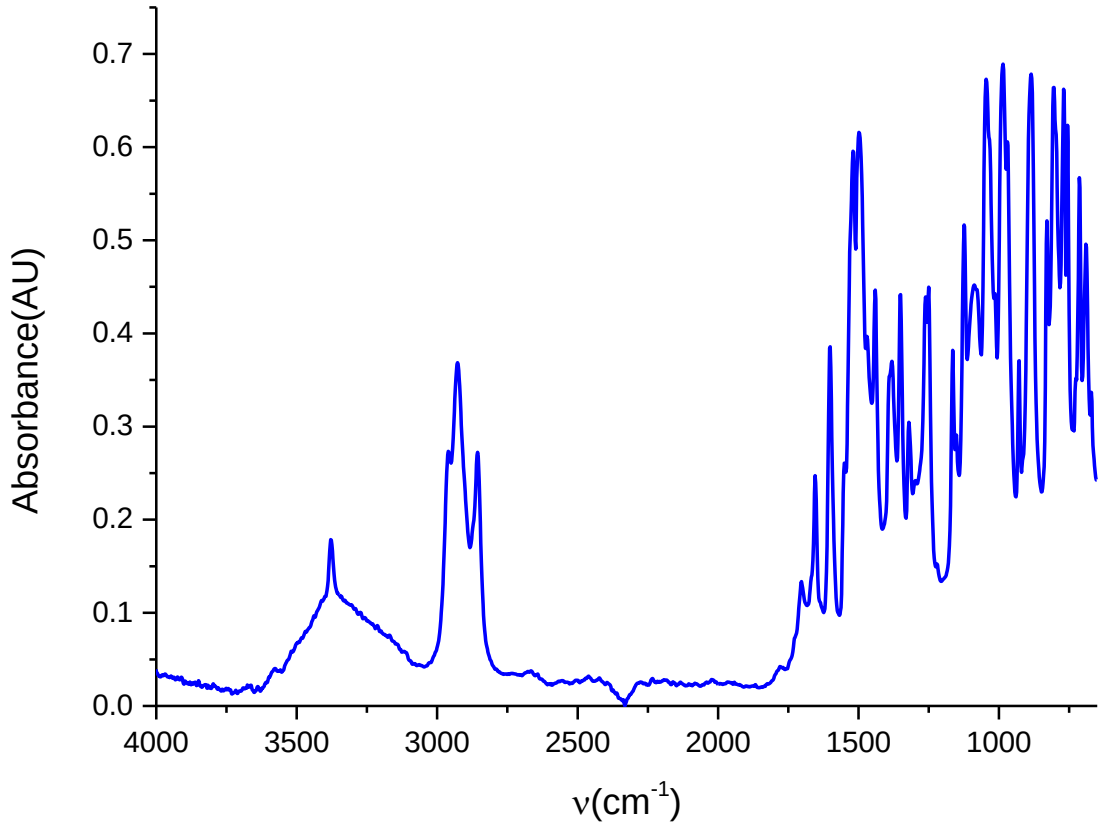

Figure S34. FT-IR spectrum of *trans*-**2**.

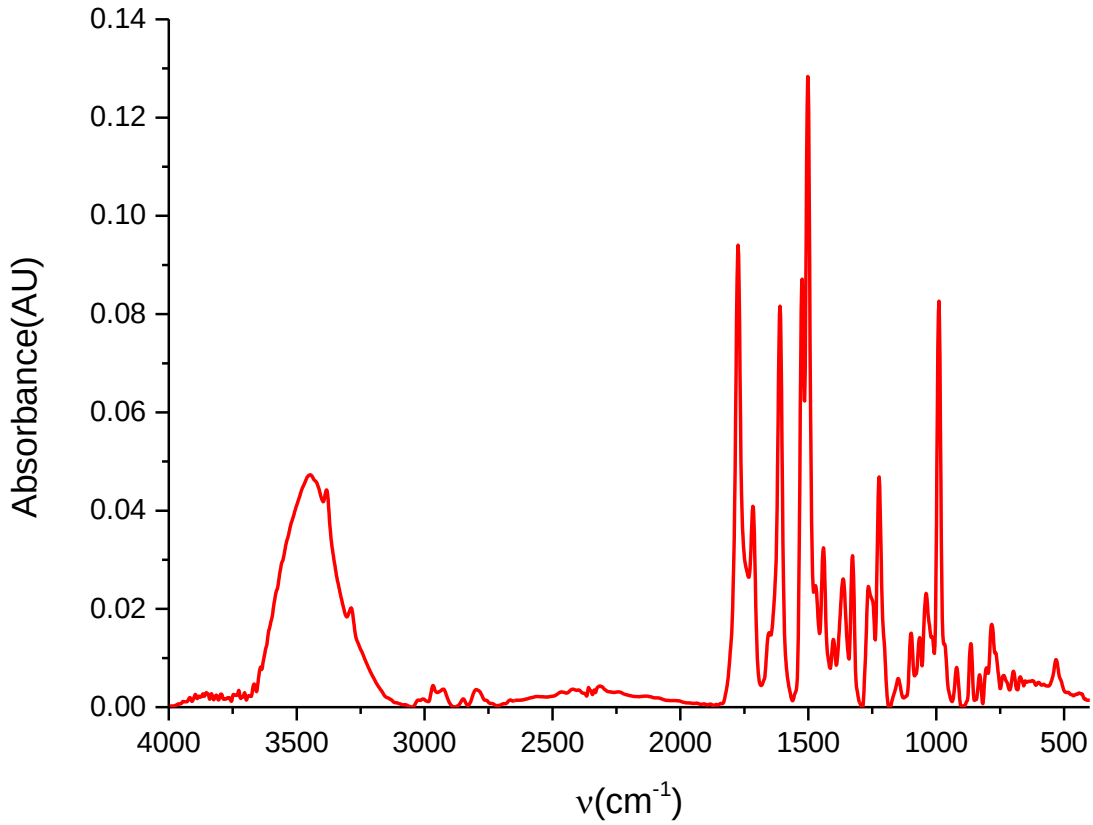

Figure S35. FT-IR spectrum of *cis*-**3**.

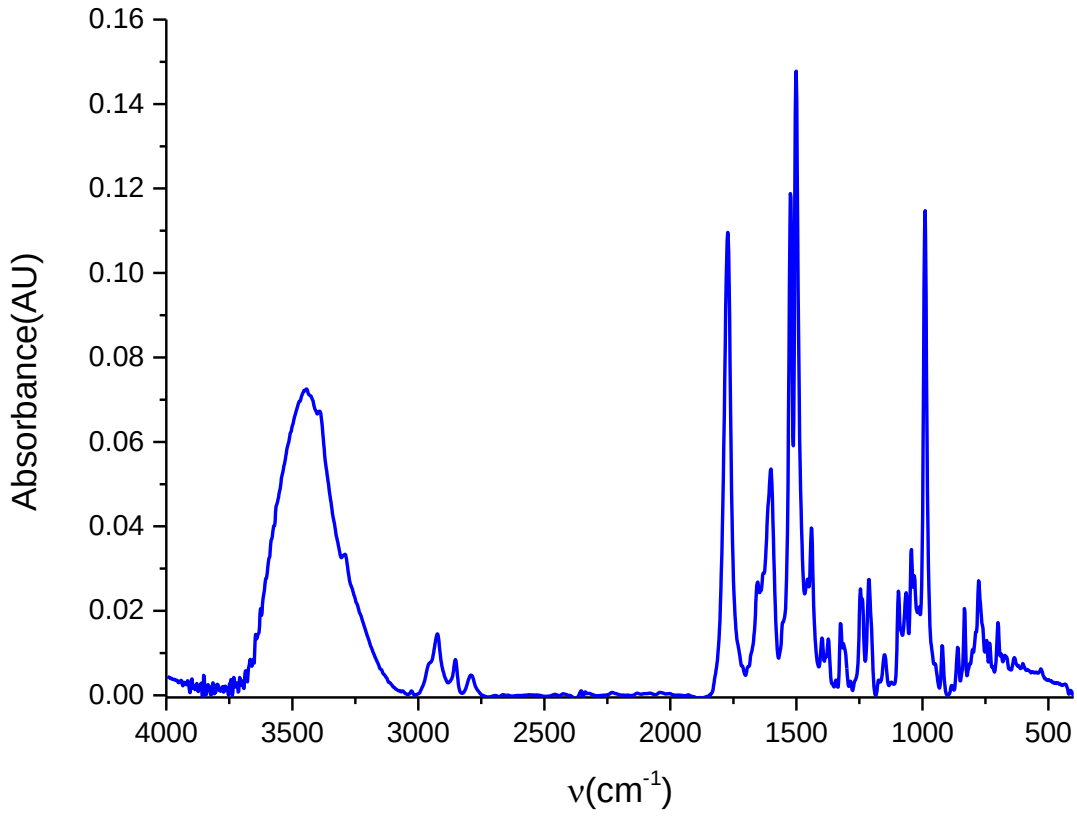

Figure S36. FT-IR spectrum of *trans*-**3**.

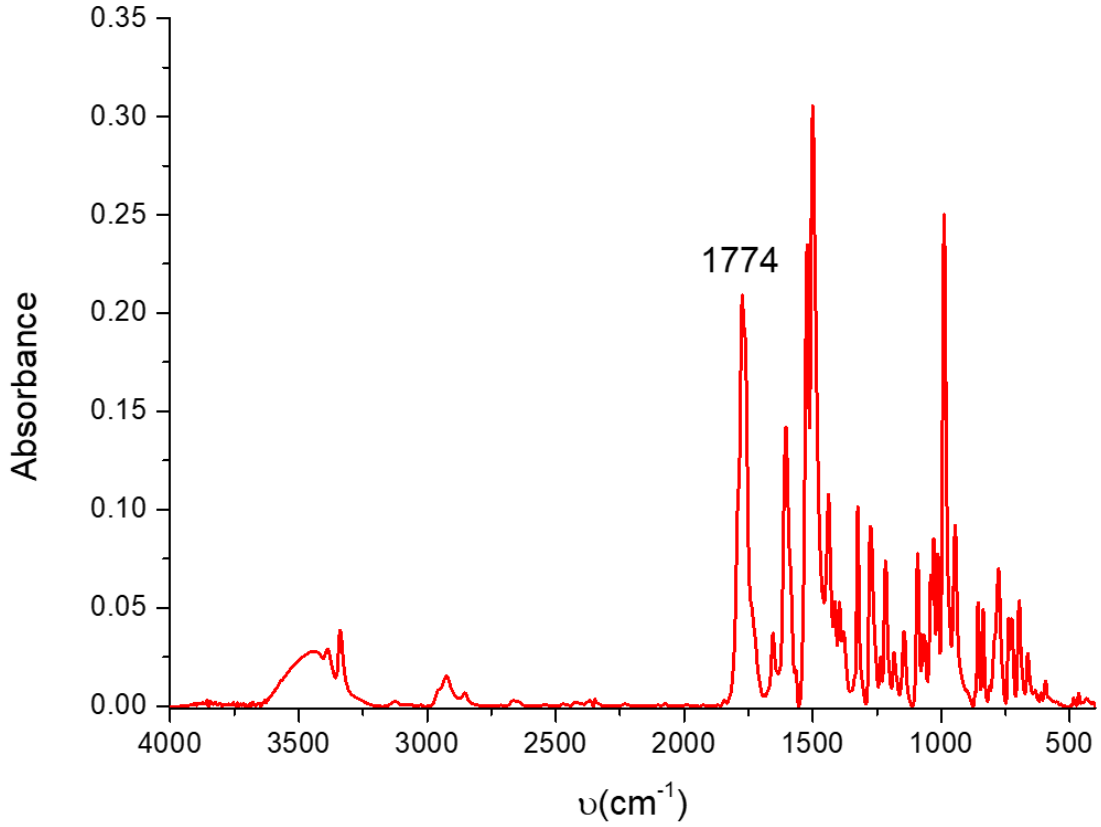

Figure S37. FT-IR spectrum of *cis*-**4**.

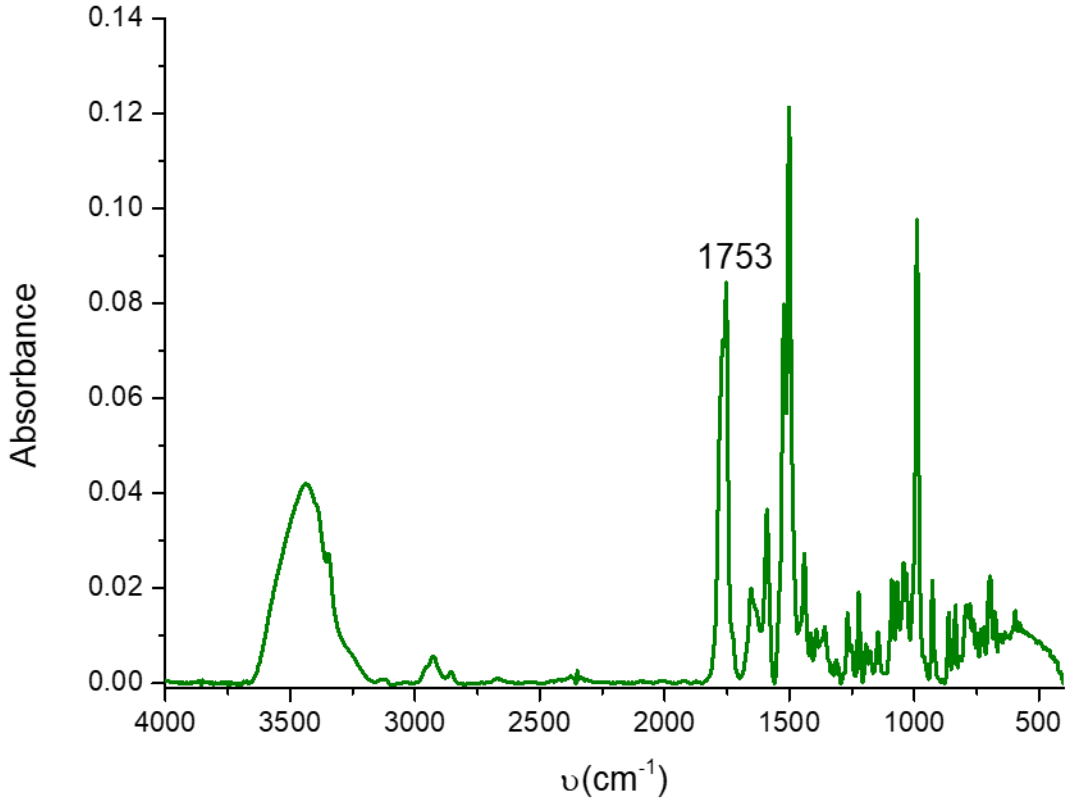

Figure S38. FT-IR spectrum of *trans*-**4**.

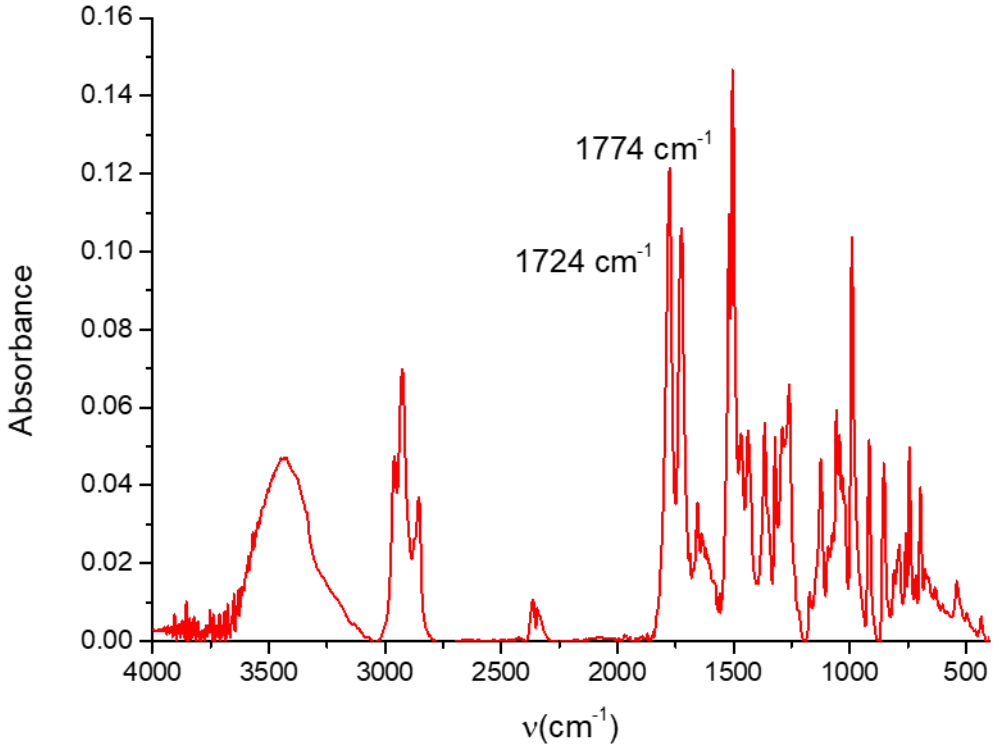

Figure S39. FT-IR spectrum of *cis*-**5**.

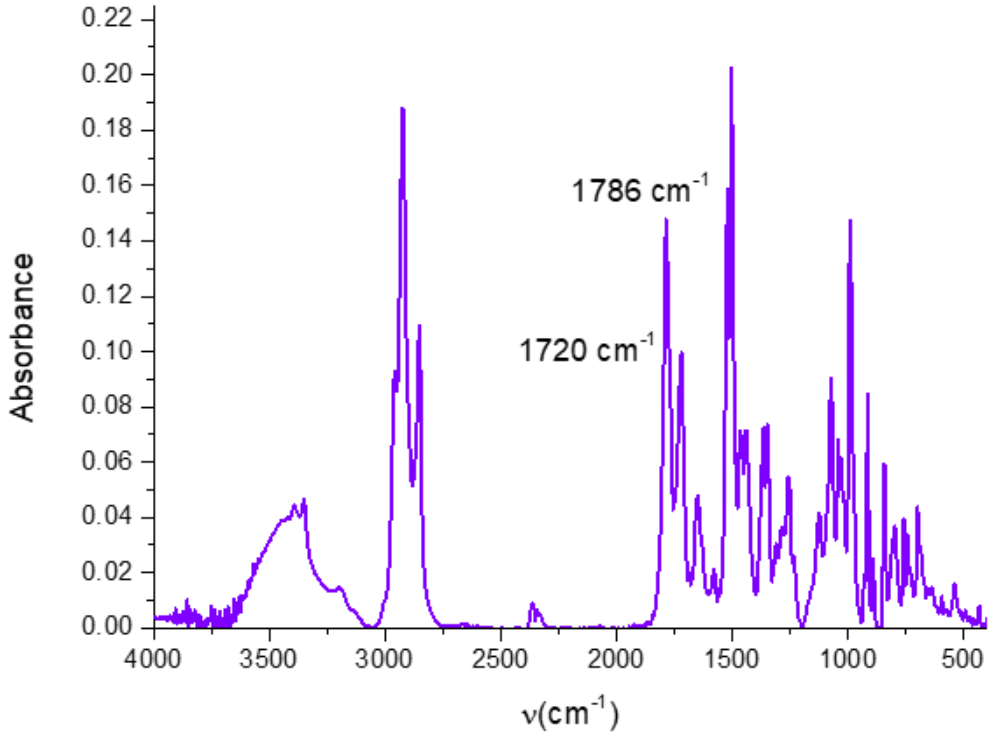

Figure S40. FT-IR spectrum of *trans*-**5**.

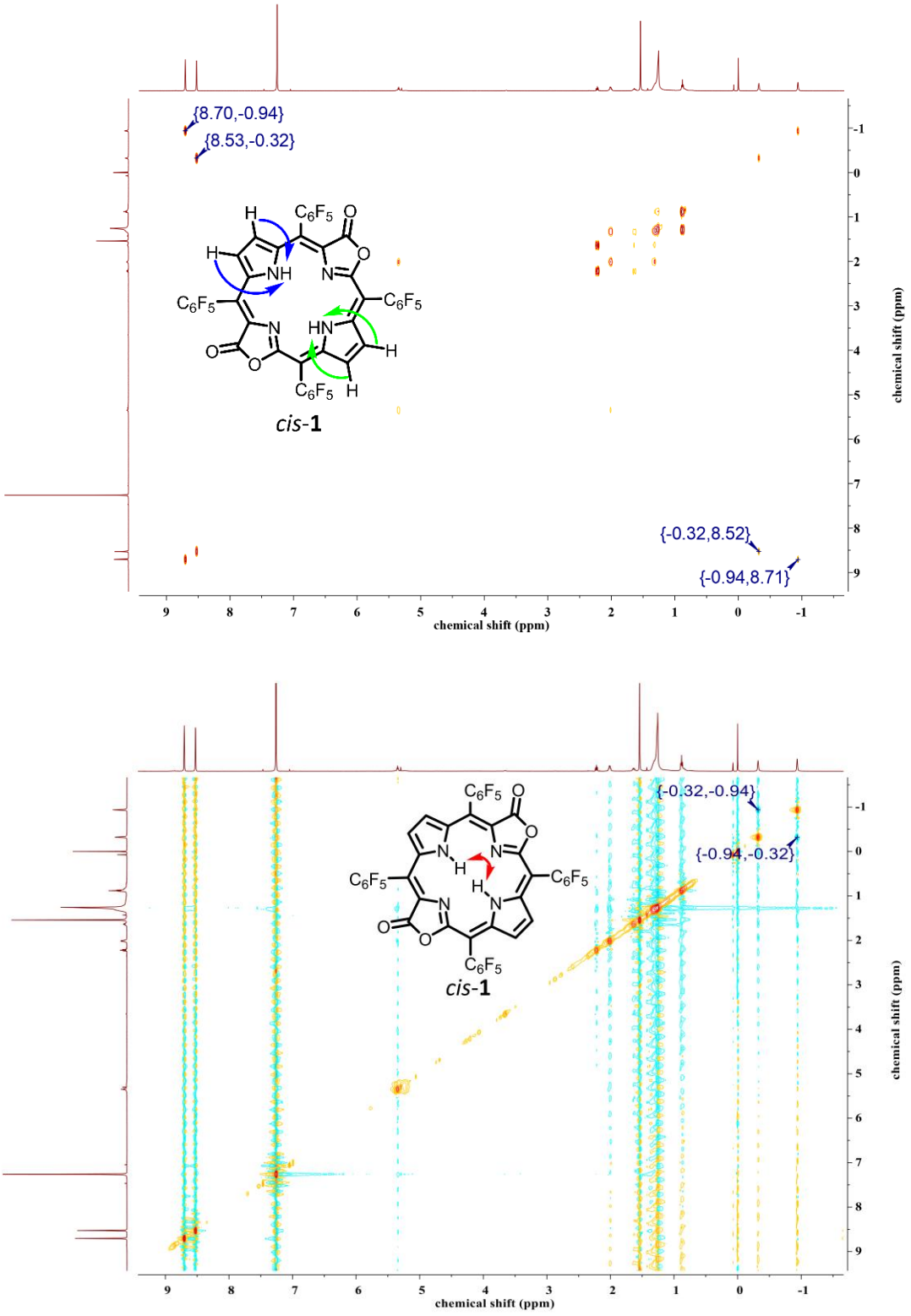

Figure S41. COSY and NOSEY spectra of *cis*-**1**.

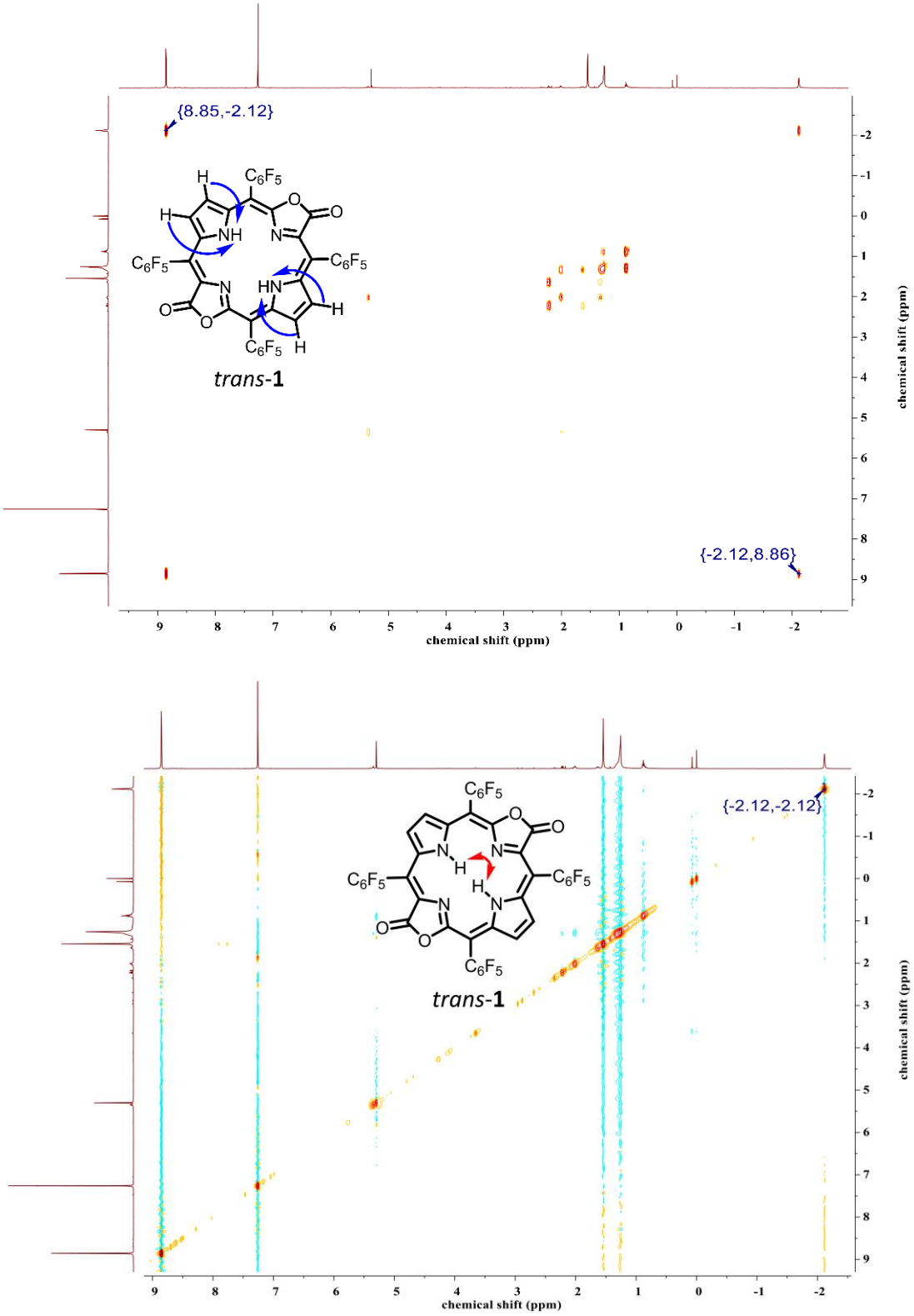

Figure S42. COSY and NOSEY spectra of *trans*-**1**.

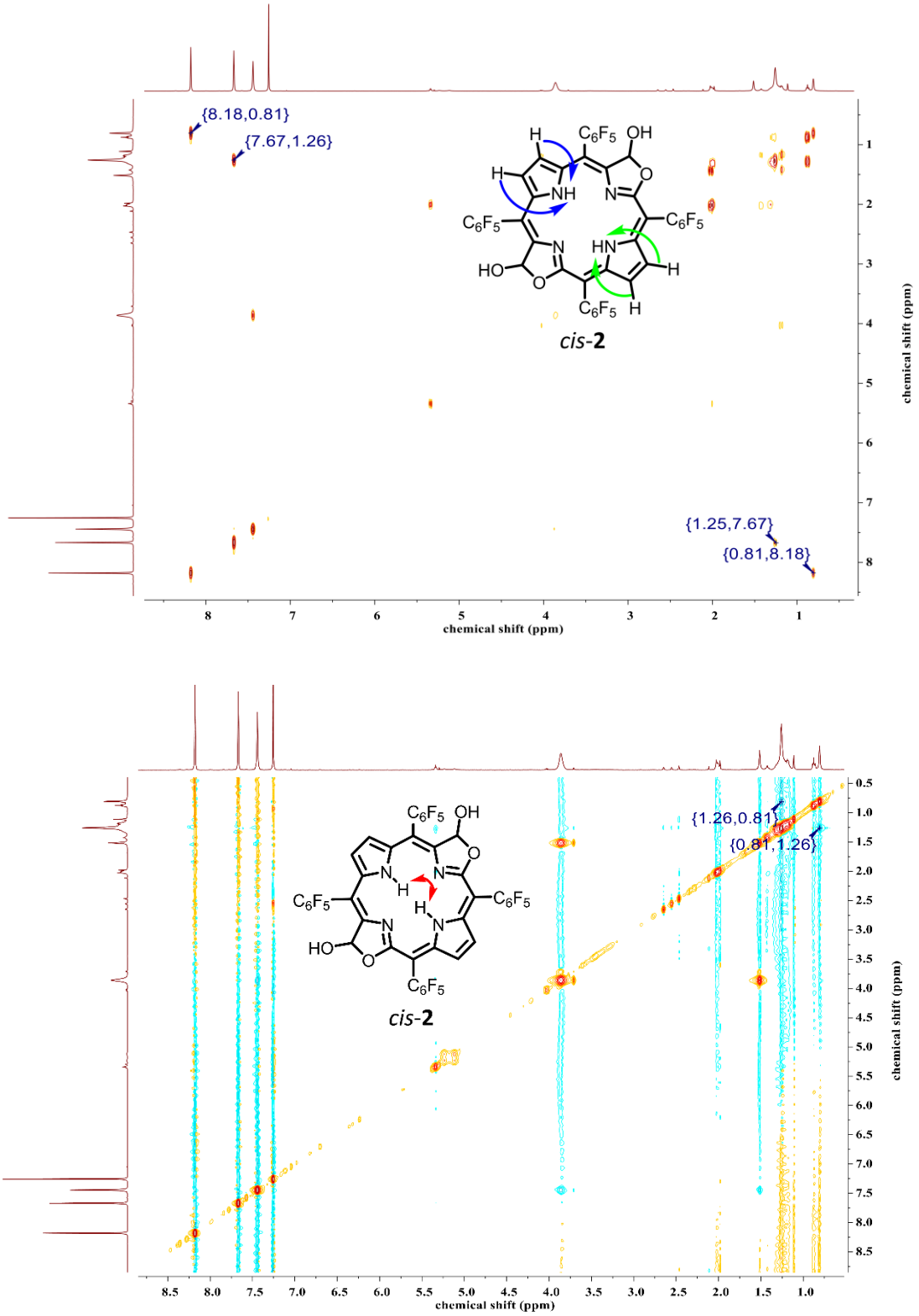

Figure S43. COSY and NOSEY spectra of *cis*-**2**.

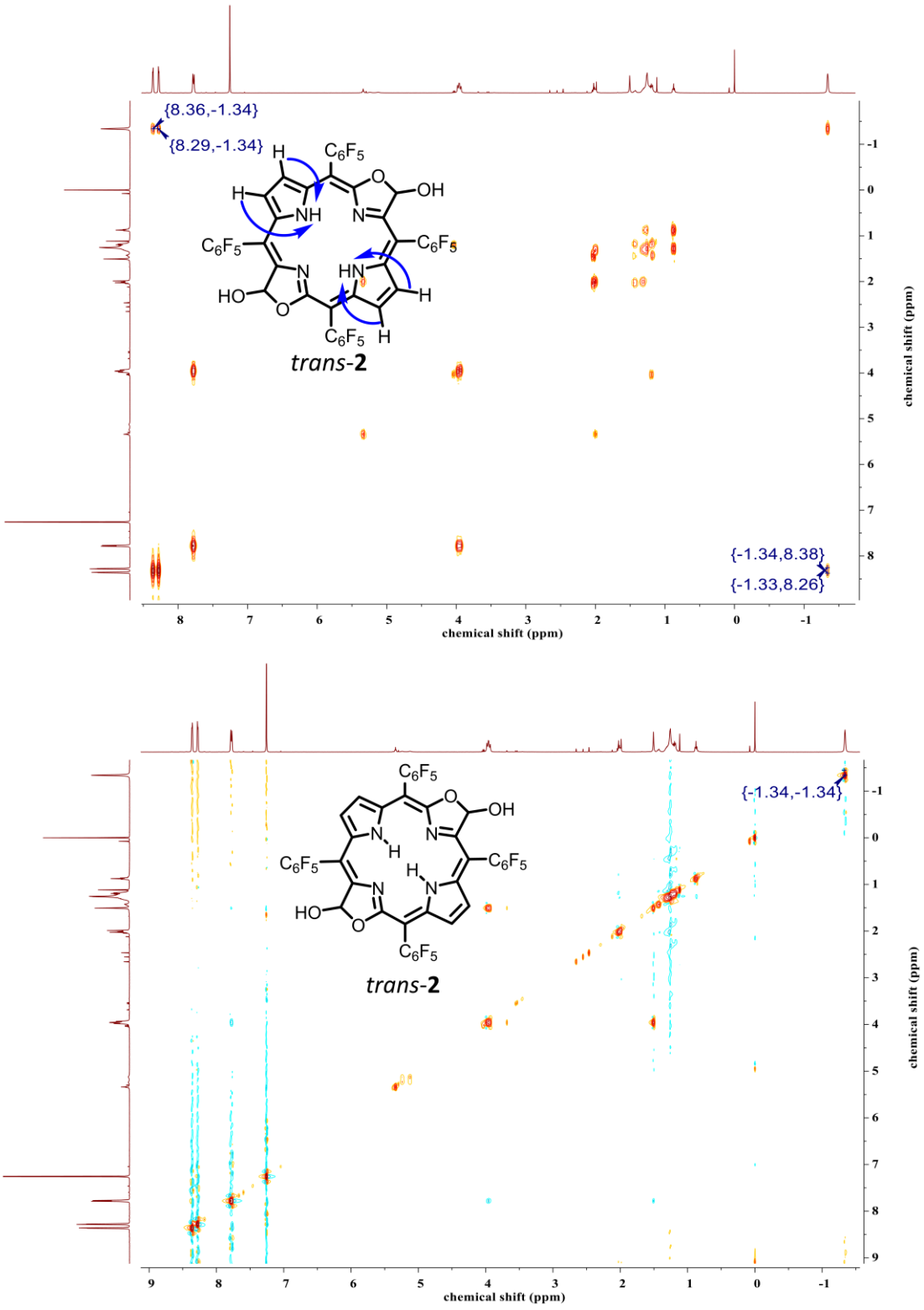

Figure S44. COSY and NOSEY spectra of *trans*-**2**.

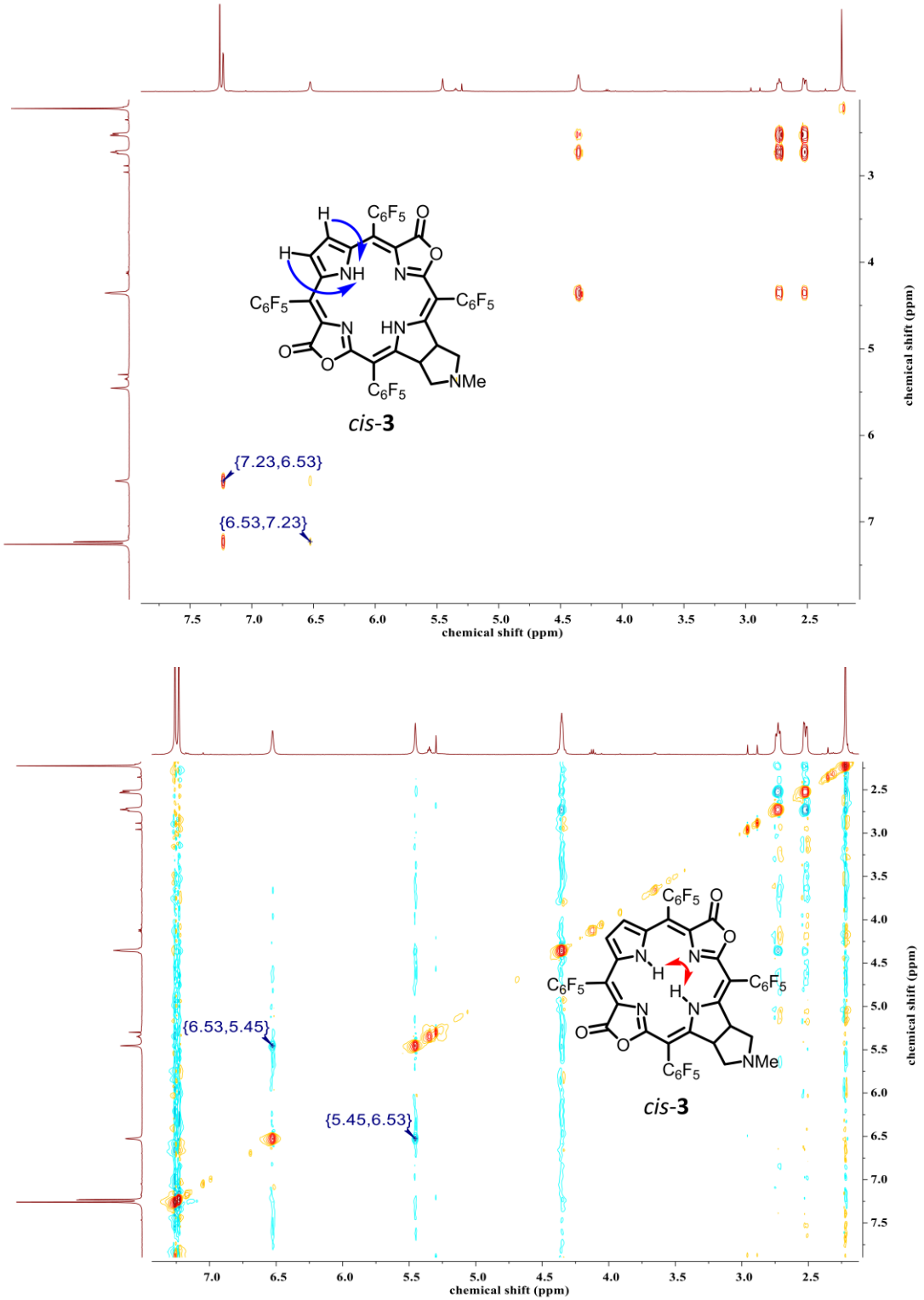

Figure S45. COSY and NOSEY spectra of *cis*-**3**.

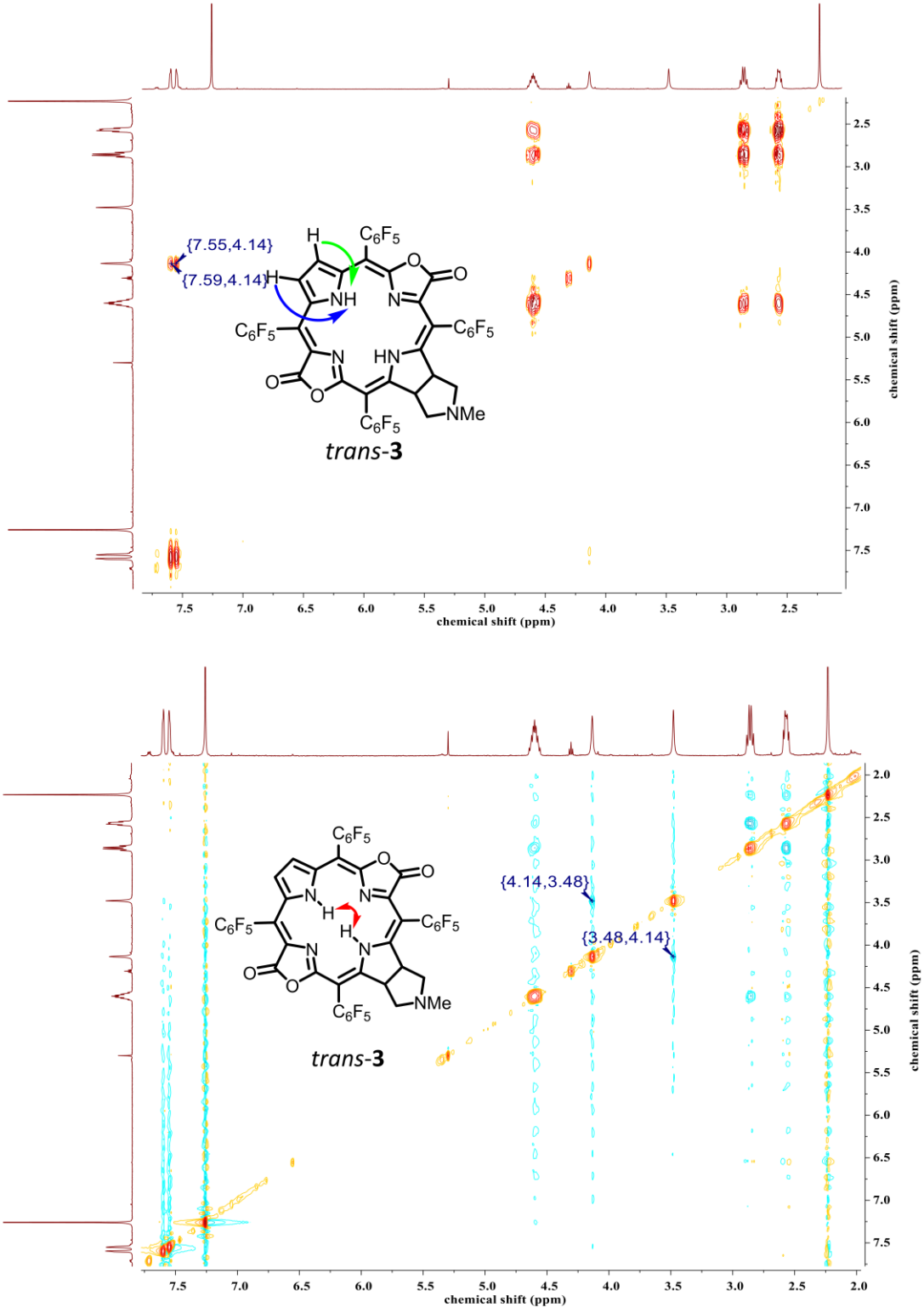

Figure S46. COSY and NOSEY spectra of *trans*-**3**.

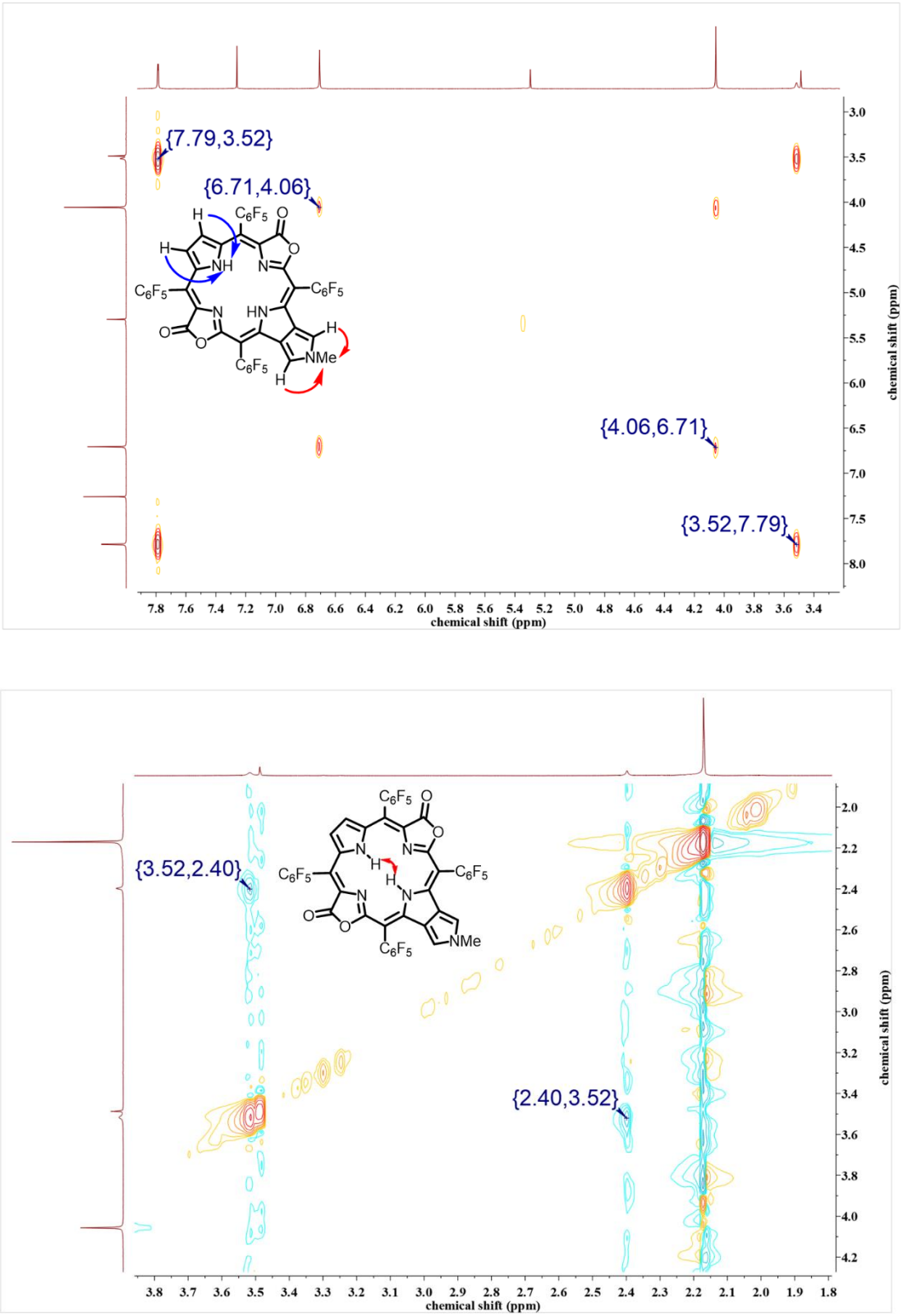

Figure S47. COSY and NOSEY spectra of *cis*-**4**.

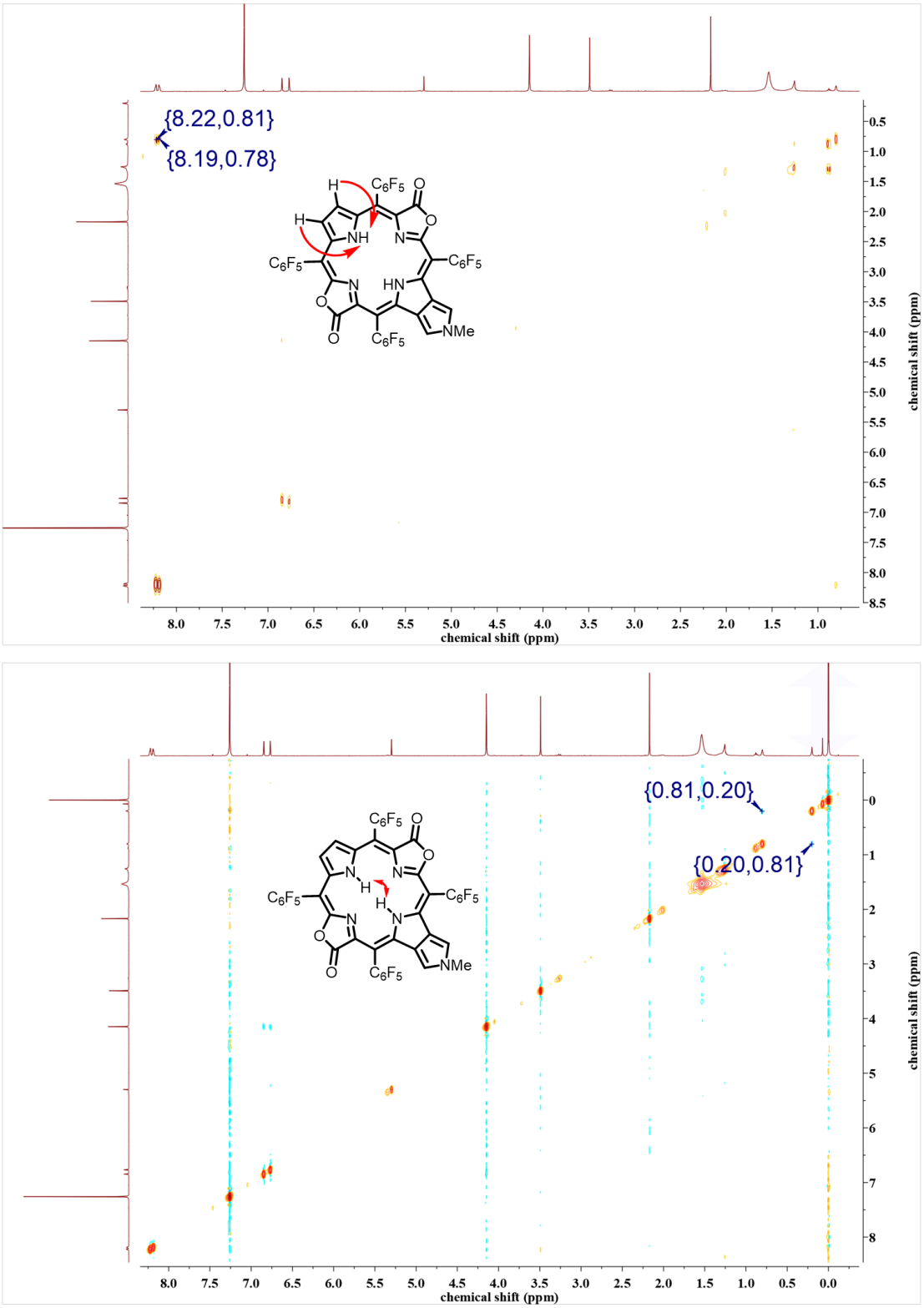

Figure S48. COSY and NOSEY spectra of *trans*-**4**.

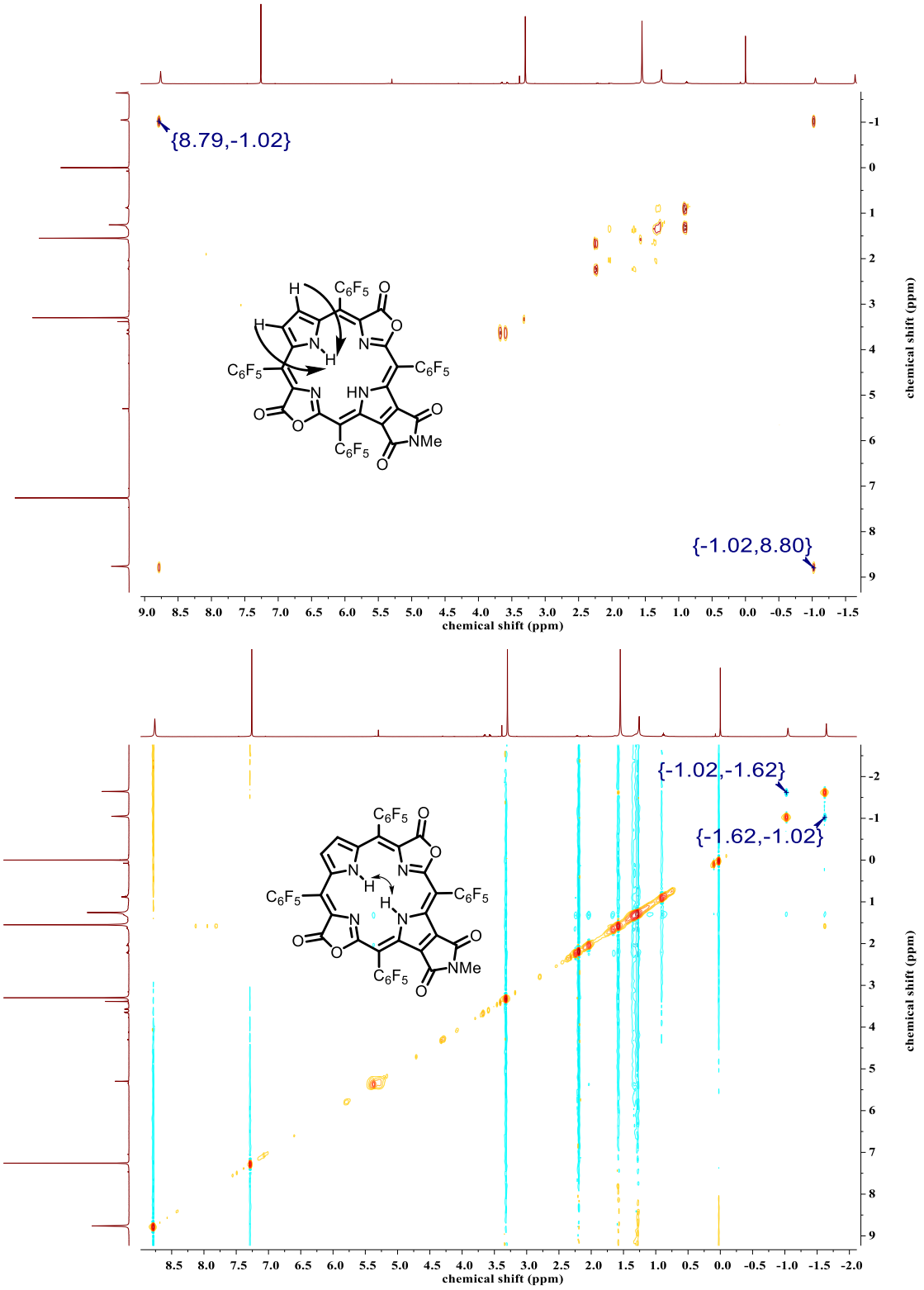

Figure S49. COSY and NOSEY spectra of *cis*-**5**.

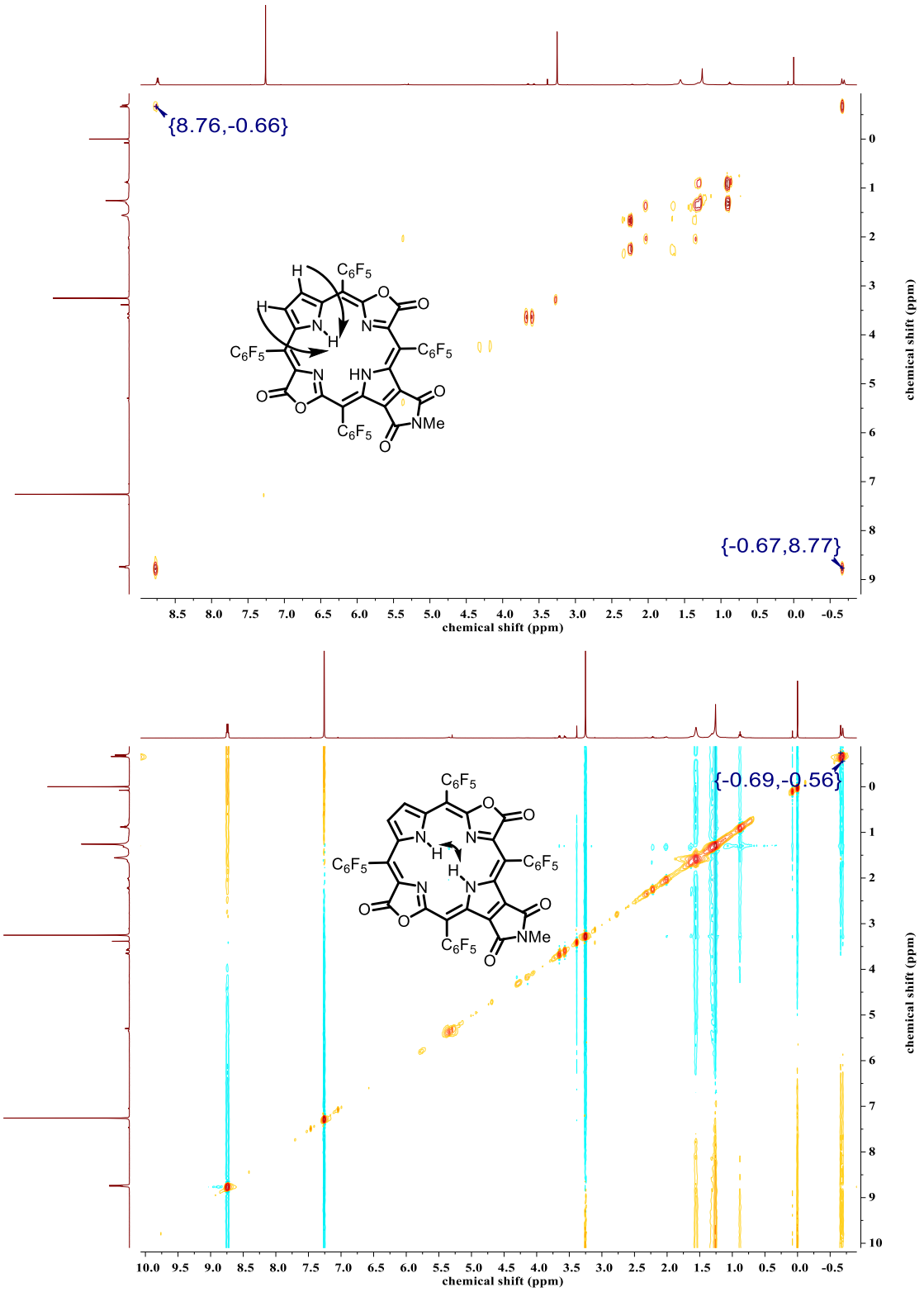

Figure S50. COSY and NOSEY spectra of *trans*-**5**.

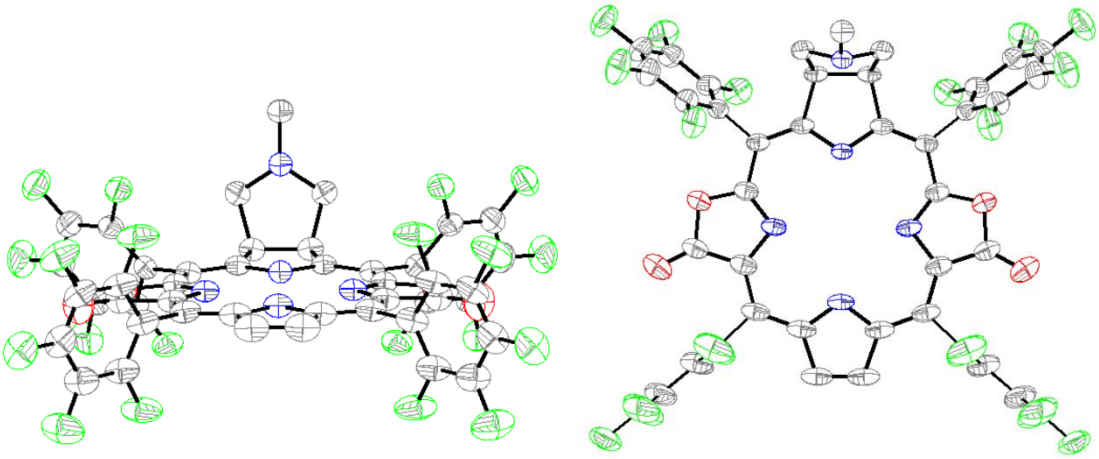

Figure S51. X-ray structure of *cis*-**3**. Thermal ellipsoids set at 50% probability (red: oxygen, gray: carbon, green: fluorine, blue: nitrogen).

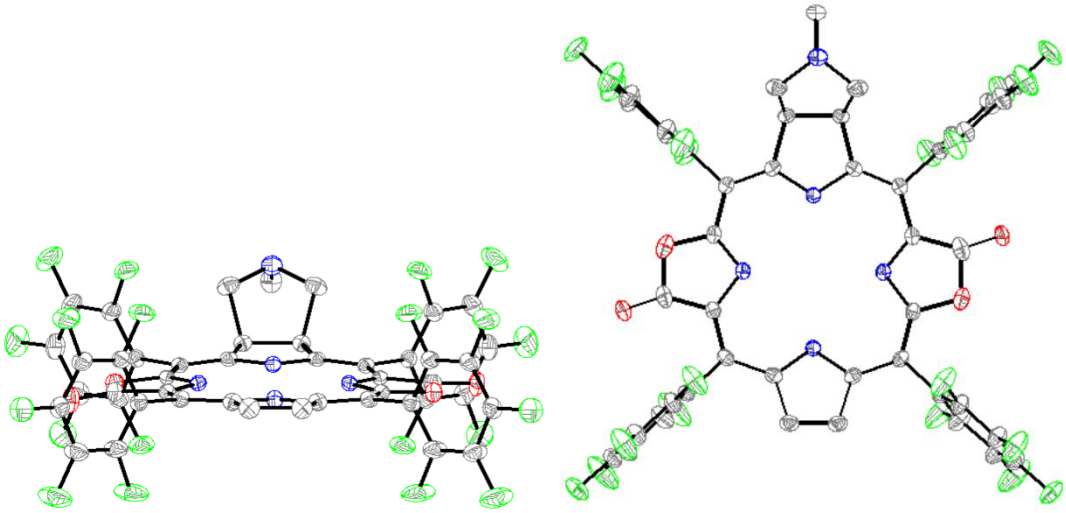

Figure S52. X-ray structure of *trans*-**3**. Thermal ellipsoids set at 50% probability (red: oxygen, gray: carbon, green: fluorine, blue: nitrogen).

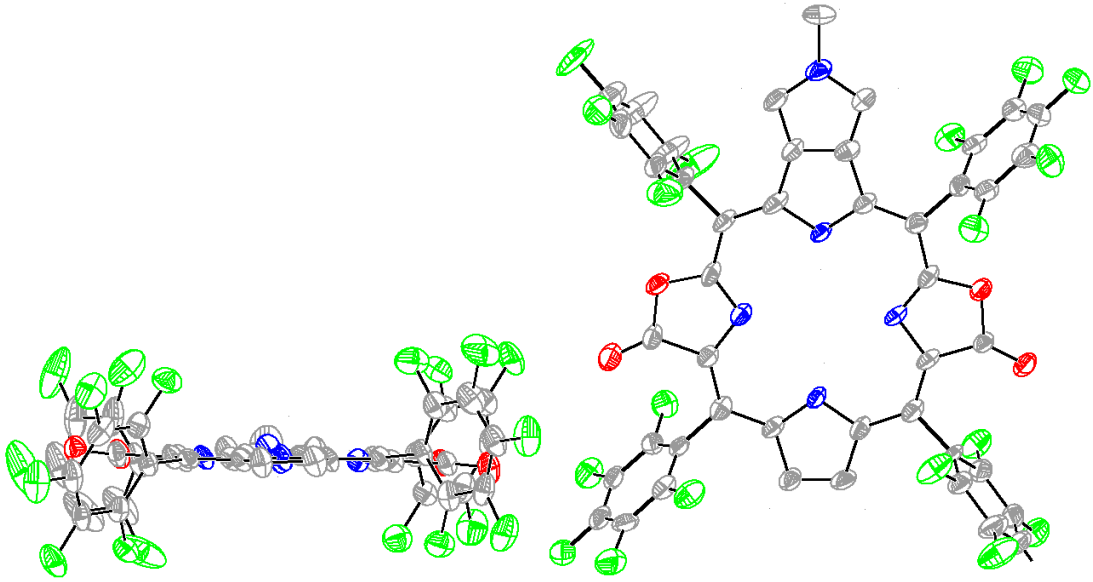

Figure S53. X-ray structure of *cis*-**4**. Thermal ellipsoids set at 50% probability (red: oxygen, gray: carbon, green: fluorine, blue: nitrogen).

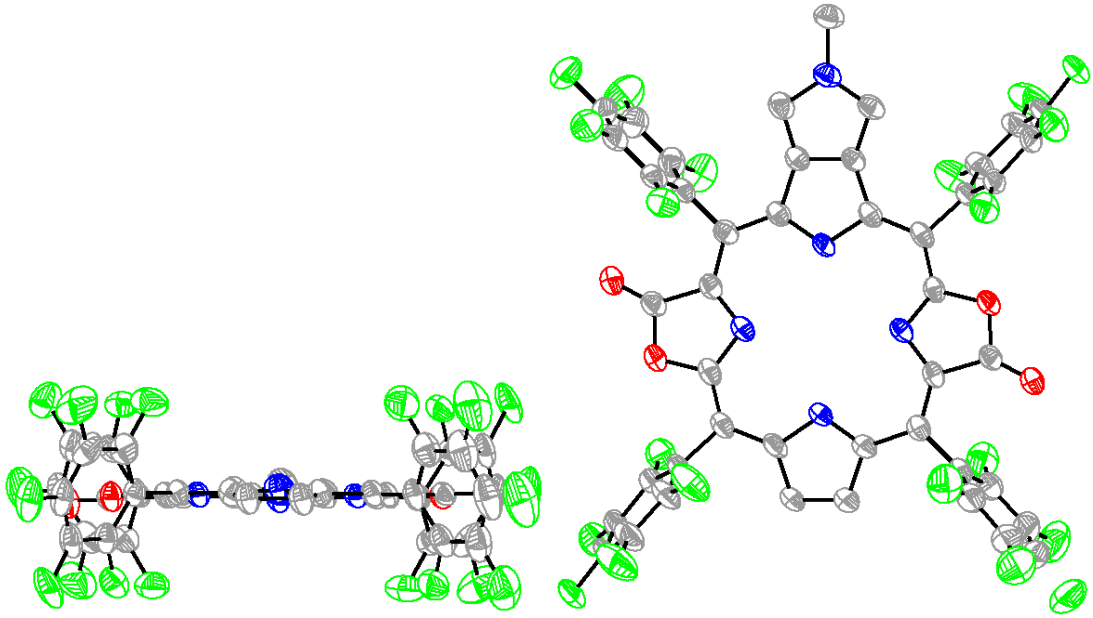

Figure S54. X-ray structure of *trans*-**4**. Thermal ellipsoids set at 50% probability (red: oxygen, gray: carbon, green: fluorine, blue: nitrogen).

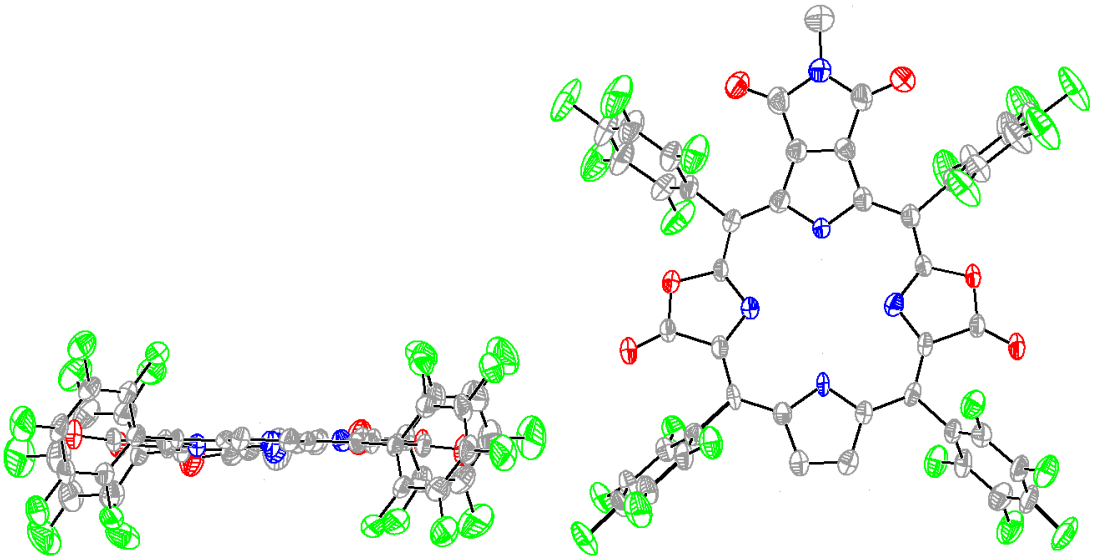

Figure S55. X-ray structure of *cis*-**5**. Thermal ellipsoids set at 50% probability (red: oxygen, gray: carbon, green: fluorine, blue: nitrogen).

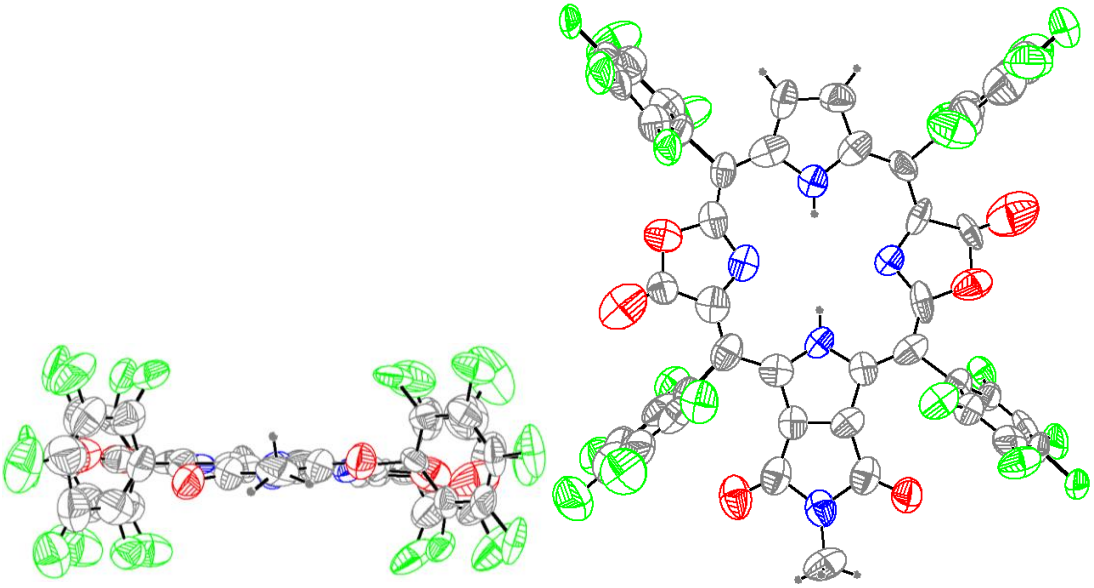

Figure S56. X-ray structure of *trans*-**5**. Thermal ellipsoids set at 50% probability (red: oxygen, gray: carbon, green: fluorine, blue: nitrogen).

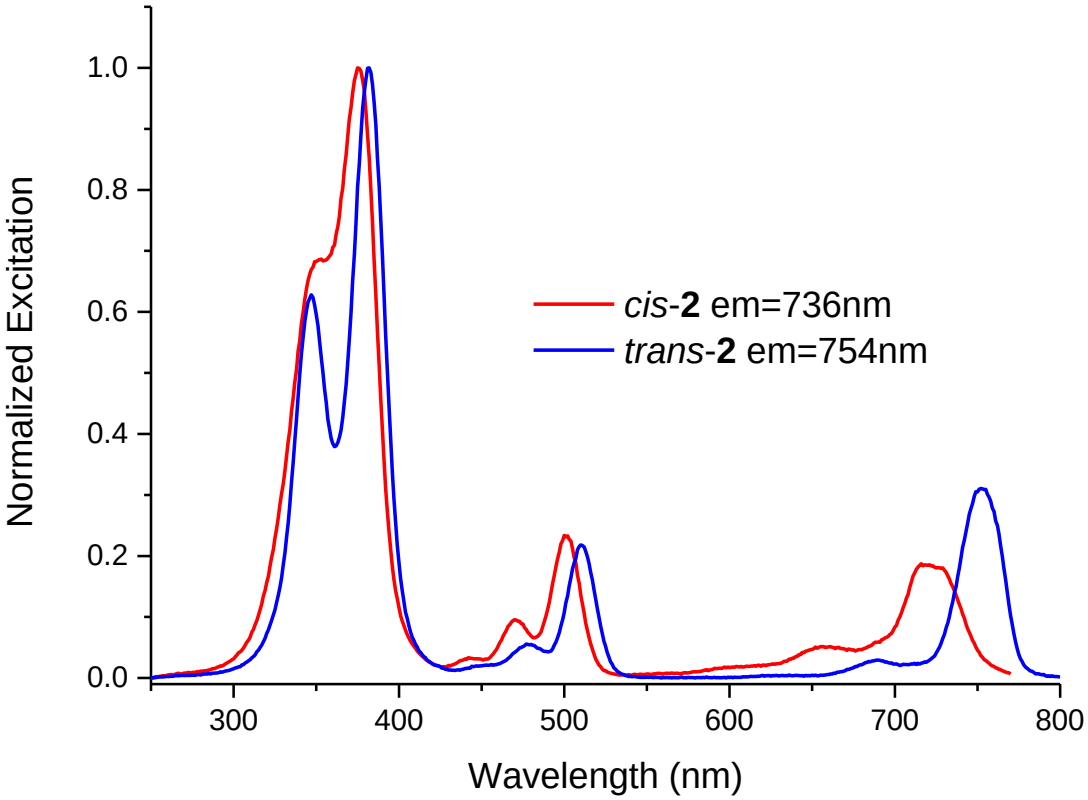

Figure S57. Normalized excitation spectrum of *cis*-**2** and *trans*-**2** in CH_2Cl_2.

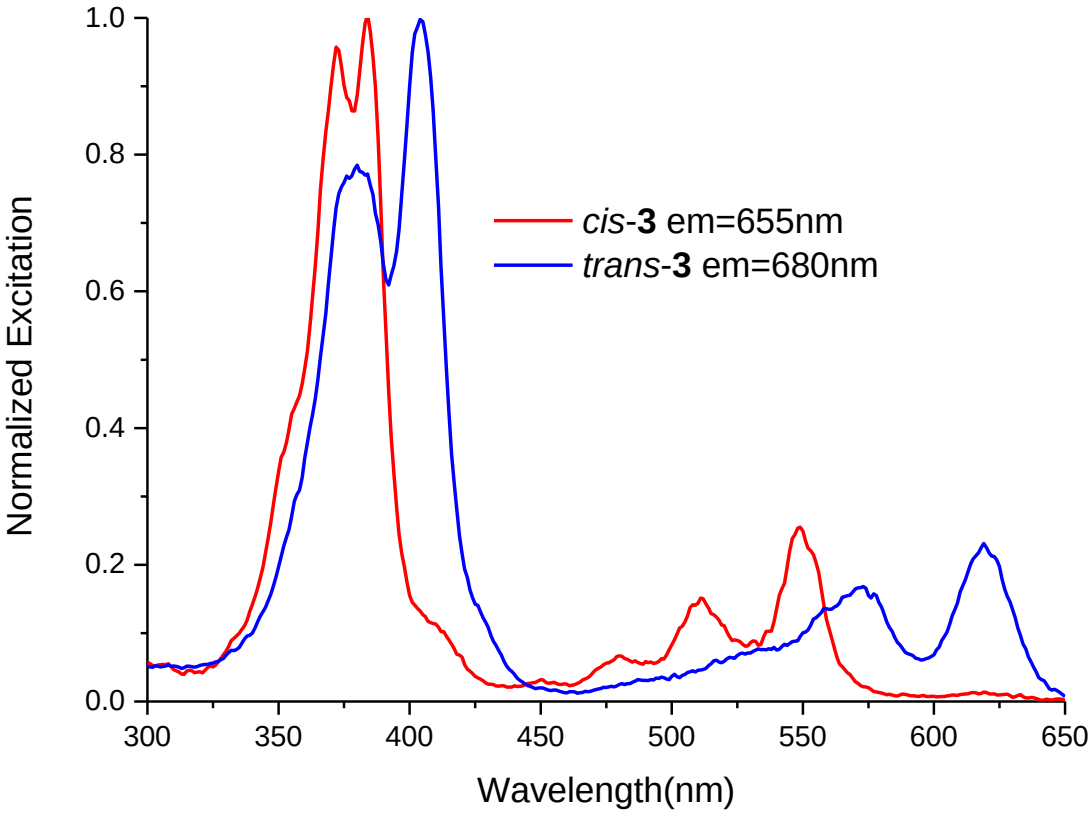

Figure S58. Normalized excitation spectrum of *cis*-**3** and *trans*-**3** in CH_2Cl_2.

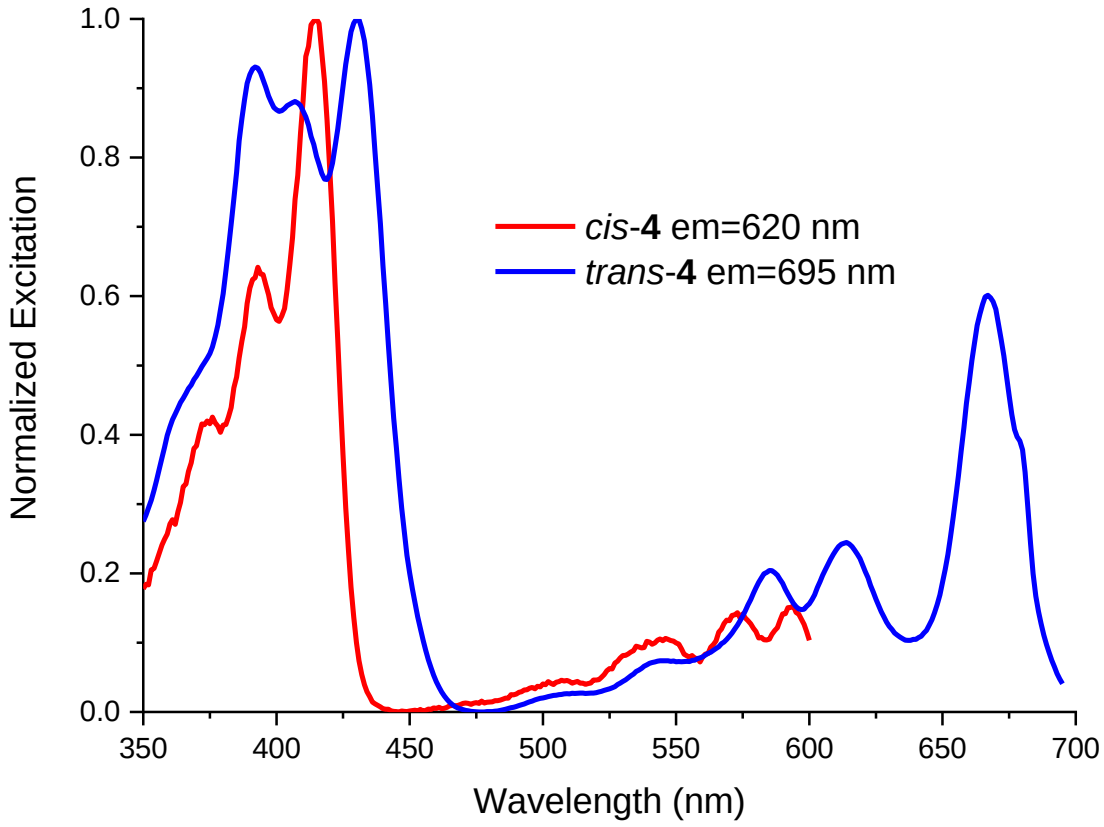

Figure S59. Normalized excitation spectrum of *cis*-**4** and *trans*-**4** in CH_2Cl_2.

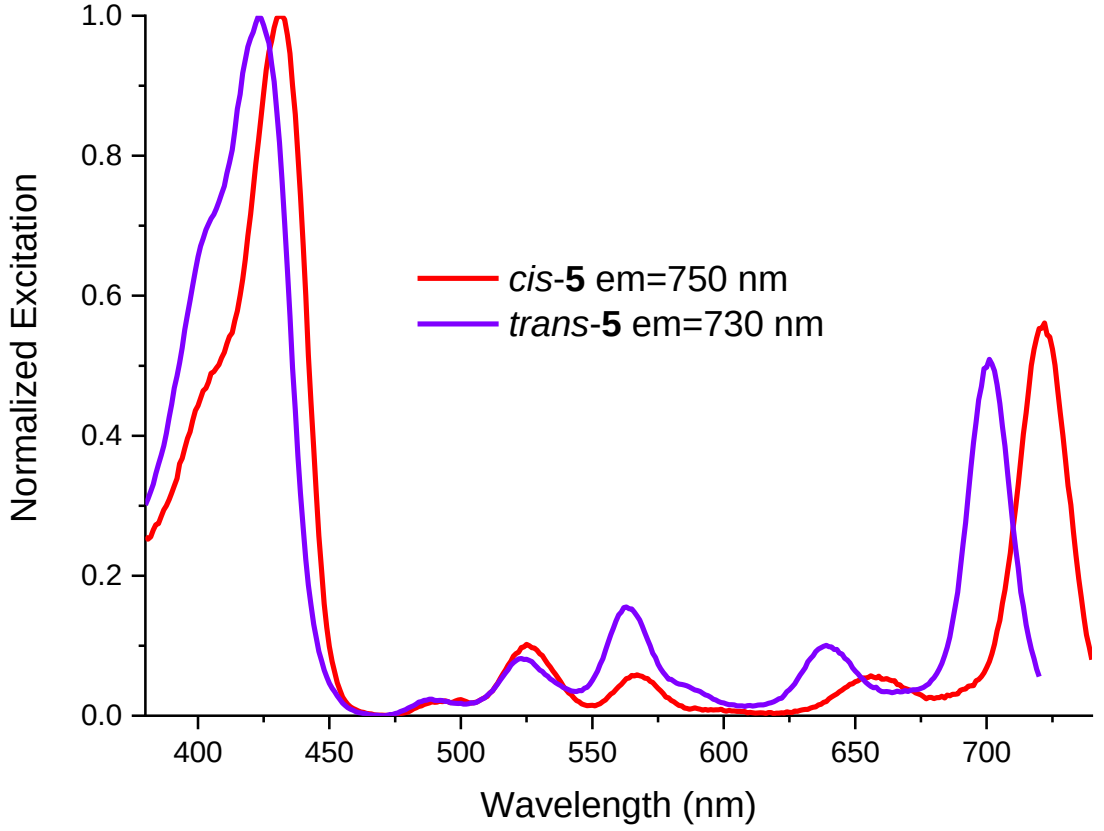

Figure S60. Normalized excitation spectrum of *cis*-**5** and *trans*-**5** in CH_2Cl_2.

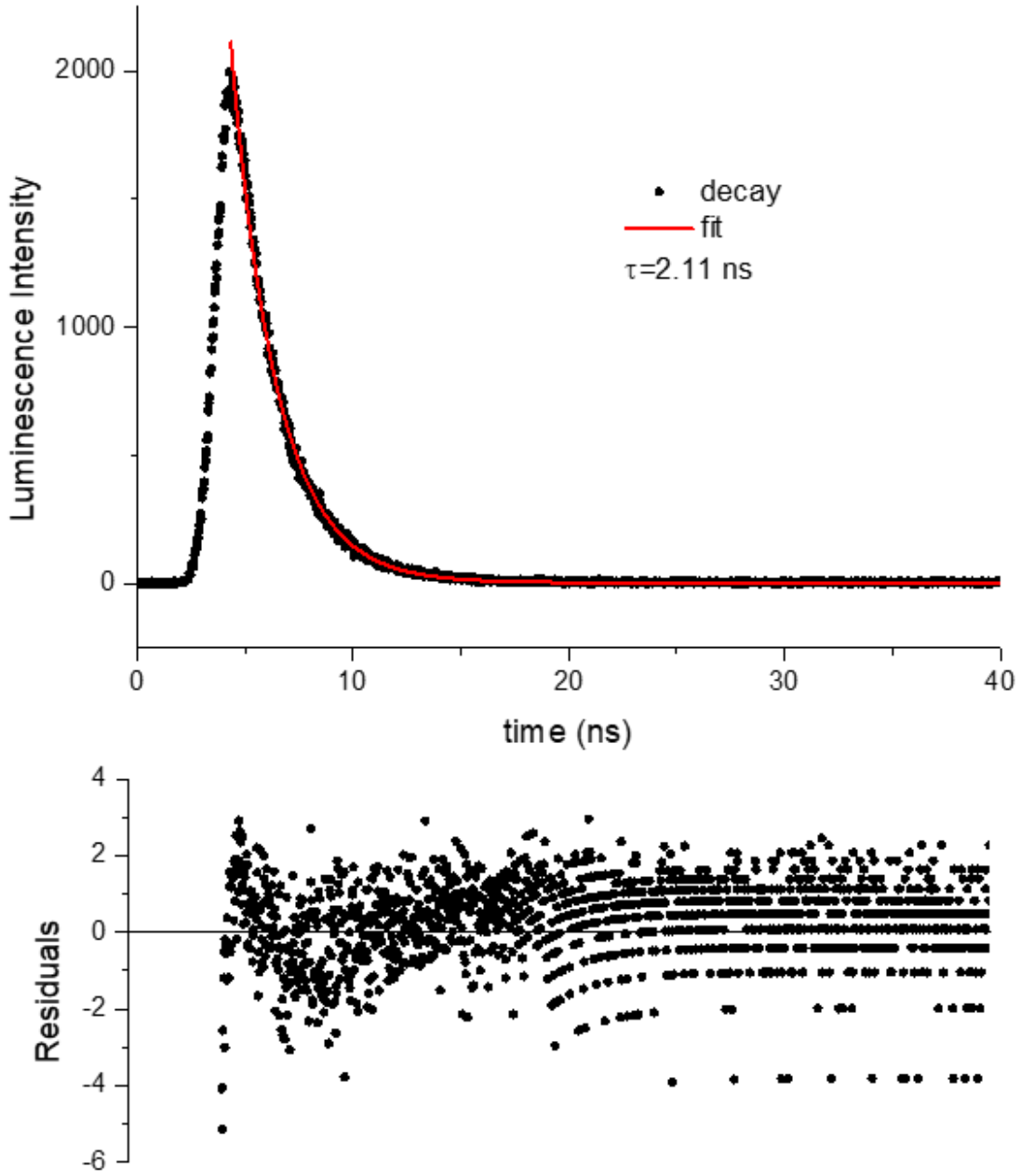

Figure S61. Lifetime measurement of *cis*-**2** in CH_2Cl_2.

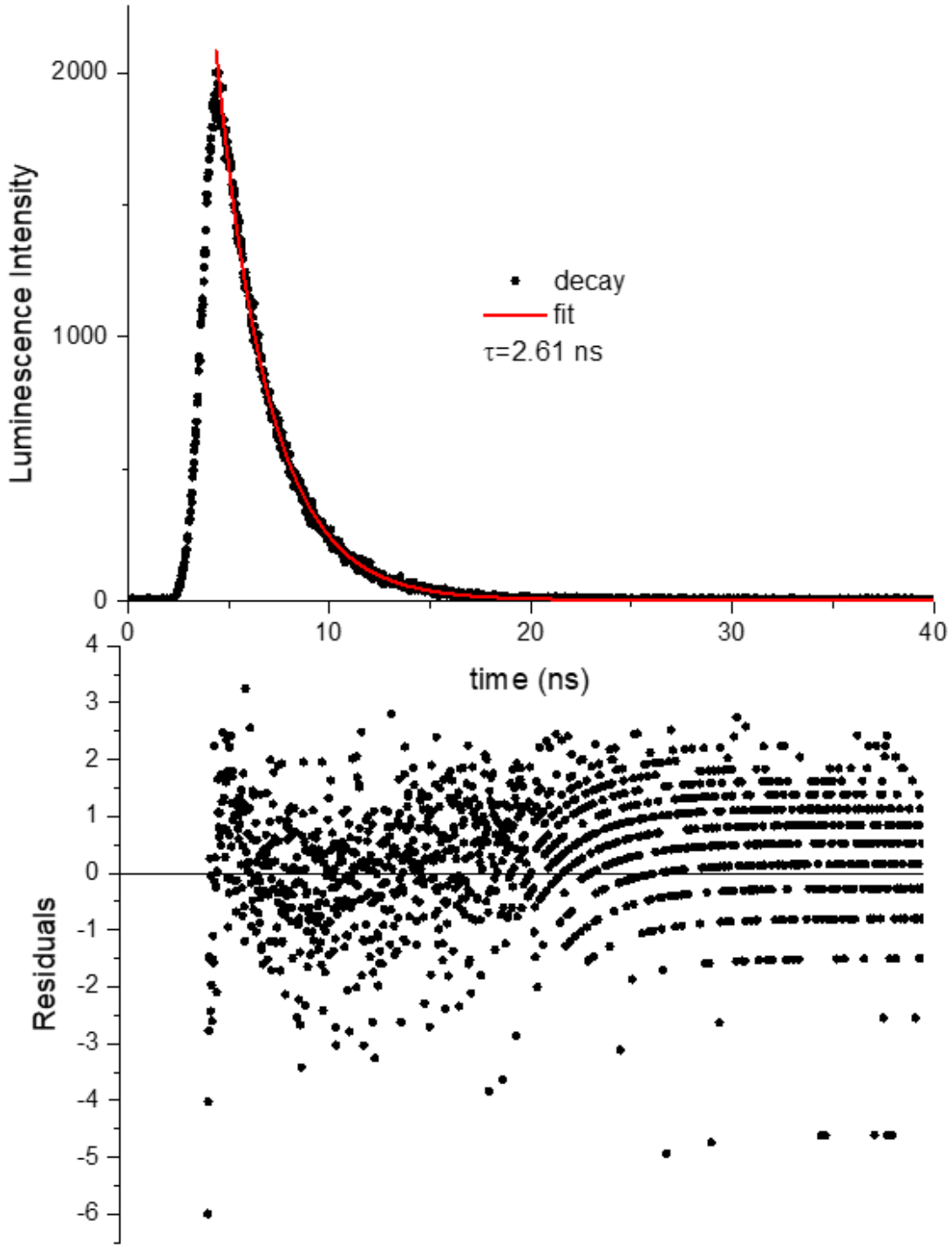

Figure S62. Lifetime measurement of *trans*-**2** in CH_2Cl_2.

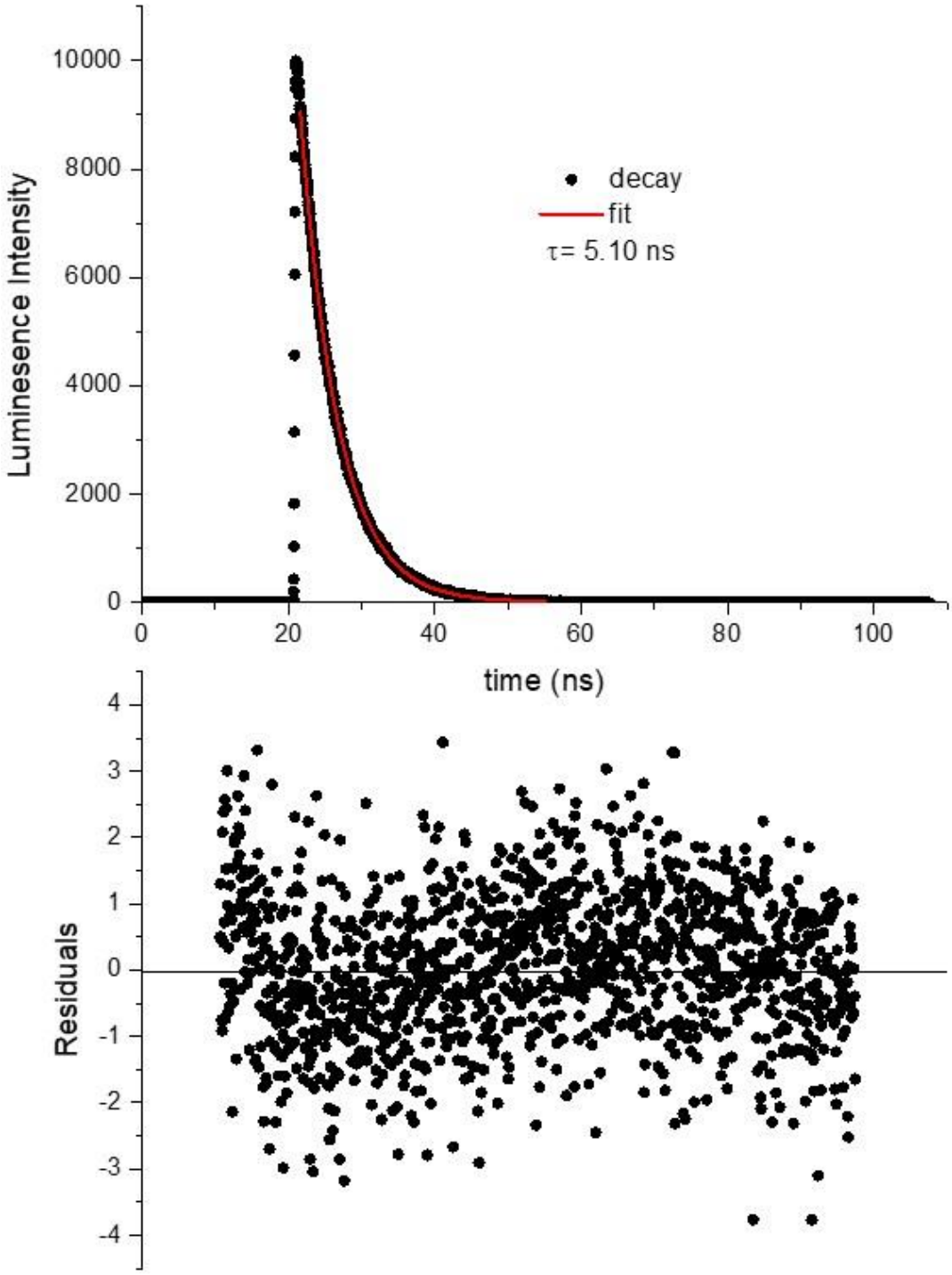

Figure S63. Lifetime measurement of *cis*-**3** in CH_2Cl_2.

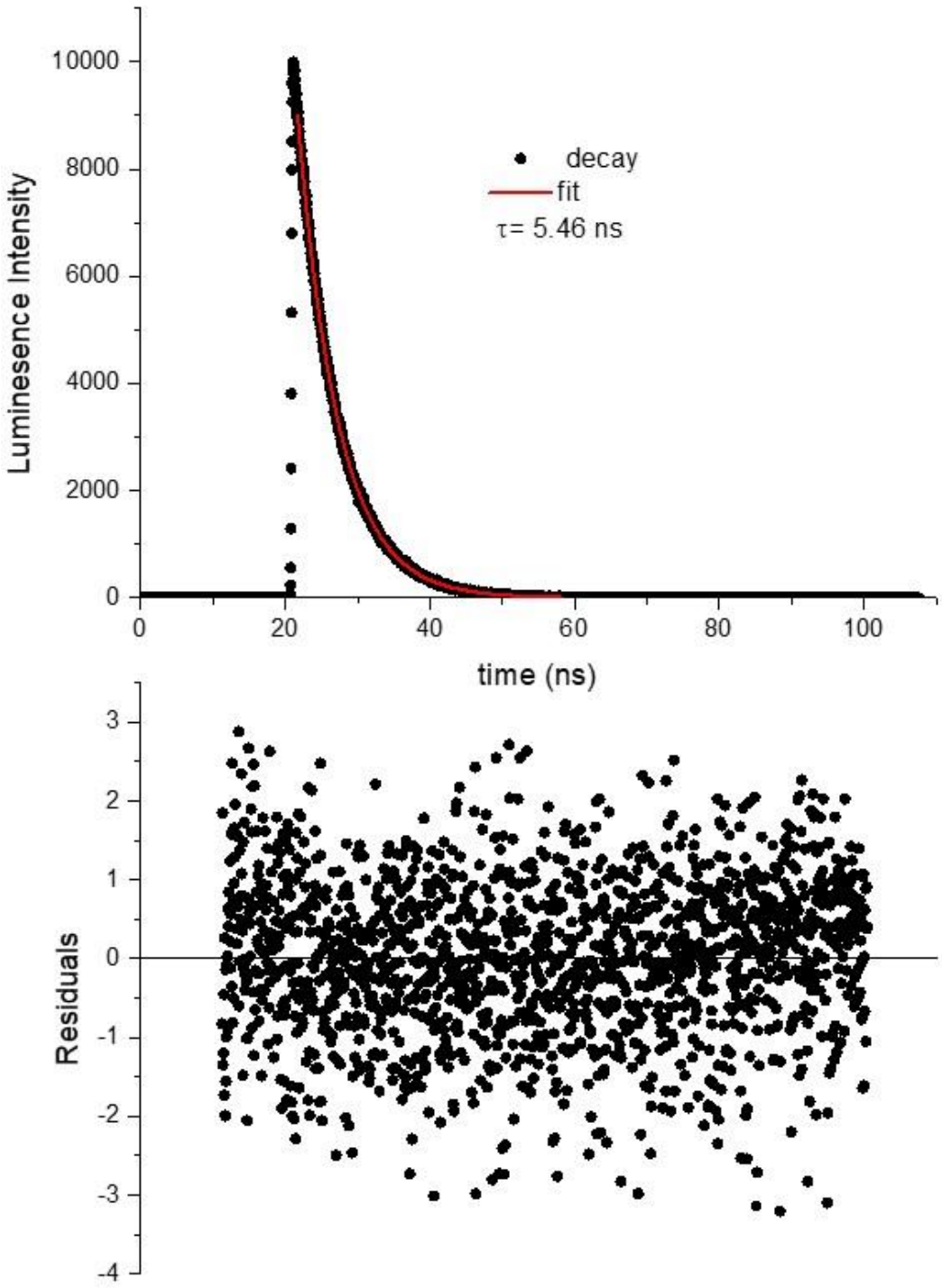

Figure S64. Lifetime measurement of *trans*-**3** in CH_2Cl_2.

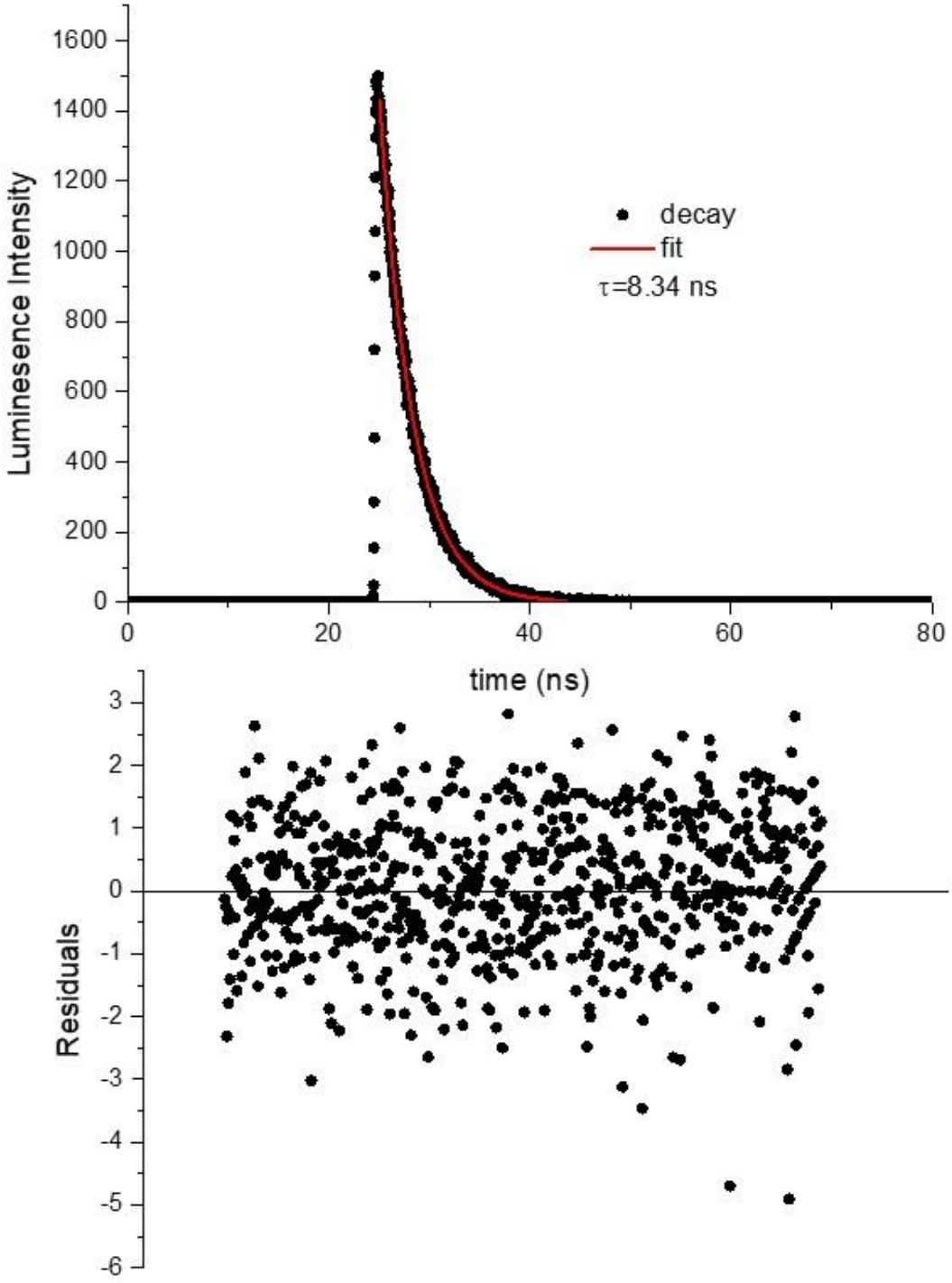

Figure S65. Lifetime measurement of *cis*-**4** in CH_2Cl_2.

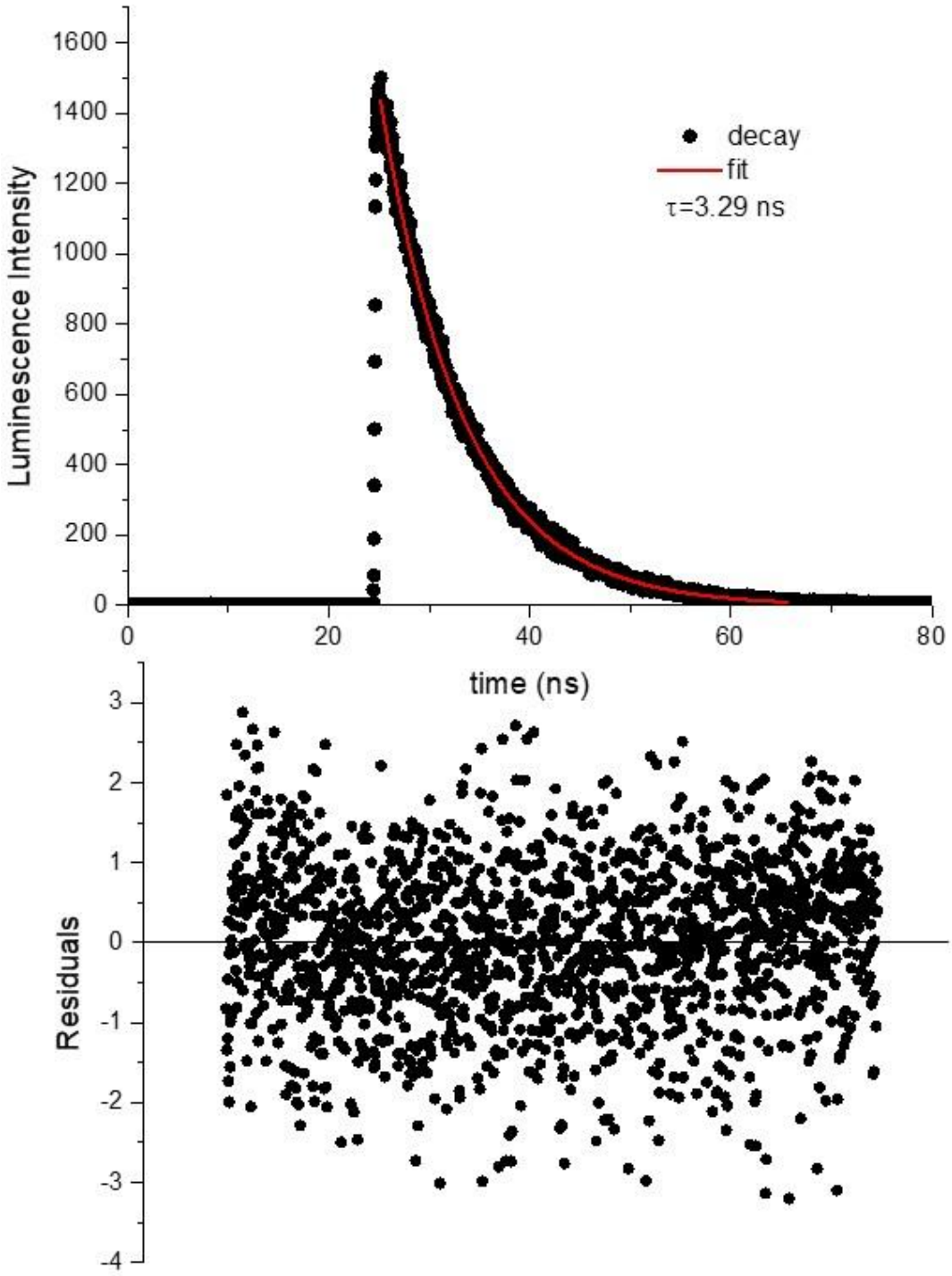

Figure S66. Lifetime measurement of *trans*-**4** in CH_2Cl_2.

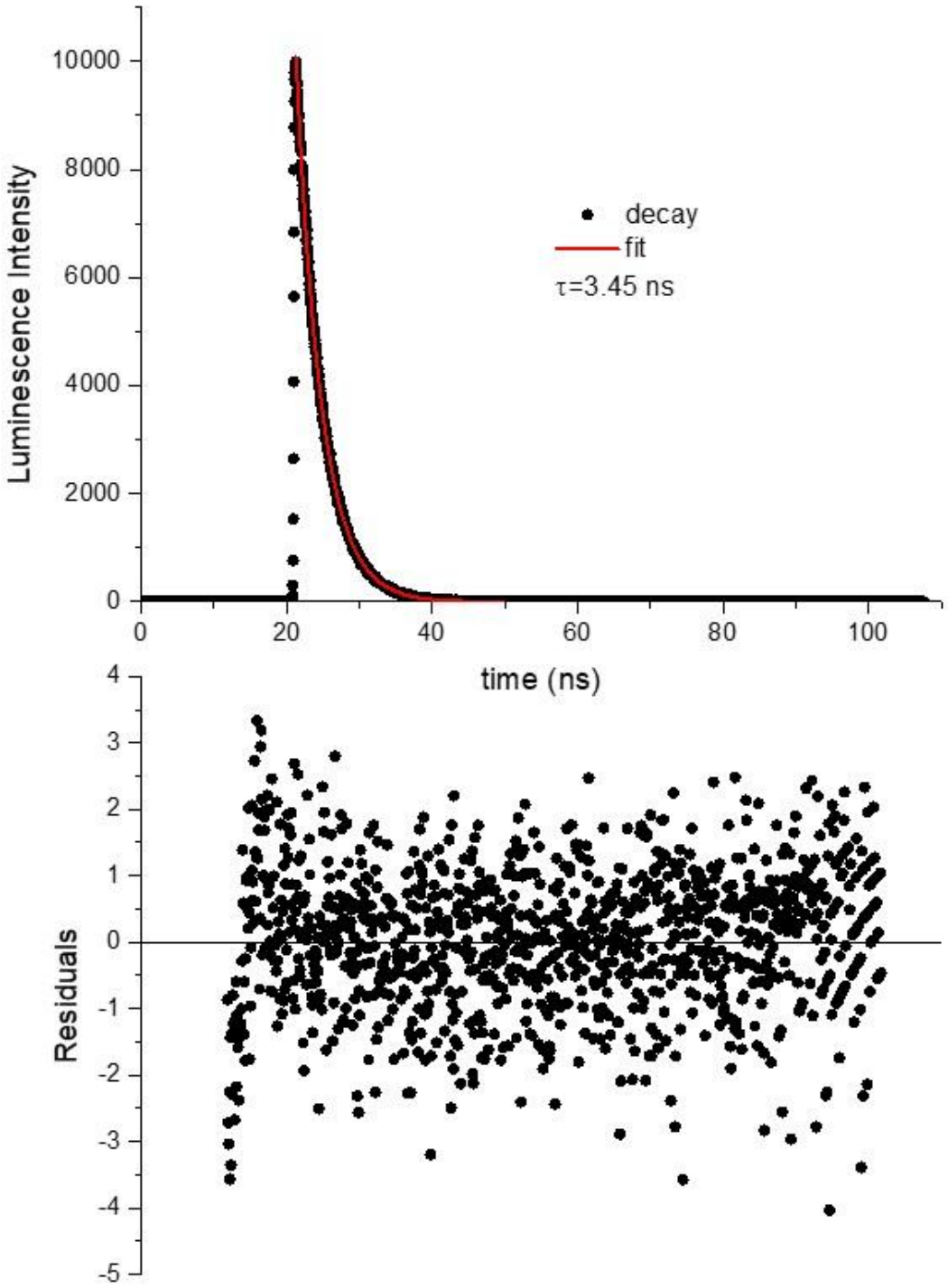

Figure S67. Lifetime measurement of *cis*-**5** in CH_2Cl_2.

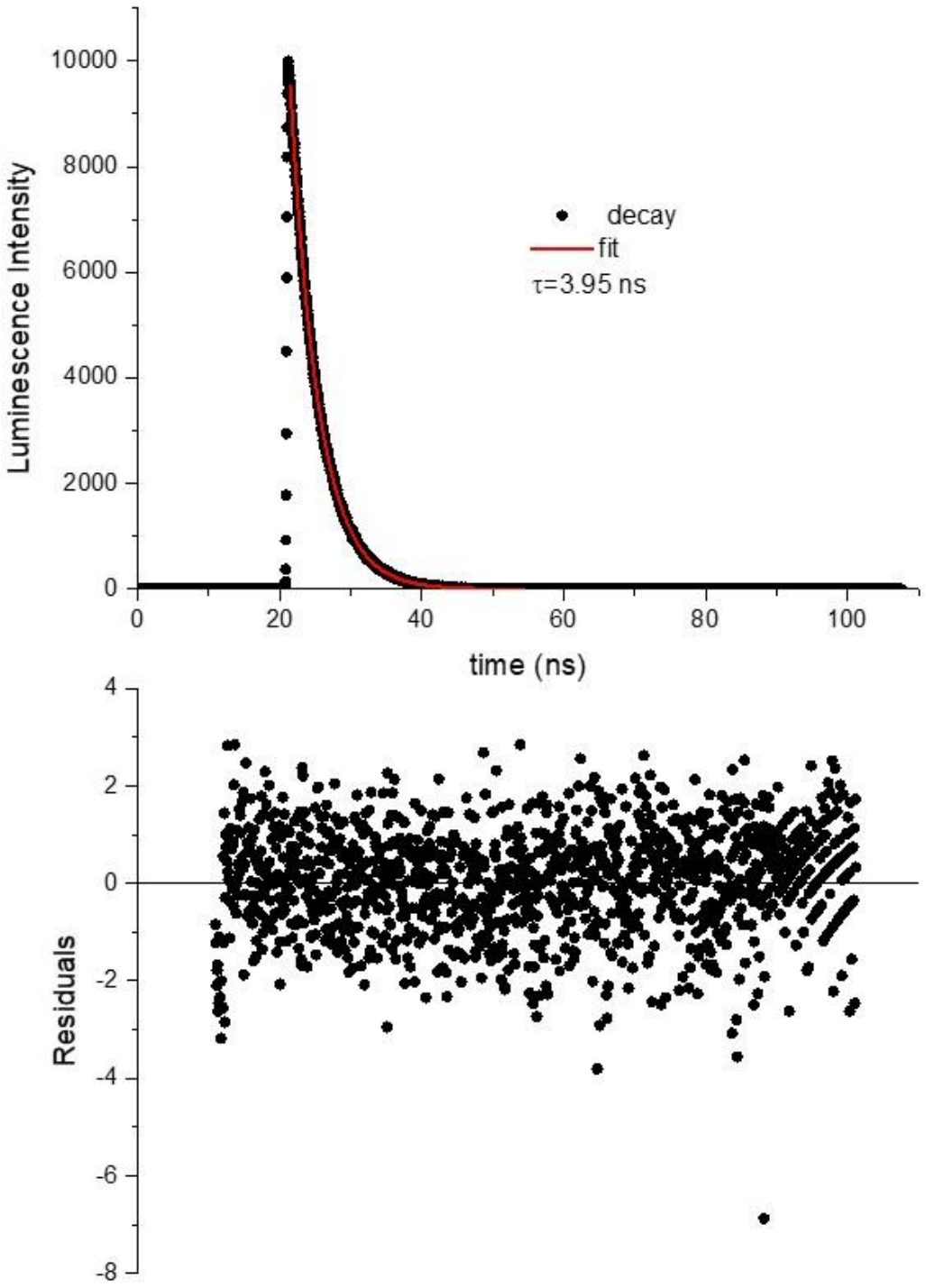

Figure S68. Lifetime measurement of *trans*-**5** in CH_2Cl_2.

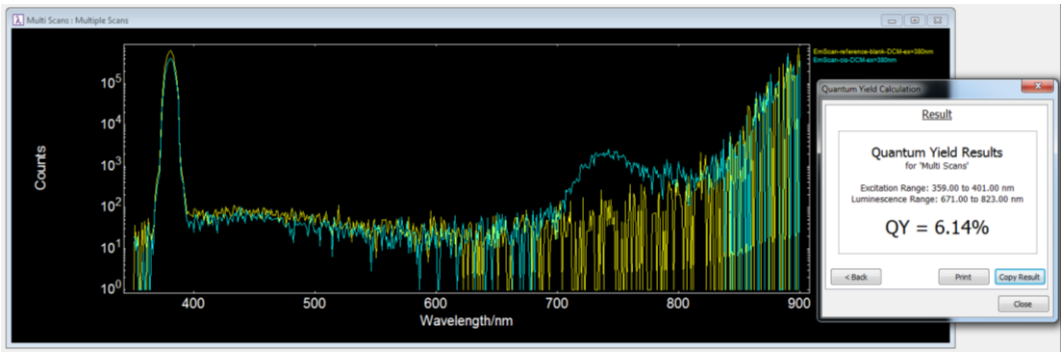

Figure S69. Absolute quantum yield of *cis*-**2** in CH_2Cl_2.

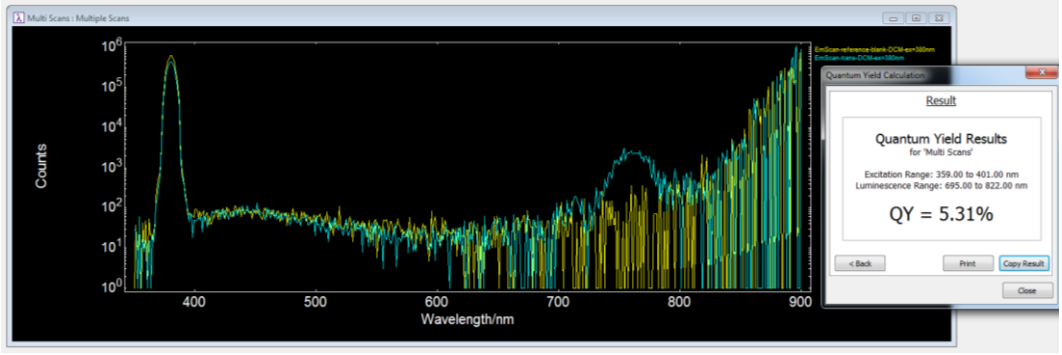

Figure S70. Absolute quantum yield of *trans*-**2** in CH_2Cl_2.

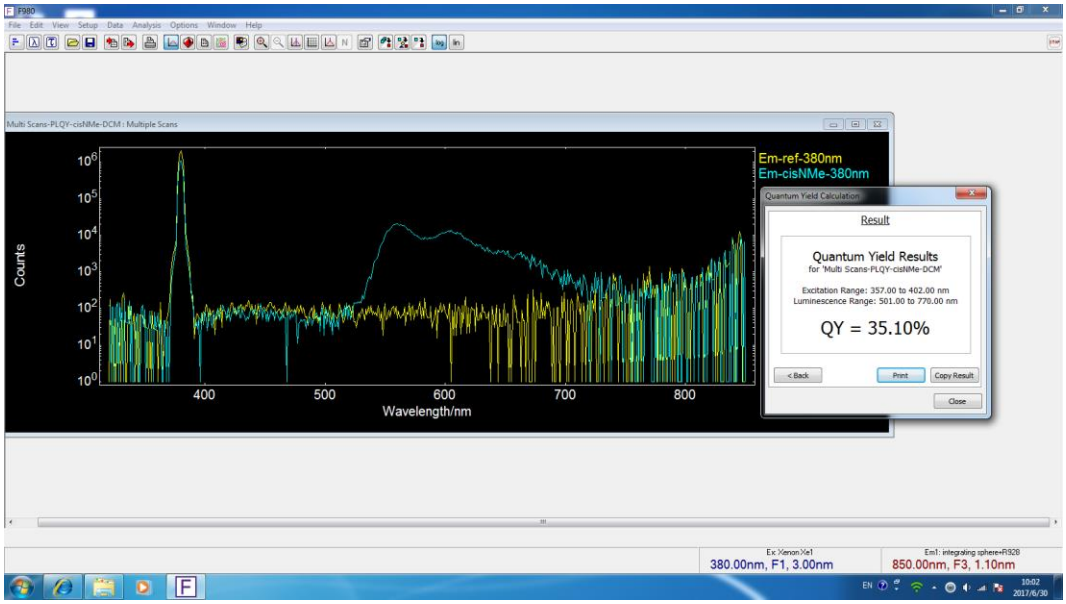

Figure S71. Absolute quantum yield of *cis*-**3** in CH_2Cl_2.

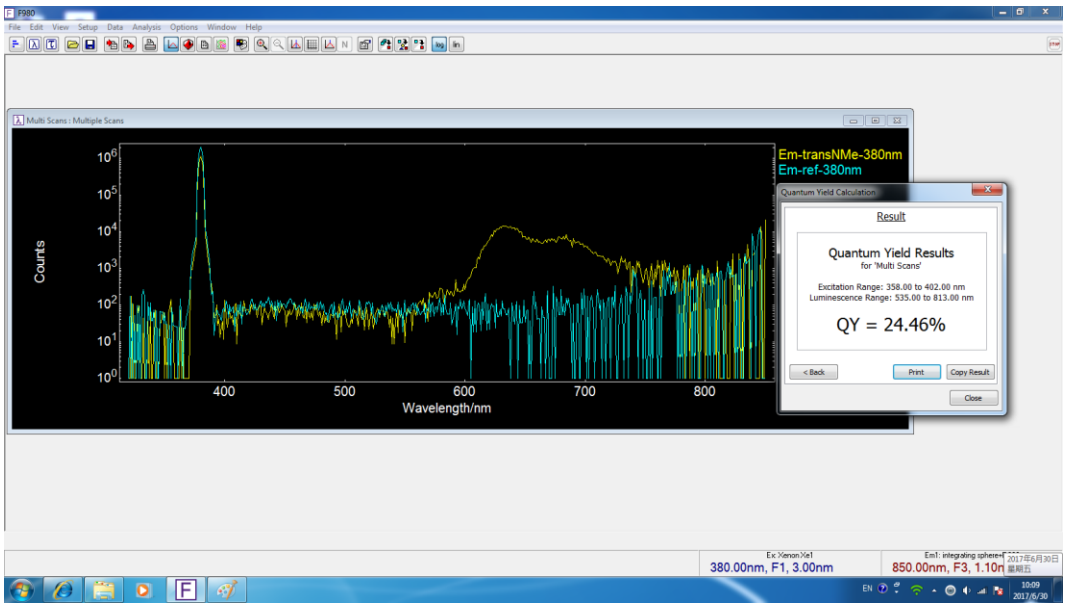

Figure S72. Absolute quantum yield of *trans*-**3** in CH_2Cl_2.

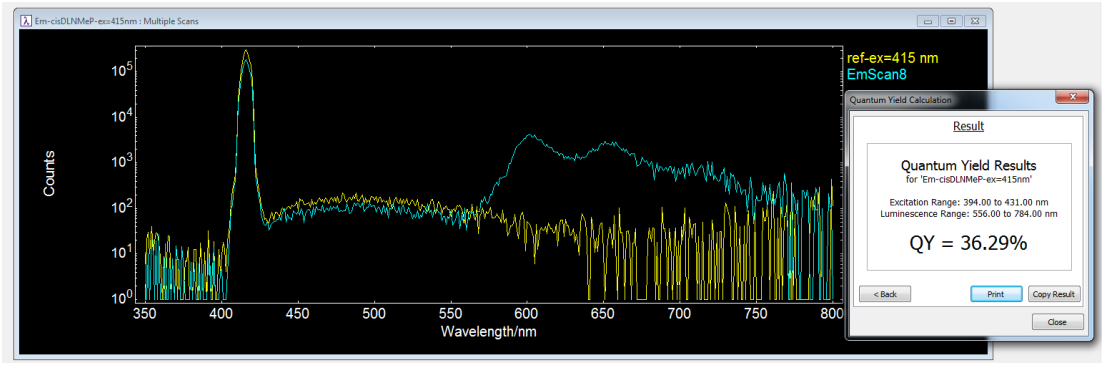

Figure S73. Absolute quantum yield of *cis*-**4** in CH_2Cl_2.

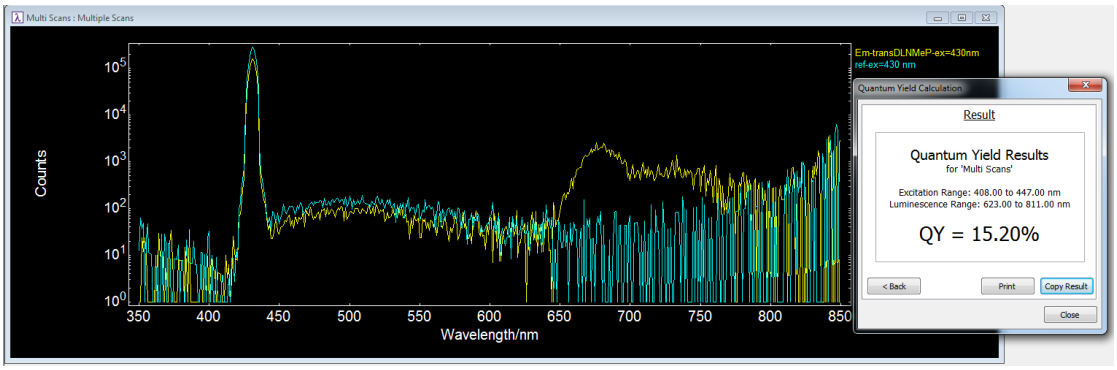

Figure S74. Absolute quantum yield of *trans*-**4** in CH_2Cl_2.

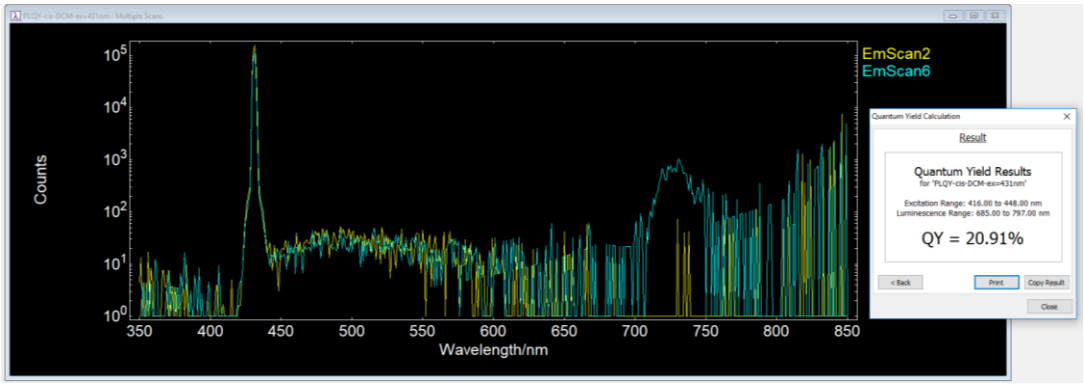

Figure S75. Absolute quantum yield of *cis*-**5** in CH_2Cl_2.

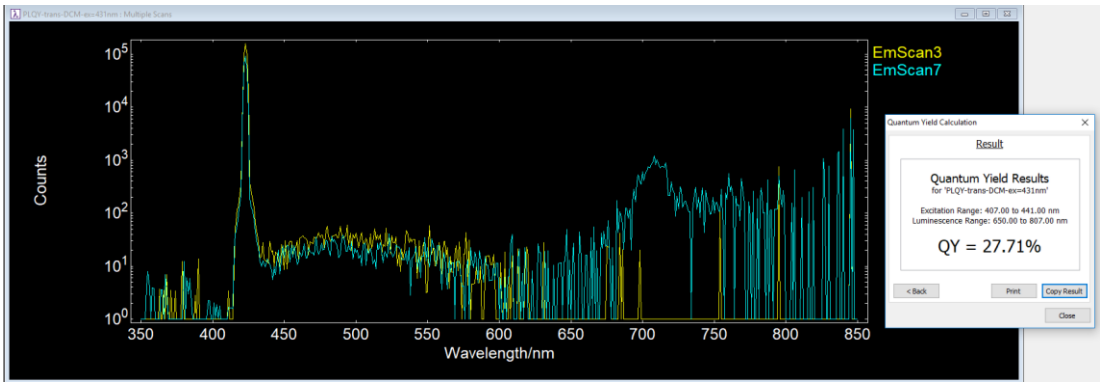

Figure S76. Absolute quantum yield of *trans*-**5** in CH_2Cl_2.

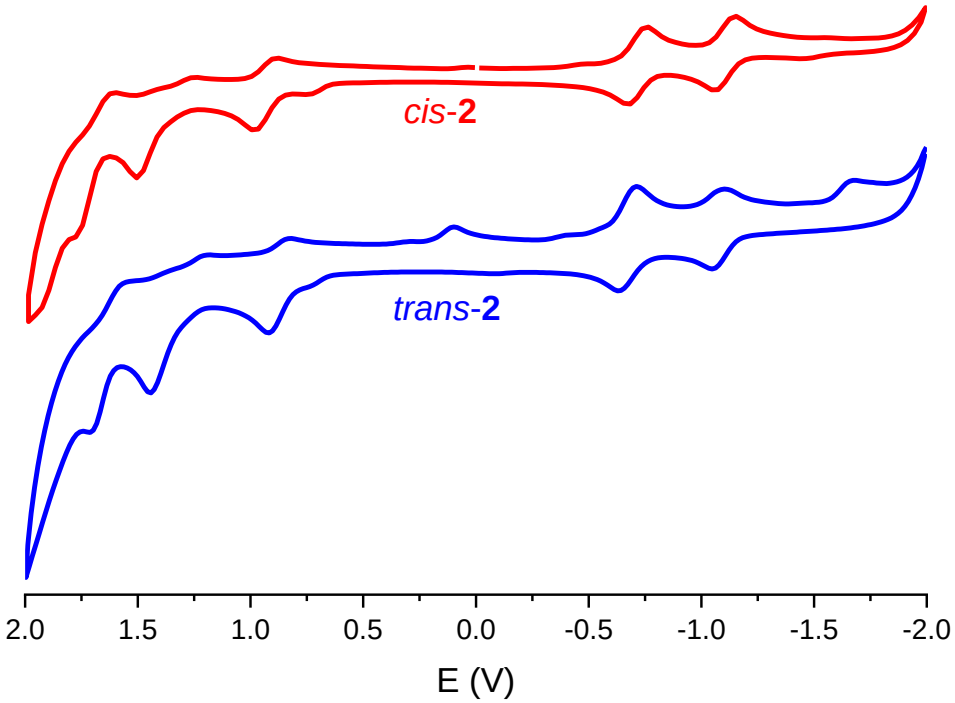

Figure S77. Cyclic Voltammograms of *cis*-**2** and *trans*-**2** in DCM containing 0.1M NBu_4PF_6 (V *vs.* AgCl/Ag).

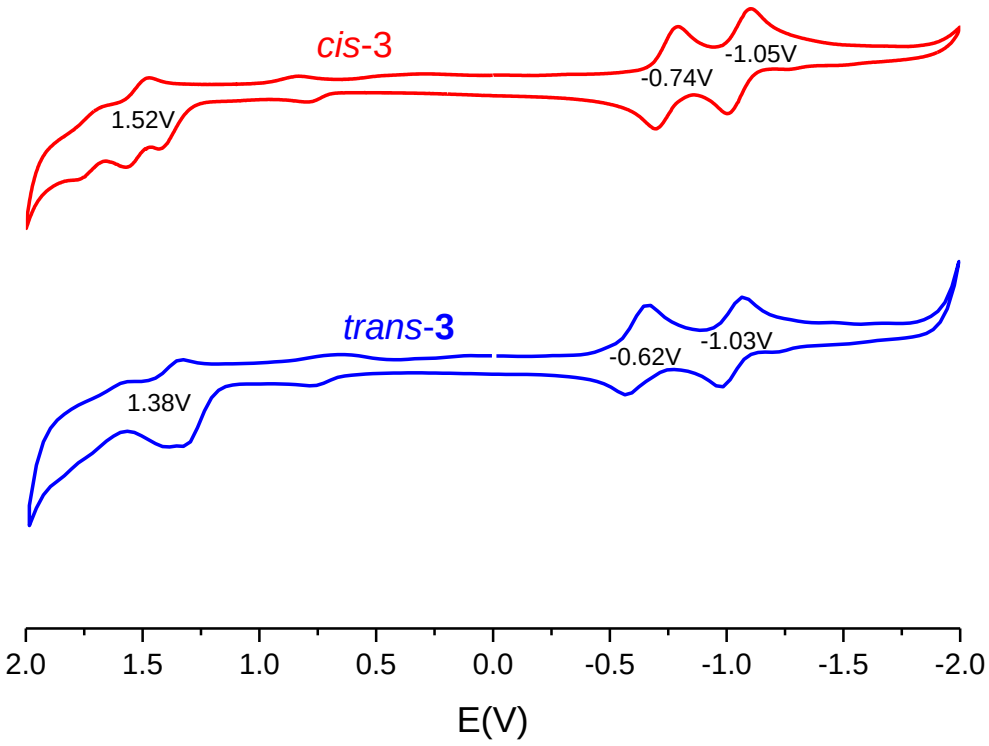

Figure S78. Cyclic Voltammograms of *cis*-**3** and *trans*-**3** in DCM containing 0.1M NBu_4PF_6 (V *vs.* AgCl/Ag).

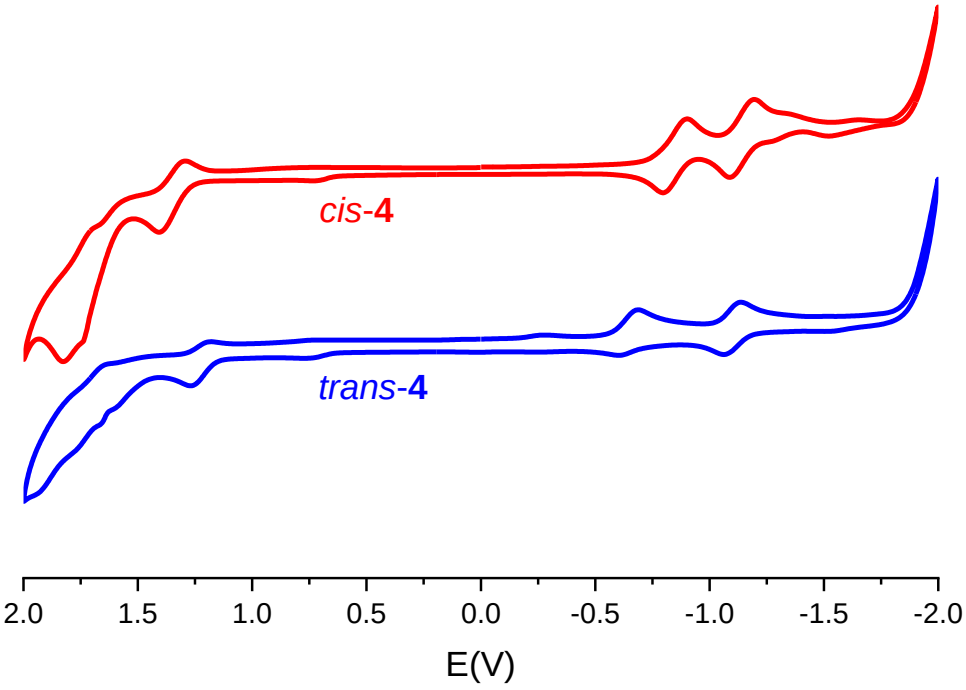

Figure S79. Cyclic Voltammograms of *cis*-**4** and *trans*-**4** in DCM containing 0.1M NBu_4PF_6 (V *vs.* AgCl/Ag).

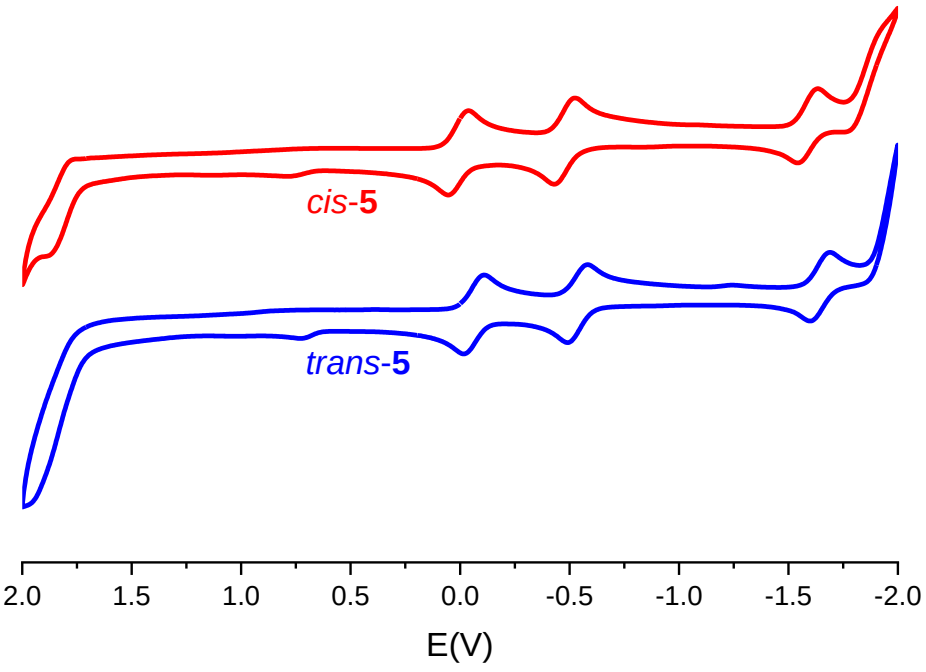

Figure S80. Cyclic Voltammograms of *cis*-**5** and *trans*-**5** in DCM containing 0.1M NBu_4PF_6 (V *vs.* AgCl/Ag).

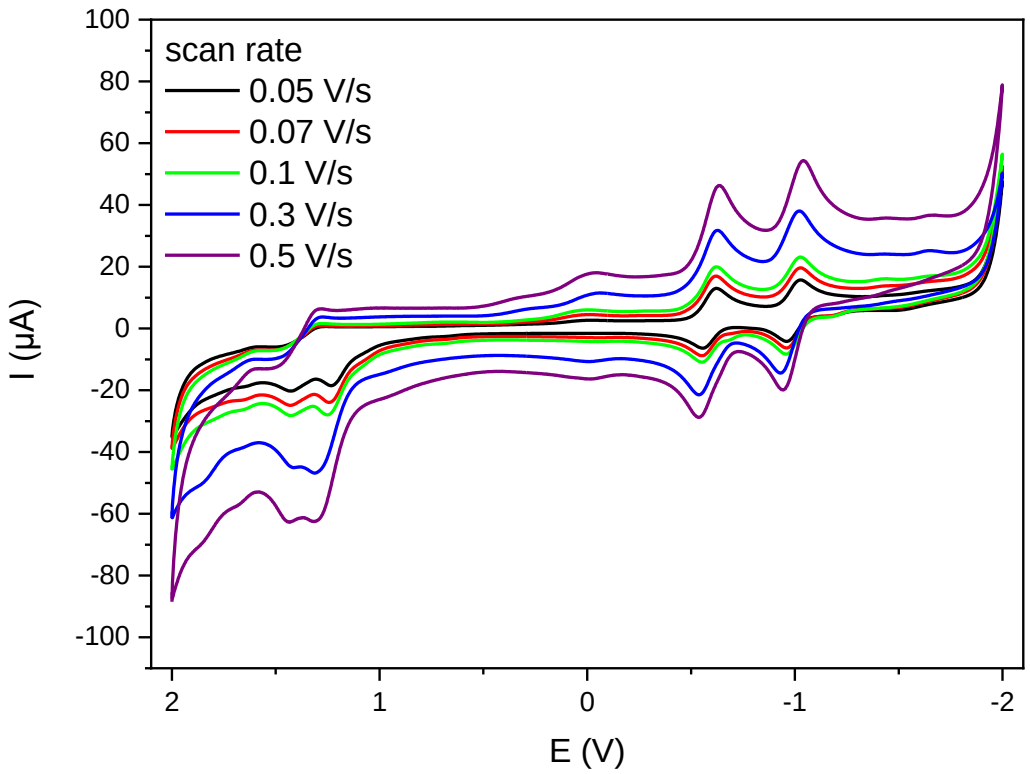

Figure S81. Cyclic Voltammograms of *cis*-**3** in DCM containing 0.1M NBu_4PF_6 (V *vs.* AgCl/Ag) with different scan rates.

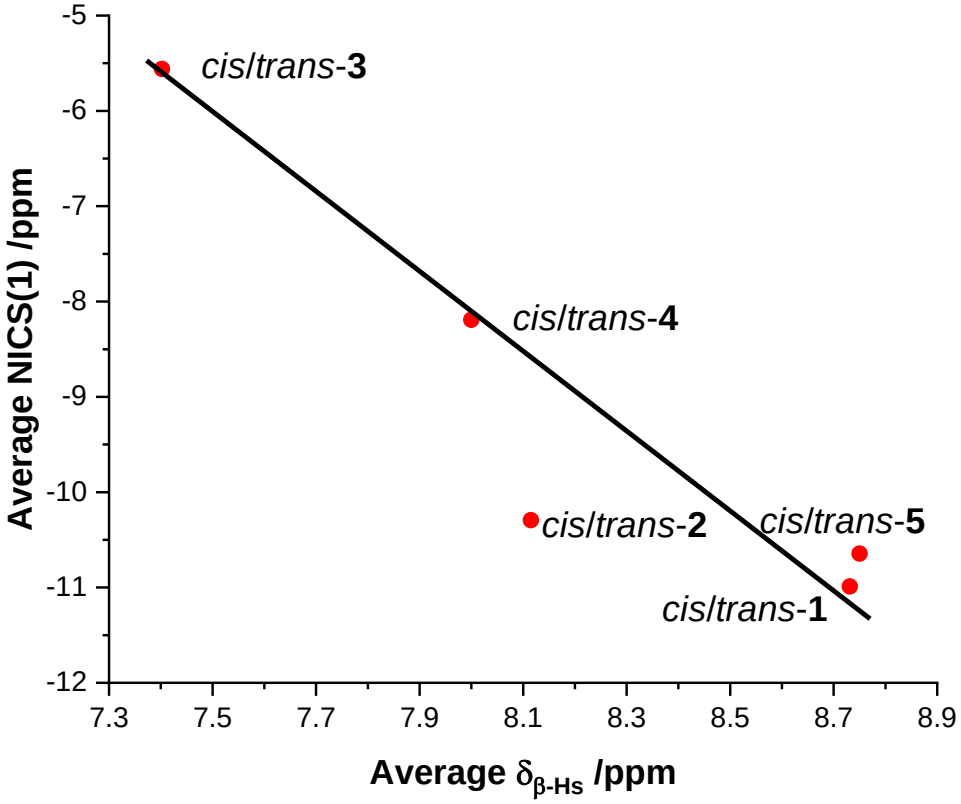

Figure S82. Average NICS(1) value *vs* average $\delta_{\beta\text{-Hs}}$ for **1**-**5** in this work.

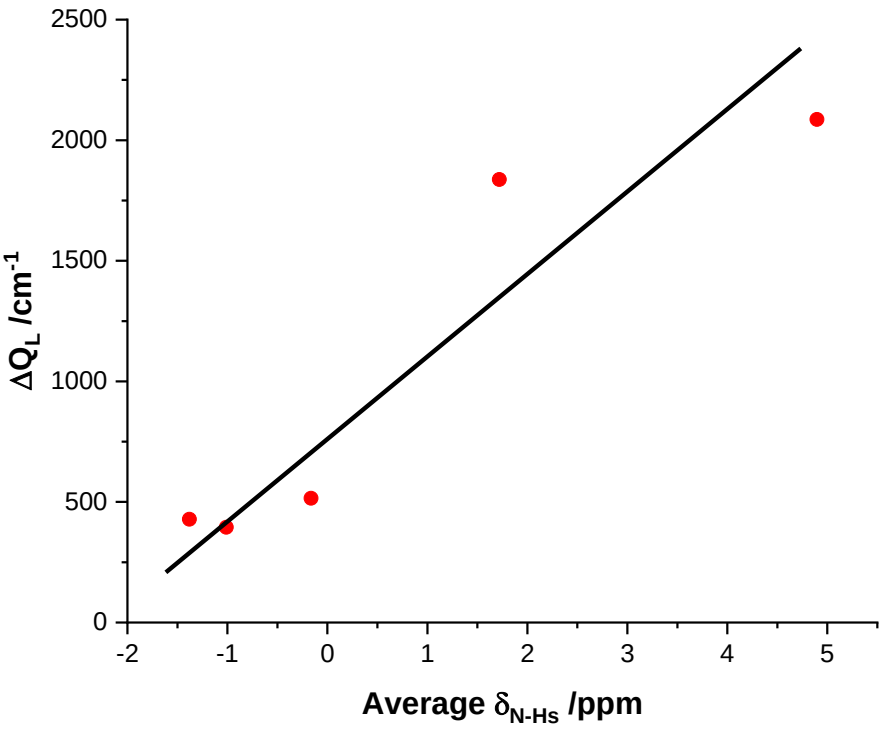

Figure S83. Correlation between regioisomeric effect and aromaticity estimated by average chemical shifts of N-Hs in cis/trans-isomers.

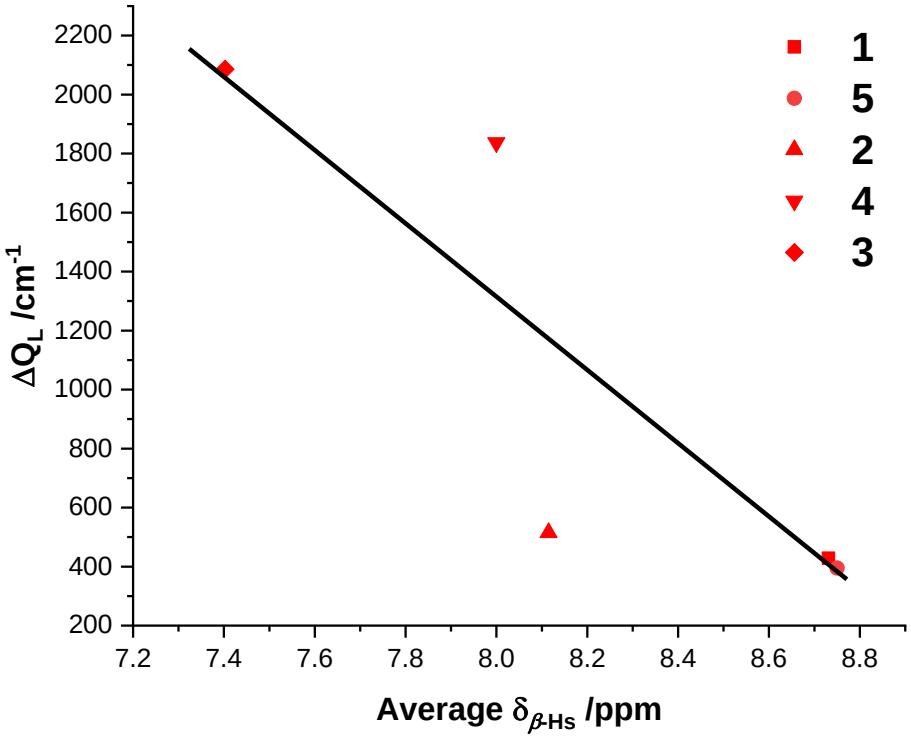

Figure S84. Correlation between regioisomeric effect and aromaticity estimated by average chemical shifts of ***β*-Hs** in cis/trans-isomers.

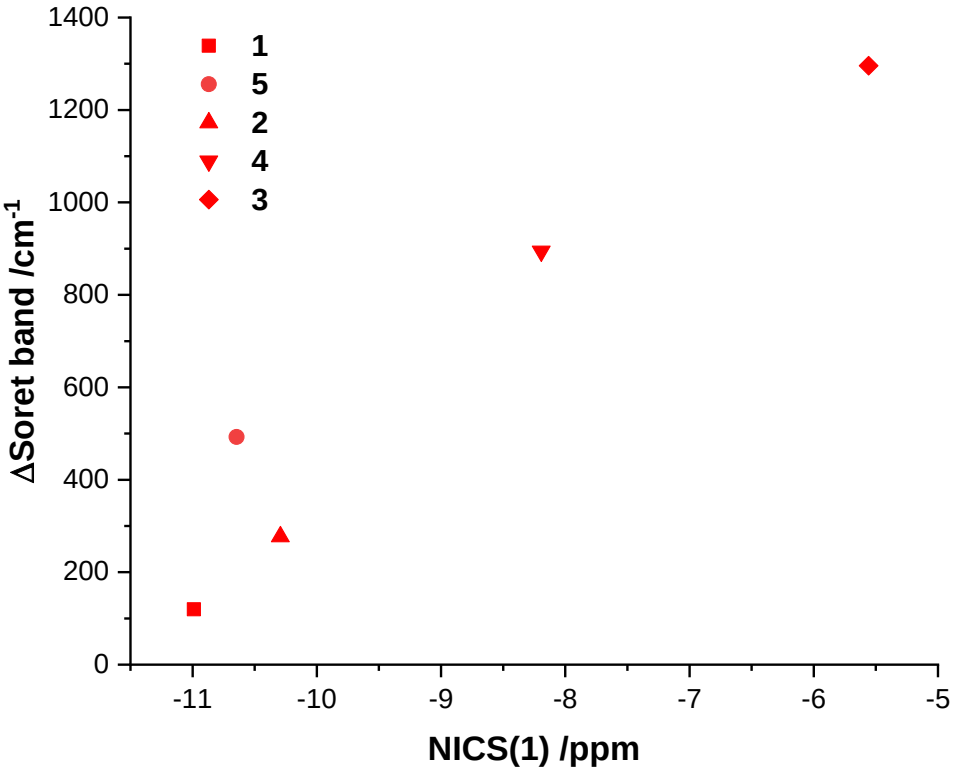

Figure S85. Correlation between regioisomeric effect (position of the Soret bands) and aromaticity estimated by the average NICS(1) value in the *cis*/*trans*-isomers.

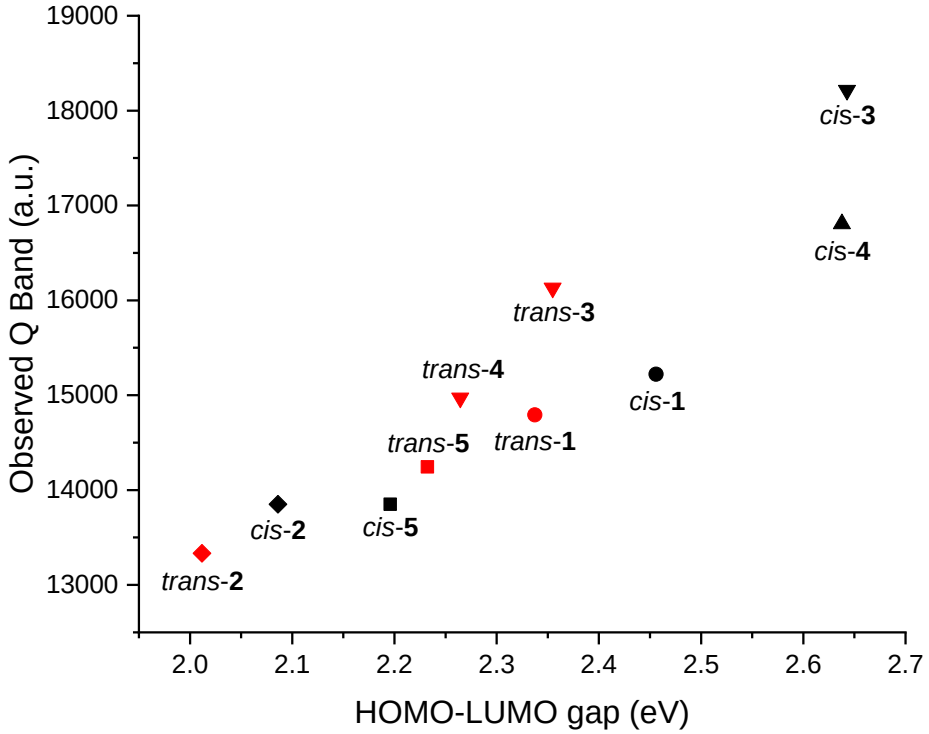

Figure S86. Observed Q band energy *versus* the calculated HOMO–LUMO gap in **1**-**5**.

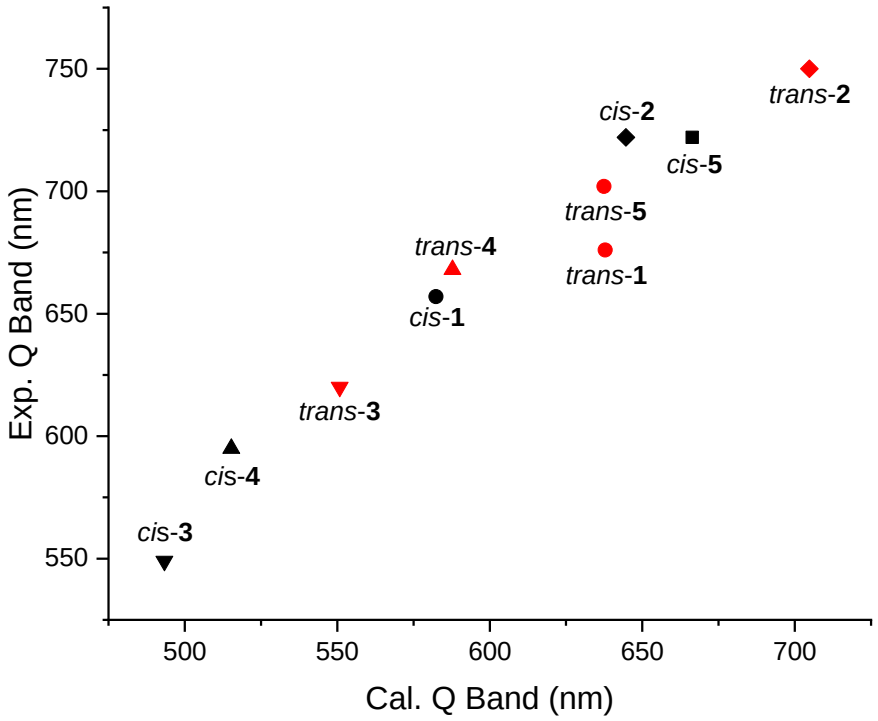

Figure S87. The experimental Q band wavelength *versus* the theoretical Q band wavelength in **1**-**5**.

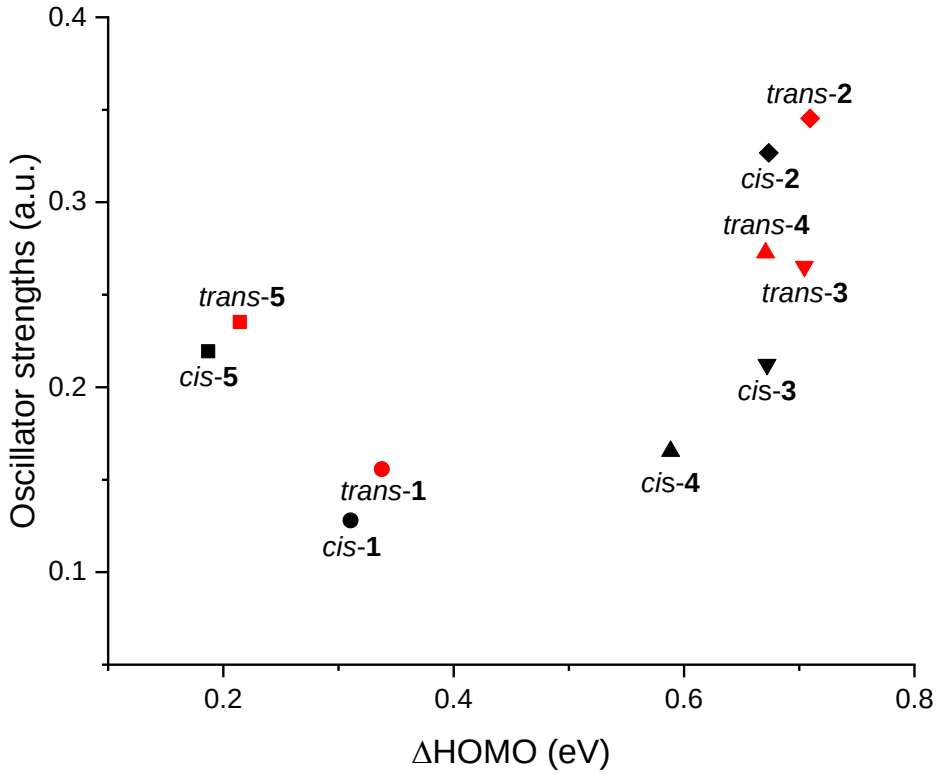

Figure S88. The oscillator strength, *f*, of the Q_L band *versus* the calculated ΔHOMO in **1**-**5**.

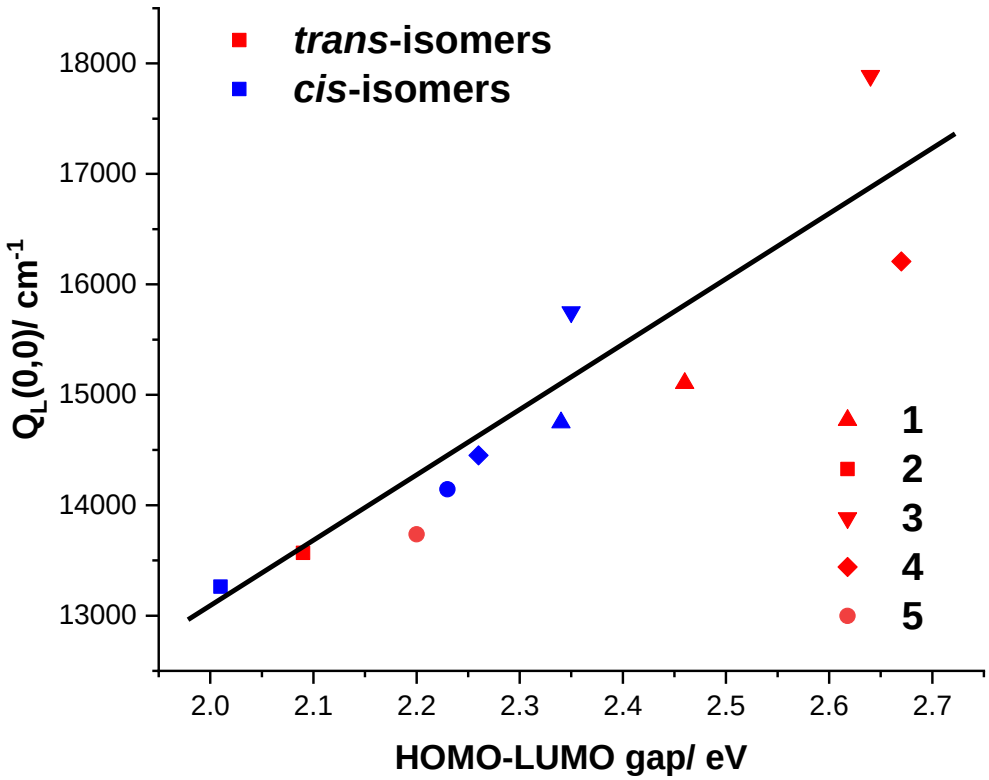

Figure S89. HOMO-LUMO gap at the optimized S_0 geometries *vs* $Q_L(0,0)$ band for **1**-**5** in this work.

4. Reference:

1. J. S. Lindsey and R. W. Wagner, *J. Org. Chem.*, 1989, **54**, 828–836.
2. a) Y. Yu, H. Lv, X. Ke, B. Yang and J. L. Zhang, *Adv. Synth. Catal.*, 2012, **354**, 3509-3516; b) X.-S. Ke, Y. Chang, J.-Z. Chen, J. Tian, J. Mack, X. Cheng, Z. Shen and J.-L. Zhang, *J. Am. Chem. Soc.*, 2014, **136**, 9598-9607.
3. a) C. Brückner, J. R. McCarthy, H. W. Daniell, Z. D. Pendon, R. P. Ilagan, T. M. Francis, L. Ren, R. R. Birge and H. A. Frank, *Chem. Phys.*, 2003, **294**, 285-303; b) J. Ogikubo, E. Meehan, J. T. Engle, C. J. Ziegler and C. Brückner, *J. Org. Chem.*, 2013, **78**, 2840-2852.
4. A. M. Silva, A. C. Tomé, M. G. Neves, A. M. Silva and J. A. Cavaleiro, *J. Org. Chem.*, 2005, **70**, 2306-2314.
5. C. Morell, A. Grand and A. Toro-Labbe, *J. Phys. Chem. A*, 2005, **109**, 205-212.
6. a) G. M. Sheldrick, *Acta. Crystallogr. A*, 2008, **64**, 112-122; b) G. M. Sheldrick, *Acta Crystallogr. C*, 2015, **71**, 3-8.
7. O. V. Dolomanov, L. J. Bourhis, R. J. Gildea, J. A. K. Howard and H. Puschmann, *J. Appl. Crystallogr.*, 2009, **42**, 339-341.
8. A. L. Spek, *Acta Crystallogr. D*, 2009, **65**, 148-155.
9. a) C. Lee, W. Yang and R. G. Parr, *Phys. Rev. B*, 1988, **37**, 785; b) A. D. Becke, *J. Chem. Phys.*, 1993, **98**, 5648-5652.
10. M. J. Frisch, G. W. Trucks, H. B. Schlegel, G. E. Scuseria, M. A. Robb, J. R. Cheeseman, G. Scalmani, V. Barone, B. Mennucci, G. A. Petersson, H. Nakatsuji, M. Caricato, X. Li, H. P. Hratchian, A. F. Izmaylov, J. Bloino, G. Zheng, J. L. Sonnenberg, M. Hada, M. Ehara, K. Toyota, R. Fukuda, J. Hasegawa, M. Ishida, T. Nakajima, Y. Honda, O. Kitao, H. Nakai, T. Vreven, J. A. Montgomery, J. E. P. Jr., F. Ogliaro, M. Bearpark, J. J. Heyd, E. Brothers, K. N. Kudin, V. N. Staroverov, R. Kobayashi, J. Normand, K. Raghavachari, A. Rendell, J. C. Burant, S. S. Iyengar, J. Tomasi, M. Cossi, N. Rega, J. M. Millam, M. Klene, J. E. Knox, J. B. Cross, V. Bakken, C. Adamo, J. Jaramillo, R. Gomperts, R. E. Stratmann, O. Yazyev, A. J. Austin, R. Cammi, C. Pomelli, J. W. Ochterski, R. L. Martin, K. Morokuma, V. G. Zakrzewski, G. A. Voth, P. Salvador, J. J. Dannenberg, S. Dapprich, A. D. Daniels, Ö. Farkas, J. B. Foresman, J. V. Ortiz, J. Cioslowski and D. J. Fox, *Gaussian 09 (Revision E.01)*, Gaussian Inc., Wallingford CT, 2009.
11. a) P. C. Hariharan and J. A. Pople, *Theor. Chim. Acta*, 1973, **28**, 213-222; b) M. M. Francl, W. J. Pietro, W. J. Hehre, J. S. Binkley, M. S. Gordon, D. J. DeFrees and J. A. Pople, *J. Chem. Phys.*, 1982, **77**, 3654-3665.
12. a) R. Herges and D. Geuenich, *J. Phys. Chem. A*, 2001, **105**, 3214-3220; b) D. Geuenich, K. Hess, F. Köhler and R. Herges, *Chem. Rev.*, 2005, **105**, 3758-3772; c) Y. Chang, H. Chen, Z. Zhou, Y. Zhang, C. Schütt, R. Herges and Z. Shen, *Angew. Chem. Int. Ed.*, 2012, **51**, 12801 –12805 ; d) J. I. Wu, I. Fernández and P. v. R. Schleyer, *J. Am. Chem. Soc.*, 2012, **135**, 315-321.
13. a) P. v. R. Schleyer, C. Maerker, A. Dransfeld, H. Jiao and N. J. van Eikema Hommes, *J. Am. Chem. Soc.*, 1996, **118**, 6317-6318; b) P. v. R. Schleyer, H. Jiao, N. J. v. E. Hommes, V. G. Malkin and O. L. Malkina, *J. Am. Chem. Soc.*, 1997, **119**, 12669-12670.

14. a) T. Keith and R. Bader, *Chem. Phys. Lett.*, 1992, **194**, 1-8; b) T. A. Keith and R. F. Bader, *Chem. Phys. Lett.*, 1993, **210**, 223-231; c) J. R. Cheeseman, G. W. Trucks, T. A. Keith and M. J. Frisch, *J. Chem. Phys.*, 1996, **104**, 5497-5509.
15. a) F. London, *J. Phys. Radium*, 1937, **8**, 397-409; b) R. McWeeny, *Phys. Rev.*, 1962, **126**, 1028-1034; c) R. Ditchfield, *Mol. Phys.*, 1974, **27**, 789-807; d) K. Wolinski, J. F. Hinton and P. Pulay, *J. Am. Chem. Soc.*, 1990, **112**, 8251-8260.